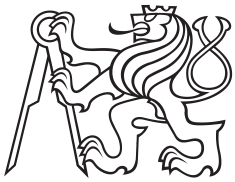

Czech
Technical
University
in Prague

F3

Faculty of Electrical Engineering
Department of Circuit Theory

Master's Thesis

Investigating the Potential Development of Antimicrobial Resistance Towards Photoactive Nanoparticles Under Illumination

Bc. Markéta Bařinková

Supervisor: **David Rutherford, Ph.D.**
Field of study: **Medical Electronics and Bioinformatics**
Subfield of study: **Medical Instrumentation**
Turn-in date: **May 2022**

MASTER‘S THESIS ASSIGNMENT

I. Personal and study details

Student's name: **Bařinková Markéta** Personal ID number: **503301**

Faculty / Institute: **Faculty of Electrical Engineering**

Department / Institute: **Department of Circuit Theory**

Study program: **Medical Electronics and Bioinformatics**

Specialisation: **Medical Instrumentation**

II. Master’s thesis details

Master’s thesis title in English:

Investigating the Potential Development of Antimicrobial Resistance Towards Photoactive Nanoparticles under Illumination

Master’s thesis title in Czech:

Výzkum potenciálního rozvoje antimikrobiální rezistence vůči fotoaktivním nanočásticím pod osvětlením

Guidelines:

This experimental project will aim to determine whether bacteria can develop resistance to bactericidal nanoparticles by re-exposing cells to sublethal concentrations and then re-exposing surviving cells to subsequent treatment. The model bacterial cells (E. coli) will be exposed to sublethal concentrations of zinc oxide nanoparticles under white light illumination with sufficient intensity to activate the nanomaterial surface. For specific applications with reverse-rotation bioreactors, custom-designed lids will be created to allow illumination of the bacterial and nanoparticle suspension during exposure. The number of viable E. coli cells will be measured at the beginning (0 hours of exposure) and at the end of the experiment (24 hours of exposure) using a standard broth dilution technique and compared to the concentration of viable cells without ZnO NP. The growth kinetics of bacteria exposed to ZnO NP under illumination will be monitored in real time and compared with illuminated cells that were not exposed to ZnO NP. The concentrations of reactive oxygen species generated by the interaction of light with the surface of ZnO NP (eg hydrogen peroxide) will also be measured.

Bibliography / sources:

[1] Panáček, A., Kvítek, L., Smékalová, M. et al. Bacterial resistance to silver nanoparticles and how to overcome it. Nature Nanotech 13, 65–71 (2018). https://doi.org/10.1038/s41565-017-0013-y
[2] Rutherford, D et al., Growth Inhibition of Gram-Positive and Gram-Negative Bacteria by Zinc Oxide Hedgehog Particles. Int J Nanomedicine. 2021; 16: 3541–3554. https://dx.doi.org/10.2147%2FIJN.S300428

Name and workplace of master’s thesis supervisor:

David Rutherford, Ph.D. Department of Physics FEE

Name and workplace of second master’s thesis supervisor or consultant:

Date of master’s thesis assignment: **05.01.2022** Deadline for master's thesis submission: **20.05.2022**

Assignment valid until: **30.09.2023**

David Rutherford, Ph.D.	doc. Ing. Radoslav Bortel, Ph.D.	prof. Mgr. Petr Páta, Ph.D.
Supervisor’s signature	Head of department’s signature	Dean’s signature

© ČVUT v Praze, Design: ČVUT v Praze, VIC

III. Assignment receipt

The student acknowledges that the master's thesis is an individual work. The student must produce her thesis without the assistance of others, with the exception of provided consultations. Within the master's thesis, the author must state the names of consultants and include a list of references.

.	
Date of assignment receipt	Student's signature

© ČVUT v Praze, Design: ČVUT v Praze, VIC

Acknowledgements

First and foremost, I would like to thank my supervisor, David Rutherford, PhD. for all his support, advice and guidance throughout the work on this thesis, for the countless discussions over results and numerous read-throughs of all my rough drafts. A big thanks also goes out to my family and partner for all their moral support.

Declaration

I declare that the presented work was developed independently and that I have listed all sources of information used within it in accordance with the methodical instructions for observing the ethical principles in the preparation of university theses.

In Prague, on _____

_____
Signature

Abstract

Antimicrobial resistance (AMR) is a significant problem for society and scientists are, therefore, constantly searching for methods of overcoming it. However, as bacteria are living organisms, bacterial resistance can develop in them over time. For this reason, when testing perspective antimicrobial agents, the effects of long-term exposure of cells to the agent should be studied to rule out the development of this resistance. In this thesis, the use of an illuminated photoactive nanoparticle (zinc oxide) as an antimicrobial agent was inspected. For this experiment, non-lethal *Escherichia coli* bacteria were repeatedly exposed to sub-lethal (100 μg/ml) concentrations of zinc oxide nanoparticles and grown in personal bioreactors. Prior to the experiment itself, preliminary experiments were carried out in order to ensure accurate results. These experiments included the measurement of the minimum inhibitory concentration and absorbance spectrum of zinc oxide nanoparticles, and other factors affecting the final measurement. For the re-exposure experiments themselves, four samples were tested - an un-illuminated sample containing zinc oxide nanoparticles, an illuminated sample, an illuminated sample containing nanoparticles, and a reference sample without illumination and nanoparticles. To evaluate the results of the two re-exposure experiments, colony forming unit (CFU) concentrations of cells after exposure to zinc oxide were measured on Mueller-Hinton agar plates. Optical density of the cell cultures (in Mueller-Hinton broth) was also measured during growth. From this data, lag phase lengths and maximum growth rates were extracted for evaluation. The data was then analyzed using a non-parametric variant of a two-factor ANOVA test called the Scheirer-Ray-Hare test. The results showed that, rather than forming antimicrobial resistance, cells exposed to zinc oxide nanoparticles became more sensitive to them over time. This effect was observed in one sample of each experiment in the third re-exposure step. Furthermore, a significant decrease in the growth rate of these suppressed samples was discovered as well as the prolongation of lag phases. Although the results of this thesis did not detect any evidence of bacteria developing resistance towards zinc oxide nanoparticles, this does not mean the material can be used with impunity. Antibacterial nanoparticles may be the long-term answer to combat AMR so if lessons are to be learned from the misuse and over-use of antibiotics, they must be used with the utmost care to prevent any possible resistance from developing.

Keywords: Antimicrobial resistance, photoactive nanoparticles, sub-lethal concentration, re-exposure, zinc oxide nanoparticles

Abstrakt

Antimikrobiální rezistence (AMR) je zásadním problémem moderní společnosti. Proto vědci stále pátrají po způsobech jejího překonání. Protože jsou bakterie živými organismy, vyvíjí se v čase, a to včetně svých rezistentních mechanismů. Citlivost bakterie vůči antimikrobiální látce v jednom časovém okamžiku tedy nezaručuje dlouhodobou funkčnost látky jako antibiotika. Z tohoto důvodu je nutné posuzovat účinky dlouhodobého působení antimikrobiálních činidel během zkoumání perspektivních antibiotik. Tímto způsobem lze alespoň částečně odhalit vývoj antimikrobiální rezistence vůči dané látce. V této práci byly zkoumány osvětlené nanočástice oxidu zinečnatého pro jejich antimikrobiální účinky. Pro výzkum byly použity neletální bakterie *Escherichia coli*, které byly několikanásobně vystaveny subletálním koncentracím (100 μg/ml) nanočástic oxidu zinečnatého a pěstovány v osobních bioreaktorech. Před samotným experimentem byl proveden předběžný výzkum pro zajištění přesných výsledků. Ten zahrnoval měření minimální inhibiční koncentrace a absorpčního spektra nanočástic oxidu zinečnatého i dalších faktorů ovlivňujících měření. Následně byly provedeny dva samostatné experimenty, ve kterých proběhlo testování čtyř samostatných vzorků – vzorku obsahujícího nanočástice oxidu zinečnatého, osvíceného vzorku, osvíceného vzorku obsahujícího nanočástice oxidu zinečnatého a reference, která byla neosvícená a neobsahovala nanočástice. Pro jejich vyhodnocení byla použita především data vývoje optické hustoty bakteriálních kultur v čase (buňky byly pěstovány v Mueller-Hintonově vývaru v osobních bioreaktorech) a měření jednotek tvořících kolonie ze vzorků odebíraných před a po vystavení oxidu zinečnatému na Mueller-Hintonově agaru. Z těchto dat byly dále získány dva parametry: délka lag fáze a maximální růstová rychlost. Data byla následně analyzována použitím neparametrického ekvivalentu dvoufaktorového ANOVA testu – Scheirer-Ray-Hare testu. Výsledky odhalily, že nevzniká antimikrobiální rezistence, ale naopak dochází u našich kultur ke zvýšené citlivosti vůči nanočásticím oxidu zinečnatého. Tento efekt byl pozorován u jednoho vzorku během obou experimentů během třetí expozice. Navíc byl pozorován pokles v rychlosti růstu a prodloužení lag fáze u těchto vzorků. Přestože výsledky tohoto experimentu nedetekovaly důkaz vzniku antimikrobiální rezistence vůči nanočásticím oxidu zinečnatého, neukazuje to na možnost bezmezného využívání této látky jako antibiotika. Antibakteriální nanočástice mohou být dlouhodobým řešením antimikrobiální rezistence, ale pokud se máme ponaučit z předchozího nadužívání a zneužívání antibiotických látek, musíme i tyto látky používat s nejvyšší opatrností, abychom zabránili vzniku další rezistence.

Klíčová slova: Antimikrobiální rezistence, fotoaktivní nanočástice, subletální koncentrace, následná expozice, nanočástice oxidu zinečnatého

Contents

Figures

Tables

Used acronyms

E. coli	*Escherichia coli*
Ag-NPs	silver nanoparticles
AMR	antimicrobial resistance
CFU	colony forming units
MDR	multidrug-resistant
MH	Mueller-Hinton
MIC	minimum inhibitory concentration
NP	nanoparticle
NPs	nanoparticles
OD	optical density
ROS	reactive oxygen species
WHO	World Health Organization

Chapter 1
Introduction

1.1 Motivation

Antimicrobial resistance (AMR) is a growing issue in today's world. Bacteria resistant to modern antibiotics pose a threat to our health, as we lack efficient means to combat infections they cause. An emerging solution to this issue is the use of nanoparticles as antimicrobial agents. Some, such as silver, have already successfully been used in applications such as the coating of surgical equipment or an ingredient in anti-fungal paints.[1] Recently, however, the development of antimicrobial resistance against silver nanoparticles has been observed, which leads to a search for different particles with antimicrobial properties. Such a nanoparticle is zinc oxide, which was used in this thesis. In addition to their antibacterial effects, zinc oxide nanoparticles are also photoactive, which offers an additional factor in the form of light to enhance the antimicrobial effects.

1.2 Goals

The goal of this thesis was to observe long-term effects of commercially available zinc oxide nanoparticles on non-pathogenic *Escherichia coli* bacterial cells. The effect of illumination of these particles using visible light was also examined. I aimed to uncover the development of antibacterial resistance against these nanoparticles in the non-pathogenic bacteria or other possible changes over a longer exposure time.

1.3 Thesis Structure

The thesis is divided into three main segments. Part one outlines the problem of antimicrobial resistance, its possible solutions and gives additional information about bacterial cells and nanoparticles as antimicrobial agents. Part two is dedicated to the description of materials and methods (both experimental and statistical) used during the practical experiment. In Part three results of the experiment are shown and discussed.

Part I

Theoretical Background

A theoretical overview of the structure of bacterial cells, antimicrobials and the formation of antimicrobial resistance, and the role of nanoparticles in the fight against it

In this section, a theoretical background to some of the important topics tied to this thesis will be given. An overview of the structure and growth of bacterial cells will be given with focus on *Escherichia coli* (*E. coli*) on which the experiments of this thesis were done. Next, information will be given on antibiotics and the development of antimicrobial resistance (AMR). Finally, I will discuss some of the nanoparticles (NPs) under examination for their antibacterial effects with a special emphasis on zinc oxide nanoparticles (ZnO NPs), which are the subject of this thesis.

Chapter 2
Bacterial cells

Bacteria are akingdom of unicellular prokaryotic organisms found everywhere in the world and make up a significant proportion of the Earth's biomass. Prokaryotes got their name from the fusion of Greek words "pro" meaning "before" and "karyon" meaning "kernel" - in other words, this kingdom is made up of organisms without a fully-formed nucleus. The genetic information of Bacteria and Archaea (the two domains belonging to this empire) is found freely in the cytoplasm with no nucleic envelope.[2]

2.1 Bacterial Morphology

As has already been said, bacteria are unicellular organisms. They are also often referred to as microorganisms, as they typically reach only micrometers in size. They can be divided into several groups based on their shape. Cocci are small spherical cells, which may form larger structures such as diplococci (a pair of cocci), streptococci (a chain of cocci), and other similar formations. Rod-shaped bacteria are dubbed bacilli and can also join together into more complex units such as bacilli chains or palisades.[2] For a comprehensive overview of bacterial morphologies, see Figure 2.1.

2.2 Bacterial Cell Anatomy

2.2.1 Surface components

Regardless of their shape, bacterial cells are commonly enveloped in a cell wall and plasma membrane. While the plasma membrane closely resembles that of eukaryotes, the structure of the bacterial cell wall is very specific to bacteria. What is more, the structure of the cell wall is the basis for the division of bacteria into gram-positive and gram-negative bacteria. While the cell wall of gram-positive bacteria (such as

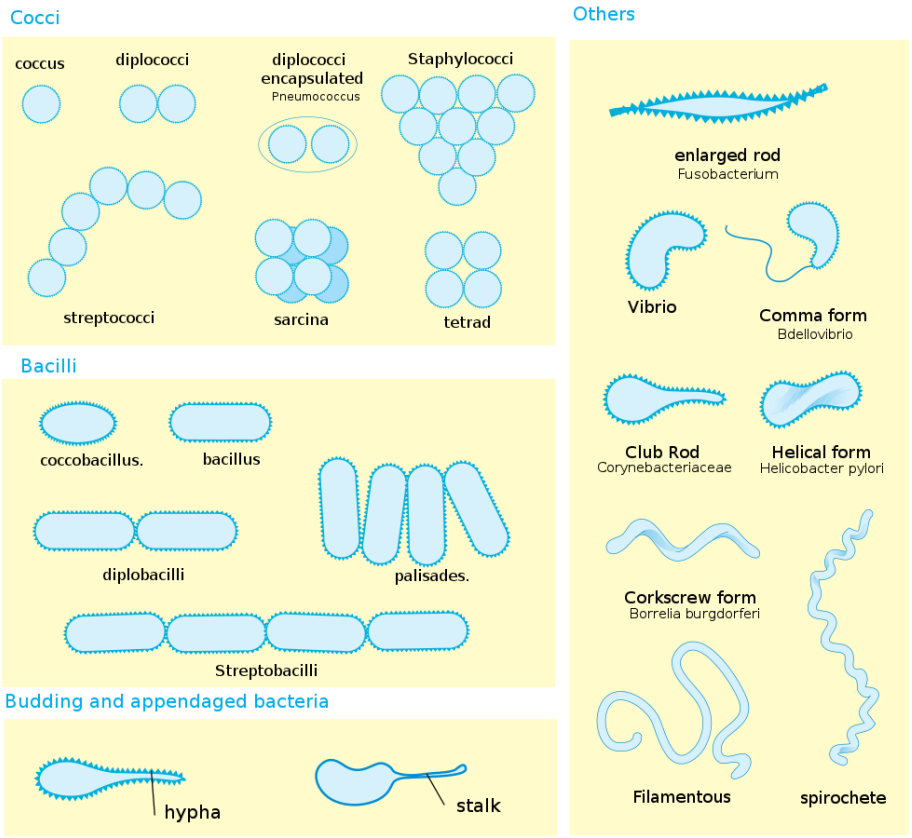

Figure 2.1: Overview of bacterial morphologies.[3]

Staphylococcus aureus) is made up mainly of a thick (20-80 nm) peptidoglycan layer sitting directly on the cytoplasmic membrane, the wall of gram-negative bacteria (such as *Escherichia coli*) is much more complex. The latter contains a thinner (1-7 nm) layer of peptidoglycan, separated from the cytoplasmic membrane by a periplasmic space. An outer phospholipid outer membrane is anchored to the peptidoglycan using lipoproteins and contains molecules of lipopolysaccharides (see Figure 2.2). When stained using Gram's method, the thick peptidoglycan layer of gram-positive cells retains the dye better, leading to the differential staining of these bacterial types.[2] It is from this histological method that gram-positive and gram-negative cells have gotten their name.[4] The plasma membrane on the other hand is common for both gram-positive and gram-negative bacteria. It constitutes a semi-permeable membrane formed by two layers of phospholipids containing many proteins and protein complexes. These can form intra-membrane pores that aid the transport of nutrients into the cells and waste out, but also take part in biosynthetic pathways. It is also the site of the respiratory chain, producing ATP for the cell.[4]

Surrounding the cell wall, a slime layer or capsule may be found, which is not essential, though may aid bacteria survival in host organisms. Two additional structures may be found on the surface of bacterial cells - flagella and pili. Flagella act as propellers for the bacterium, rotating thanks to ATP lysis at their base. The

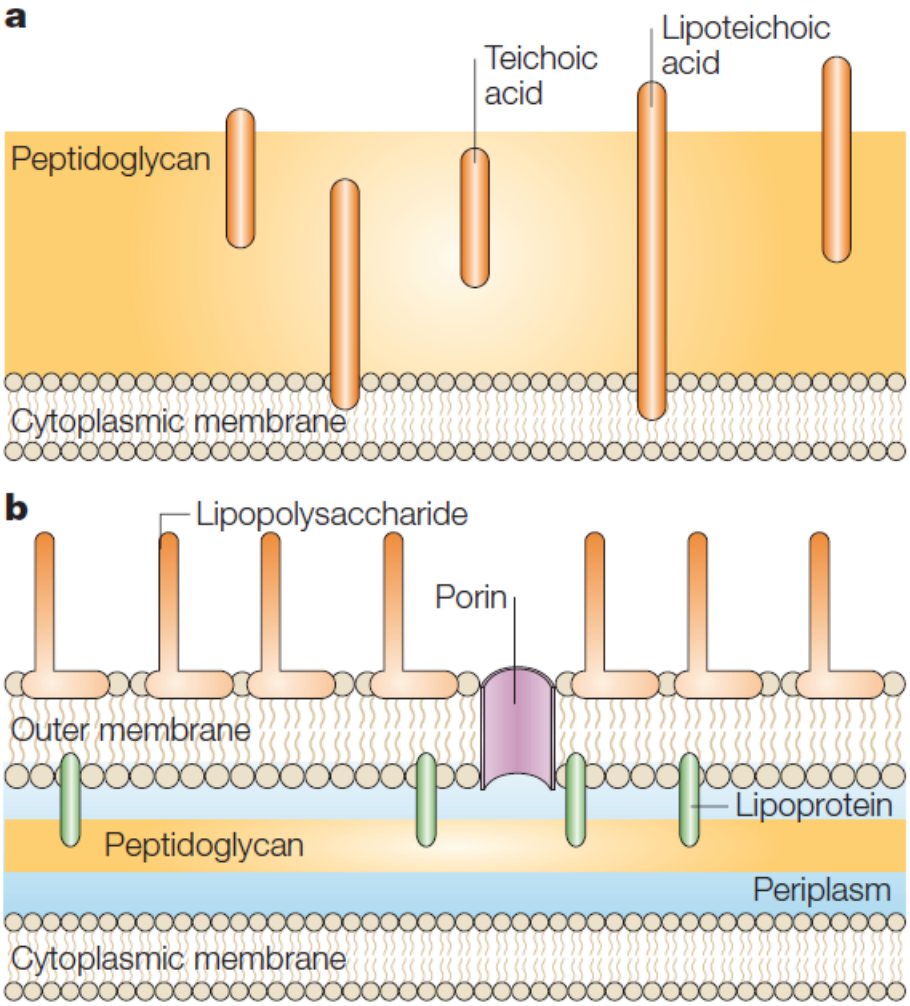

Figure 2.2: Schematic image of gram-positive (a) and gram-negative (b) bacterial cell walls.[4]

number of flagella and their placement differs and is useful for identifying bacterial strains. Additionally, two types of pili may be found on the cellular surface. Shorter pili, sometimes also called fimbrae, serve as attachment structures of the bacterium to a surface or host cell. Longer pili, also known as sex pili, are less abundant and play an important role in the transfer of bacterial genetic material during conjugation between two bacterial cells.[5]

2.2.2 Intracellular components

Inside the bacterial cell, many organelles are found, as in most cellular organisms. Genetic information in the form of one double-strand DNA molecule is found in a structure called the nucleoid, which is typically attached to the cytoplasmic membrane.[5] Other nucleic acid elements called plasmids are found freely in the cytoplasm and usually carry genetic information for additional (and often inessential)

bacterial characteristics such as genes for antimicrobial resistance. These are usually found as circular DNA molecules, can be transferred to other cells both vertically (from a parent cell to daughter cells during cell division) and horizontally (between two cells other than parent-daughter pairs, for example through the aforementioned mechanism of conjugation), and are especially useful as transforming agents for biological experiments.[2]

Apart from nucleic acids, the cytoplasm contains several organelles. Prominent among them are free ribosomes, ribonucleoproteins which take part in the translation of RNA to amino-acid sequences. Bacterial cells also contain a cytoskeleton, which is homologous to that of eukaryotes. These filamentous molecules help the trafficking of proteins and organelles to specific regions of the cell as well as aid cell division.[6] In addition to these organelles, many distinct structures may be found inside the cells for the storage of nutrients and other substances. These structures include inclusions, vacuoles, carboxysomes, and magnetosomes.[2]

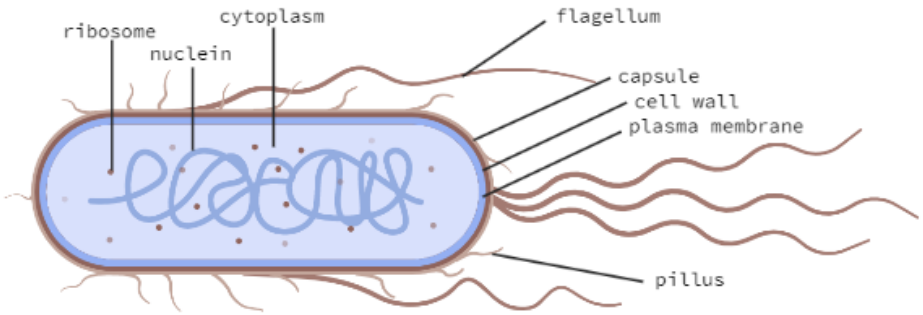

Figure 2.3: Schematic anatomy of a bacterial cell. This image was created with BioRender.com

2.3 Bacterial Metabolism and Growth

Just as bacteria differ in their shape or cell anatomy, so do they vary in their metabolic types. In addition, many bacteria may prefer one specific metabolic pattern, but change to a different one under stress or during lack of nutrients. Bacteria exhibit both autotrophic (utilizing CO_2 as a carbon source) and heterotrophic (utilizing organic substances as carbon sources) metabolic strategies. This in itself isn't unusual, as eukaryotes may also be found as both autotrophs (such as photosynthesizing plants) and heterotrophs (such as animals). However, bacteria are unique in their vast number of modifications of these main patterns. While eukaryotic autotrophic cells are exclusively photooxygenic (meaning they rely on energy from the sun and produce oxygen as a byproduct and water as an electron donor), bacterial cells may produce different byproducts (while oxygenic bacteria produce oxygen, anoxygenic bacteria do not create this byproduct), utilize different molecules as electron donors (apart from water, hydrogen, organic carbon, or iron may all act as electron donors) or rely on a different energy source (unlike phototrophs, lithotrophs utilize inorganic compounds

as a source of energy). Similarly, while eukaryotic heterotrophs rely mainly on aerobic respiration (a respiratory process whose terminal electron acceptor is oxygen), bacteria may utilize both aerobic and anaerobic respiration (in which inorganic compounds such as carbon dioxide or sulfates are terminal electron acceptors) as well as fermentation (which is a non-respiratory energy source resulting in the production of byproducts such as ethanol).[7]

In addition to the vast amount of metabolic pathways through which bacteria obtain energy, prokaryotic cells in general have also adapted to survive in much harsher conditions than eukaryotic ones. This explains why bacteria are so widely spread over the globe. While eukaryotic cells require temperatures, acidity and salinity of defined parameters of what we would call optimal life conditions on Earth, certain bacterial strains grow at high temperatures (up to 120°C, these are called thermophiles) and low temperatures (subzero temperatures, these are called psychrophiles). They can also tolerate wide ranges of pH (from pH < 1 to a pH of 11) and salinity (some halophile can tolerate up to 30 % salinity). Some bacterial strains have even been shown to be resistant to UV radiation.[7]

Under optimal conditions, bacteria can grow at an exponential rate, owing to the fact that each parent cell can divide into two daughter cells. Scientists have studied bacterial growth under laboratory conditions in culture media and have discovered a typical growth curve containing four main growth phases that can be seen in Figure 2.4. When initially put into a fresh medium, bacterial cells undergo the so-called "Lag" phase, during which the culture exhibits no replication as it adjusts to the new surroundings. Next, bacteria enter a "Log" phase, a state of exponential growth, which continues as long as optimal conditions are maintained (the bacteria have enough nutrients and space). When nutrients start being depleted, bacterial division slows and a portion of the cells begins to die, this is called the "Stationary" phase. This continues until most nutrients are depleted, cells then enter the "Death" phase, during which the amount of viable cells in the medium falls rapidly.[8]

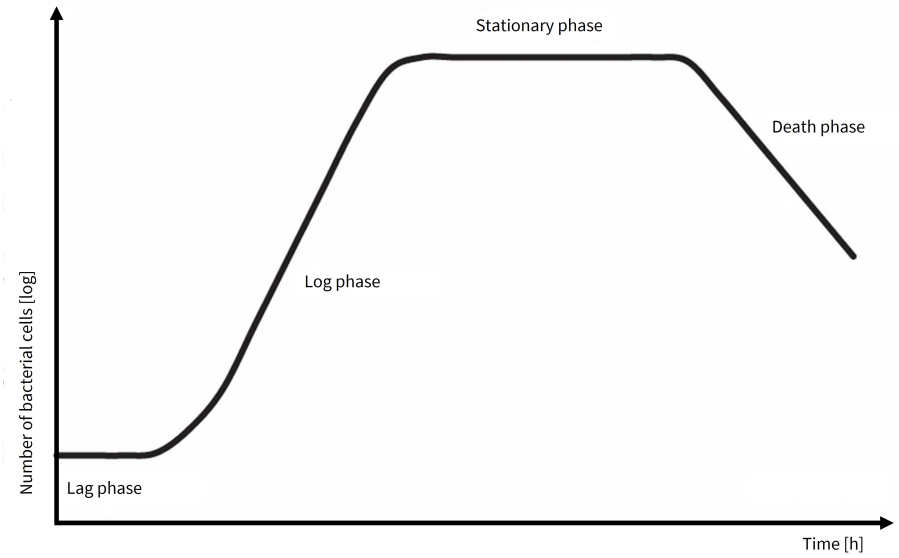

Figure 2.4: Typical bacterial growth curve.

2.4 *Escherichia coli*

The bacterium used in this thesis is a Gram-negative *Escherichia coli* (*E. coli*) strain. These bacteria have spherical to rod-like shapes (An image of *Escherichia coli* can be seen below in Figure 2.5) and are facultative anaerobes, meaning they do not need oxygen to thrive, but can occasionally utilize it under adverse conditions. Although most serogroups of this bacteria are non-pathogenic and are actually found in the digestive tract of warm-blooded animals, including humans, some strains have been shown to cause diseases in humans (e.g. *E. coli* 0157:H7). Most pathogenic strains of this bacterium cause digestive issues and fever, though some are known to cause renal failure, seizures, central nervous system disorders, etc[9] and produce toxins such as the deadly enterohemmorhagic verotoxin.[10]

E. coli is an ideal model organism for experiments on antimicrobial resistance for a number of reasons. It is small, easy to manipulate, inexpensive to proliferate, and has been thoroughly studied and described. In addition, these bacterial cells are found in the human body and some strains are pathogenic - it is therefore a good model organism for testing the effect of antibiotics and the development of antimicrobial resistance.[11,12] Under laboratory conditions, bacteria are grown in either liquid broth, or on semi-solid agarose petri dishes. In the case of broth, where they are found as individual cells, we obtain information about the number of bacterial cells using measurements of optical density (OD) and assume that the number of bacterial cells in broth is approximately proportional to optical density of the broth at a defined wavelength. Cells may, however, also be grown on agar plates. Here, each cell divides multiple times to create a colony - a cluster of cells originating from one individual and often detectable with the naked eye. *E. coli* cells form two basic types of colonies - rough, which are flat and irregular, and smooth, which are higher and circular. More colony morphologies have also been discovered,[13] however, the two mentioned above are the most readily distinguishable from agar plates.

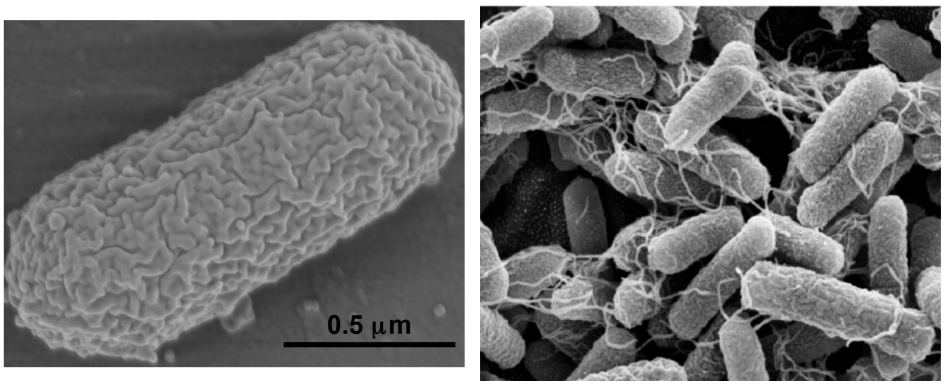

Figure 2.5: Microscopic images of *E. coli* cells.[12]

Chapter 3

Antimicrobial resistance

Antimicrobial resistance (AMR) is among the more prominent hurdles we will have to overcome in the following years. The World Health Organization (WHO) has labeled AMR as one of the top 10 global health threats. Several steps have been put forward in order to combat this threat, one of which is the attempt of researchers to find novel antimicrobial substances. Nanoparticles are among such materials, currently under scrutiny for their antimicrobial effects.

Antimicrobial agents have been around for thousands of years. The first use of antibiotics dates back more than two millennia when natural antimicrobial substances were used by ancient Greeks, Egyptians and other nations. It wasn't until the beginning of the 20th century, in 1910, when the first synthetic antibiotic, Salvarsan, came into use. The discovery of penicillin some twenty years later marked the beginning of the golden age of antibiotics. Only ten years after its discovery, however, the first bacteria with penicillin resistance emerged. In the 1940s to 1960s many natural and synthetic antibiotics were discovered. After this period of significant development of antimicrobials, the introduction of new antibiotics waned, while AMR against existing pharmaceuticals continued to evolve.[14] The rapid spread of bacterial strains resistant to antibiotics is thought to be caused by improper prescribing and use of antibiotic drugs, as well as poor infection prevention in many facilities.[15] An even bigger issue arises, when bacterial strains resistant to a certain antimicrobial substance acquire resistance against a different antibiotic, becoming a so-called multidrug-resistant (MDR) organism.[16] This has led us to a time some are now calling the "post-antibiotic era".[17]

3.1 Traditional Antibiotics and Mechanisms of Antibiotic Resistance Against Them

The primary aim of antibiotics is to rid the body of pathological bacteria while causing as little damage to host cells as possible. The idea behind ensuring this specificity to bacteria is the usage of substances targeting mechanisms or molecules specific only to bacterial cells. These targets may be the bacterial cell wall, which has a different composition to the cellular envelopes of eukaryotic cells, bacterial ribosomal subunits, or other proteins associated with bacterial growth and replication. Antibiotics are divided into multiple groups based on structural elements.

The development of antimicrobial resistance is usually a spontaneous process in

which a genetic mutation proves to be advantageous to the bacterium when subjected to the bactericidal substance. Environmental pressure acts in favor of the "survival of the fittest" - those bacteria able to withstand the effects of the antibiotic replicate and dominate subsequent generations. The selection of resistant bacteria cells is aided by their significantly shorter life cycles compared to those of their human hosts and as well as the ability of bacterial cells to take in genetic material from their surroundings via pili and exchange genetic information (usually from plasmids) with other bacterial cells through conjugation.[18] Figure 3.1 shows a schematic representation of three examples of antibiotic groups chosen to illustrate the different mechanisms through which antibiotics target bacterial cells, as well as the ways in which bacteria combat these substances.

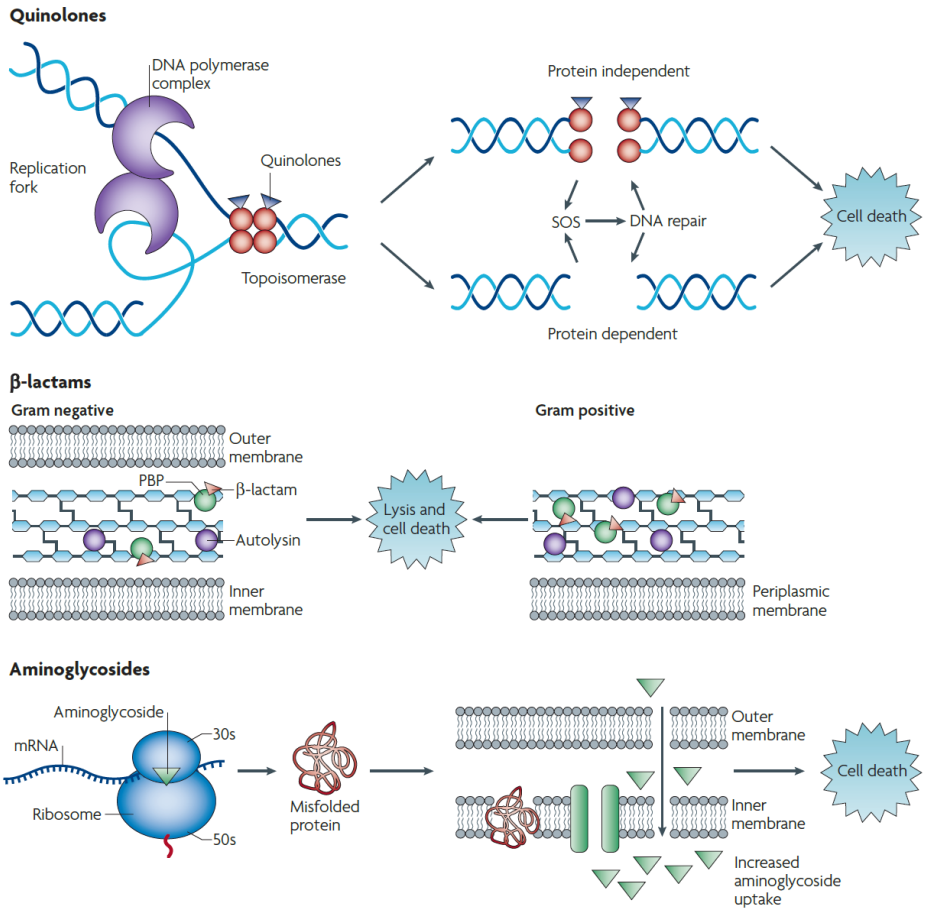

Figure 3.1: Schematic representation of the mechanisms of antimicrobial effects of quinolones, animoglycosides, and β-lactams.[19]

Quinolones

Quinolones typically inhibit the action of DNA gyrase and topoisomerase IV, which are both essential for correct DNA transcription into RNA. During this process, the mother DNA double strand is unwound from the middle of the strand, which

causes tension on the still-wound ends of the strand. This tension is released by the DNA gyrase, without which DNA transcription can never be completed. Similarly, topoisomerase IV aids DNA replication by untangling newly formed DNA strands. Without it, bacterial cells cannot replicate.[10] Among the mechanisms known to protect cells against these antibiotics are the expression of efflux pumps to expel the quinolone molecules, a decrease in membrane permeability (both these mechanisms lower the amount of the quinolone in the cell), the modification of the antibiotic, and the expression of enzymes, which compete for binding sites on the target molecules.

β-lactam antibiotics

β-lactam antibiotics were among the first discovered, as their best-known members is penicillin. These antibiotics bind to so-called penicillin-binding proteins, which are responsible for cross-linking peptidoglycans. This bond between the antibiotic and the penicillin-binding protein disrupts the formation of the bacterial wall and result in the lysis of bacterial cells. Since human cells have no penicillin-binding proteins, these antibiotics are selective towards bacterial cells. As penicillin was among the first discovered antibiotics, many defense mechanisms against β-lactam antibiotics have already cropped up. Many bacteria have developed β-lactamases, which are enzymes capable of hydrolyzing the antibiotic molecule and rendering it incapable of binding to its target molecule. Another pathway of β-lactam resistance is the modification of penicillin-binding proteins into such a form, which the antibiotic cannot target.[10,18,19]

Aminoglycosides

Another group of antibiotic substances which has been around for several years is the group of aminoglycosides. Among the representatives of this group are streptomycin, neomycin, or kanamycin. These antibiotics bind the 30S sub-unit of bacterial ribosomes and prevent the correct translation of proteins. In effect, this also leads to better membrane permeability, due to the incorporation of misfolded proteins and more antibiotic perfusion into the cells. As with β-lactam antibiotics, several resistance mechanisms have evolved in bacteria. Among these are the active efflux of the antibiotic from the cell, decrased permeability through the plasma membrane, ribosome alteration (this modifies the target of the antibiotic to make it less susceptible to the antibiotic), and inactivation of the aminoglycoside itself.[10,18,19]

- From the examples, we have seen three primary mechanisms of antimicrobial effects:
  - inhibition of cell wall synthesis, leading to lytic cell death,
  - inhibition of the translation apparatus,
  - inhibition of DNA or RNA synthesis.
- We have also seen five mechanisms of bacterial defense against these antibiotics:
  - modification of the target molecule,

- increased efflux,
- decreased membrane permeability,
- antibiotic hydrolysis or inactivation by other means,
- competition for binding spots on target proteins.

In addition to these genetically encoded methods of antimicrobial resistance, some bacteria are able to randomly slow their metabolism and become so-called "persister cells". These cells are more tolerant towards the antibiotic. Intracellular pathogens also have some level of protection against antibiotics, as these substances are created not to enter or harm host cells. Apart from these mechanisms, which protect individual cells, bigger cell complexes such as biofilms (groups of cells attached to a surface) or swarms of cells (multicellular formations of differentiated swarm cells) also possess antimicrobial properties.[20]

3.2 Investigation of the Development of Antimicrobial Resistance

For the investigation of possible development of antimicrobial resistance in bacterial cells, long-term exposure to a sub-lethal concentration of an antimicrobial is often used. Sub-lethal concentrations of these substances are meant to stress the cells in order to put selective pressure on them without killing them. The cells are exposed long-term to a constant concentration of an antibiotic in order for multiple generations to be allowed to evolve. This is usually secured by a periodical change of fresh medium with the antimicrobial substance.[21–23]

Chapter 4

Nanoparticles

Prominent among the solutions of overcoming antimicrobial resistance issues seems to be the usage of nanoparticles (particles less than 100 nm in size) as antimicrobial agents. Though many types of nanoparticles are being examined for their antimicrobial properties (carbon based polymers, synthetic polymers, quantum dots, etc.),[24] the focus of this thesis will be mainly on metallic nanoparticles, specifically zinc oxide (ZnO).

4.1 Metallic Nanoparticles as Antimicrobial Agents

Unlike traditional antibiotic substances, which target specific structures or pathways in bacterial cells, metallic nanoparticles affect the cell through several mecha-

nisms at once, making the development of antimicrobial resistance much less likely (though not impossible).

Apart from their extensive antimicrobial capacity, metallic nanoparticles are nature's original antimicrobials and can therefore be produced biogenically (isolated from bacterial strains which produce these substances as a defense mechanism against competing bacteria).[25] This would make the theoretical large-scale production of these materials as antibiotics a more ecological choice. In addition, such molecules are highly stable and biocompatible.[20]

Many metallic molecules (such as gold, copper, palladium, or titanium) are being examined for their antimicrobial effects,[20] the most widely used being silver nanoparticles (Ag-NPs). The antibiotic effect of silver has been known for several centuries. Today, it is mainly used in ointments used to combat infection, but also in anti-fungal paints, surgical masks, catheters, and many others.[1,20,26] However, the development of antimicrobial resistance to Ag-NPs has recently been discovered. In 2017, Panáček et al. published an article, which showed the development of antimicrobial resistance towards Ag-NPs through bacteria-induced aggregation. In their work, they showed that the enhanced production of the bacterial protein flagellin led to the aggregation of nanoparticles, which diminished their antimicrobial properties.[27] This discovery shows the demand for more antibacterial nanoparticles as well as for a more thorough exploration of possible antimicrobial resistance development towards them. Viable alternatives to silver nanoparticles could be nanoparticles of copper, palladium, titanium dioxide, or zinc oxide. The latter will be discussed in more detail in the following section (Section 4.2), as it is the topic of this thesis, however basic information will be given about the former three in the following paragraph.

Copper nanoparticles have strong antimicrobial effects against both Gram-positive and Gram-negative bacteria.[20] They are currently used as antimicrobials in textiles and paints, but have many other industrial uses, not relevant to this thesis.[28] Although their antibacterial efficacy is lower than that of silver nanoparticles, they are less costly to produce, which could speak in their favor as a potential mass-produced antibiotic.[29] Titanium dioxide nanoparticles are also already in use for their antimicrobial properties. The advantage of TiO_2 molecules is their photocatalytic activity, which is similar to that of zinc oxide and will be discussed more in Section 4.2. Today titanium dioxide is mainly used in the disinfection of both water and air. The nanoparticles are efficient even against biofilms as opposed to traditional antibiotics.[30] The final nanoparticle I would like to mention before moving on to the crucial molecule for this thesis is platinum (though many more, such as gold, manganese, or palladium, could be mentioned). These nanoparticles are especially interesting in their uses as medicaments for ovarian and testicular cancer. However, as these molecules are cytotoxic even towards healthy cells and need to be modified in order to specifically target cancerous cells, their use as an antimicrobial drug is, for now, improbable.[31]

4.2 Zinc Oxide Nanoparticles

Zinc oxide is an n-type semi-conductive material with properties suitable for use as an antimicrobial agent. It is highly biocompatible, non-toxic to human cells,

heat-resistant and has photocatalytic properties, which could further enhance its effects.[32] ZnO NPs have applications in many fields, such as in the targeted treatment of certain types of cancers (including both a specific toxicity of the nanoparticles to some cancer cells or as an anticancer-drug carrier), anti-inflammatory and diabetic treatment, but also in agriculture as a fertilizer and an ingredient in cosmetics such as sunscreens.[25,33,34] Another thoroughly researched quality of ZnO NPs is their antimicrobial potential.[33,35] Although it is still unclear through which mechanism ZnO eradicates microorganisms, many pathways have already been discovered as well as some properties which have a profound effect on the antimicrobial capacity of the nanoparticles.

4.2.1 Mechanisms of Antibacterial Effects of ZnO NPs

Despite being studied by numerous teams, the exact mechanisms in which zinc oxide nanoparticles act against microorganisms is still not fully understood. Among the possible mechanisms, summarized schematically in Figure 4.1, is the production of reactive oxygen species (ROS) both under illumination and in the dark, mechanical interactions with bacterial cells, the release of cytotoxic Zn^{2+} ions, and the internalization of ZnO NPs by the cell itself.[32,36] Of these, the generation of ROS is the most plausible mechanism.

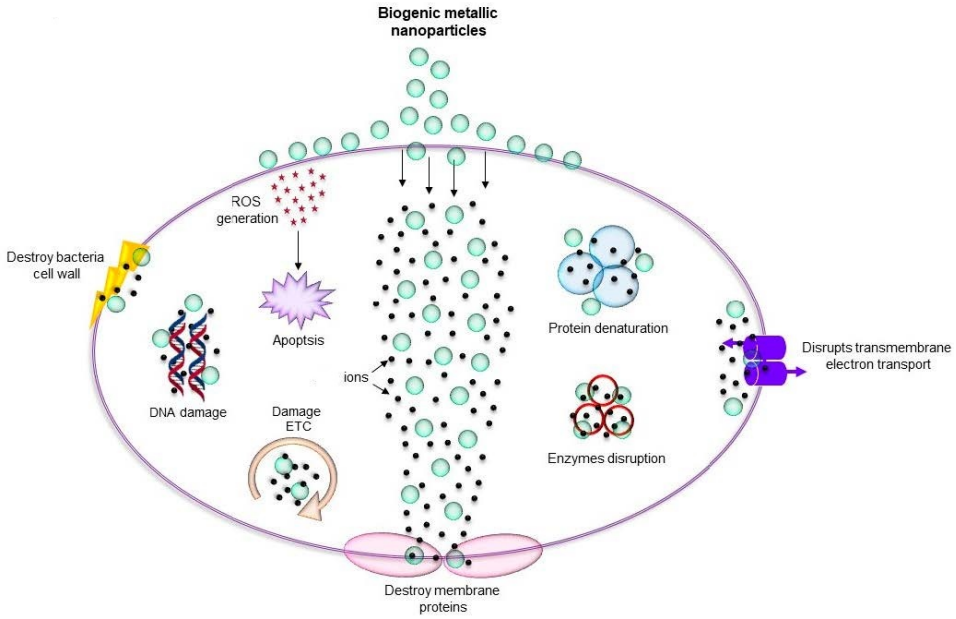

Figure 4.1: Mechanisms of antimicrobial effects of metallic nanoparticles.[20]

Production of ROS

Reactive oxygen species (ROS) are found in many cell signaling pathways, where they affect mostly cell proliferation or cell death mechanisms.[37,38] While a slight increase in ROS concentration can be stimulating to cell growth, a local increase in

ROS production in the cells surroundings leads to its toxicity and cell death.[38] ROS include superoxide anions, hydroxyl radicals and hydrogen peroxide. ZnO molecules have a wide band gap of 3.3 eV between their valence band (VB) and conduction band (CB). In addition to this, they also possess a large exciton-binding energy (60 meV), which allows them to generate many electron-hole pairs. Under illumination with photons of energies higher than the band gap (this corresponds to photons of wavelengths around 375 nm, eg. on the lower border of visible light) electrons are excited from the valence band creating in it a surplus of positively charged holes with a comparable build-up of electrons in the conduction band. In an aqueous environment, these particles then enter redox reactions, which lead to the lysis of water molecules and the generation of OH^- radicals on both the CB and VB as well as an HO_2^- radical and H_2O_2 on the CB. The reaction pathways describing the formation of these specific ROS can be seen in Figure 4.2. However, it has also been shown, that ZnO NPs are capable of forming ROS without illumination due to crystal lattice defects.

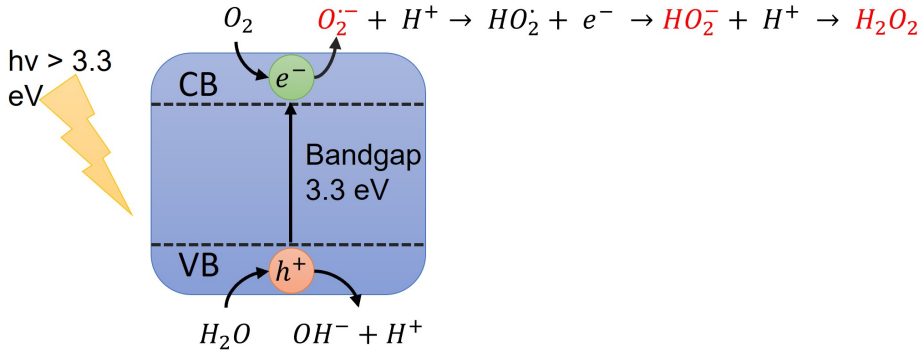

Figure 4.2: Formation of reactive oxygen species (ROS) by ZnO nanoparticles. Reactive oxygen species are highlighted using red text.

Negatively charged ROS radicals (superoxide ions and hydroxyl radicals) are unable to penetrate the negatively charged bacterial cell wall and act upon the microorganism externally, while hydrogen peroxide, an uncharged molecule, is able to penetrate the bacterial cell wall and cause oxidative stress, DNA damage, and ultimately leads to cell death.[25,32,39] In addition to this, charged radicals exhibit a shorter half-life as opposed to the neutrally charged H_2O_2 molecule.

Cellular Integrity Disruption

ZnO NPs also interact directly with cell membranes. Particles of sizes > 10 nm accumulate on the outer membrane, neutralizing the negative charge and disturbing membrane polarity, which leads to cell death through multiple mechanisms. Nanoparticles of sizes smaller than 10 nm are able to pass through the cell envelopes and penetrate bacterial cells. This internalization of ZnO NPs leads to the damage of cellular organelles and again to cell death.[39] However, even the accumulation of zinc oxide on the outer membrane of bacteria has been shown to have a profound effect on the cytotoxicity of these nanoparticles – electrostatic interactions prolong contact between nanoparticles and cell walls and strengthen the bactericidal effect.[40] This

shows that cells with a greater surface charge are more susceptible to ZnO as an antimicrobial agent.

Zn^{2+} Ion Production

The final mechanism in which ZnO NPs have been shown to have an antimicrobial effect is the release of Zn^{2+} ions. Similar to ROS, Zn^{2+} ions are required for normal cell function. Around 5 % of all bacterial proteins are thought to incorporate zinc ions, many of them essential for cell survival. A high concentration of zinc ions surrounding the cell however, causes osmotic stress on the bacterium by oxidizing its surroundings. An increased intake of these ions may also inhibit certain enzymes and act as a competitor to other metallic ions.[41] The thicker the bacterial wall, the less susceptible the strain to this form of mechanical stress. This could explain the stronger effect zinc oxide nanoparticles have towards gram-negative bacteria, due to their thinner cell wall.[32,39]

4.2.2 Parameters Influencing ZnO NP Toxicity

The antimicrobial effect of ZnO NPs is influenced by a number of parameters including nanoparticle shape and size, the presence of dopants, nanoparticle concentration, illumination, exposure time, etc.

The main parameter found to have an effect on the efficiency of the antimicrobial capacity of ZnO nanoparticles was size. Smaller nanoparticles performed better overall as an antibiotic. This may be due to the fact, that smaller particles are able to penetrate through the cell wall into the cytoplasm. However, smaller particles also release proportionately more Zn^{2+} ions, therefore enhancing another of the pathways through which these nanoparticles kill bacterial cells[32,42] as well as fungi.[43] Interestingly, it has been shown, that differences as small as tenths of nanometers in nanoparticle sizes have significant effects on antimicrobial properties.[44] This property should, therefore, be investigated further to find optimal parameters for ZnO as an antimicrobial agent.

Another parameter determining the efficacy of ZnO as an antibiotic is nanoparticle morphology. ZnO nanoparticles occupy many distinct morphologies such as nanorods, platelets, nanospheres, hedgehog particles, etc.[32,39,45,46] Some examples of different ZnO NP structures can be seen in Figure 4.3. In effect, flower-shaped and spherical nanoparticles were more efficient in their antimicrobial effects than differently shaped particles. This, along with the fact, that porous particles generally had a more significant antibacterial effect suggests, that the advantage of these NP shapes is their greater surface to volume ratio, which allows for more ROS production from an identical particle concentration.[32] More studies have also shown the efficacy of hedgehog particles, whose needle-like protrusions help mechanically disrupt cell walls.[45]

The efficacy of antimicrobial NPs can also be affected by doping - the introduction of different ions into the crystal lattice. This modification can lead to the ability to obtain smaller nanoparticles, which can improve their antimicrobial effects, as mentioned earlier. In addition, these dopants can introduce defects into the lattice, enhancing the formation of ROS. Among dopants shown to enhance the antimicrobial

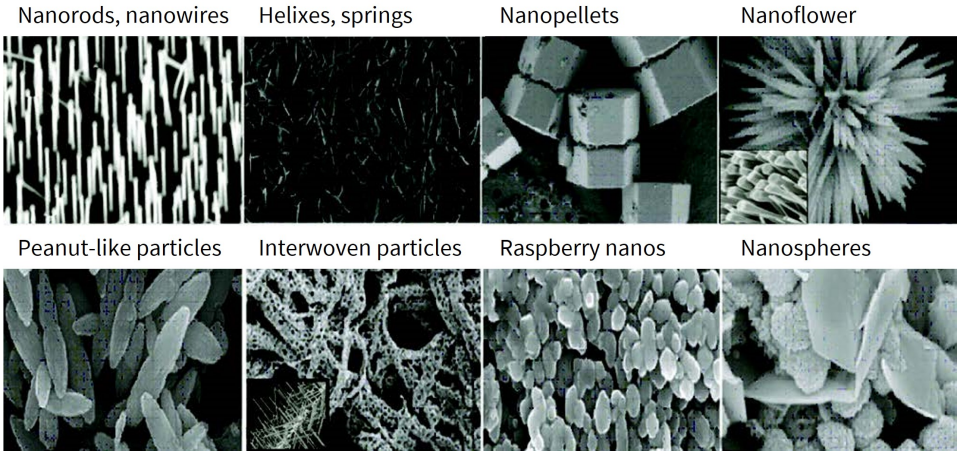

Figure 4.3: Possible morphologies of ZnO nanoparticles. Adapted from 46

effect of ZnO NPs are iron, copper, or manganese. Ion release is thought to play a major role in this enhancement. Other modification of the molecules are also possible - surface modifications to block aggregation or enhance contact with bacterial cells are also effective at improving the antimicrobial activity of ZnO NPs.[32]

It is also important to note that not every microorganism reacts to exposure to ZnO NPs identically. Zinc oxide nanoparticles have been shown to act differently against both Gram-positive and Gram-negative bacteria. Many studies have shown ZnO to be a better antimicrobial agent for Gram-positive bacteria, for which its minimum inhibitory concentration (MIC) is significantly lower than for Gram-negative bacteria.[25,32,39] This is thought to be a result of different cell membrane composition, as discussed previously in Section 2.2. However, there are also studies contradicting this finding, which may indicate another mechanism (such as the presence of catalase or cytochrome oxidase, which can combat ROS[32]) in play.[47]

4.3 Investigation of Inhibitory Concentrations of Antimicrobials

To find the threshold for the minimum inhibitory concentration (MIC) of antimicrobial substances, two methods are most often used - broth microdilution[48] or disk diffusion.[49] In broth microdilution, 96-well plates are typically used in which consecutive dilutions of an antimicrobial agent are added to a concentration of cells of about $5*10^5$ CFU/ml. The concentration at which no cell growth after 24 hours of incubation is observed is determined as the MIC.[48] Disk diffusion on the other hand takes place on agar plates. Cells are spread on plates and disks containing the desired antimicrobial are applied to the agar. Plates are then incubated overnight. The MIC is then determined based on the diameter of the inhibition zone, where no cells have grown from the point of application of the disk.[49] An example of these methods can be seen in Figure 4.4

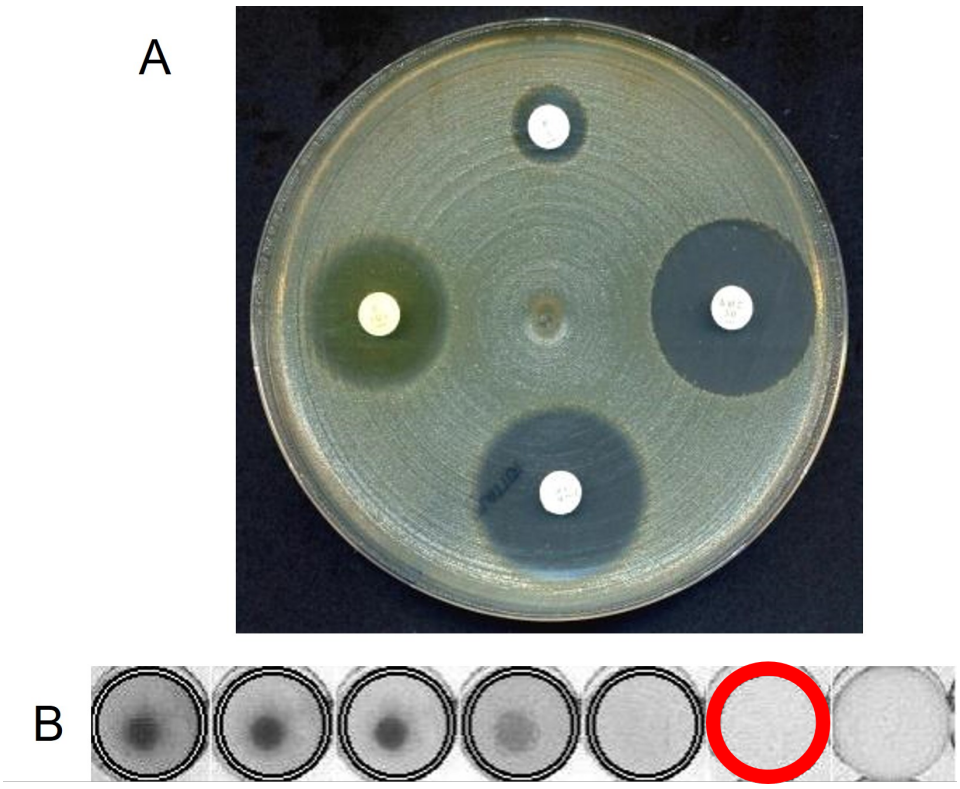

Figure 4.4: An example of methods investigating the minimum inhibitory concentration of antimicrobials. Adapted from 48, 49. A - disk dilution method. White dots show diffusion disks containing antibiotic substances. Distinct circles containing no cells can be seen around them. B - broth microdilution method. Here we can see 7 wells with a decreasing amount of bacterial biomass. The circled well contains the MIC of the antimicrobial, as the broth is completely clear.

Such contradictions in the literature on the antibacterial effects of ZnO nanoparticles highlights the need for further research. Here, I employed commercially available ZnO nanoparticles at concentrations close to minimum inhibitory concentration and model non-pathogenic *Escherichia coli*. I will attempt to investigate the long-term effects of zinc nanoparticles on these bacteria as well as the possibility of illuminating the NPs with light in order to compare the antibacterial effect with and without illumination.

Part II

Materials and Methods

This section will give an overview of the materials and methods used in this thesis. For an overview of the exact chemicals and machines used, please, refer to Appendices A and B. Results of these experiments can be seen in the Results section. It is important to note, that all work was done in a sterile environment (flowbox), in protective equipment (gloves and a lab coat), and using materials sterilized by autoclaving, dry heat sterilization, or UV sterilization.

Chapter 5
Materials

5.1 Bacteria

For this experiment the *Escherichia coli* (Migula 1895) Castellani and Chalmers 1919[50] strain of the bacteria supplied by the Czech Collection of Microorganisms (CCM 3954) was used. This strain is an international standard reference strain for antibacterial disc susceptibility testing, making it ideal for this experiment. Furthermore, its genome is fully sequenced, which can be an advantage when looking for changes in the genome linked to antimicrobial resistance. Although *E. coli* is pathogenic to both humans and animals (and therefore falls under risk group 2 according to TRBA 466), it has also been granted the "TA" identifying flag, which denotes strains, "which have been handled safely over many years in technical applications. These proven strains can therefore be assigned to the risk group 1 according to the classification criteria."[51] This makes working with them much simpler, as simpler safety measures are implemented.

5.2 Nanoparticles

For the experiment, zinc oxide nanoparticles with a primary particle size of 50 nm were used. In addition, the nanoparticles contained 6 % of an aluminium dopant. To ensure minimum agglomeration of the nanoparticles, a new stock solution with a concentration of 2 mg/ml or 1 mg/ml was prepared every week using the following approach:

1. 10 mg of ZnO NPs was weighed using an analytical balance.
2. To this, 10 ml (for the 1 mg/ml stock solution) or 5 ml (for the 2 mg/ml stock solution) HPLC grade water was added.
3. The mixture was stored in the refrigerator and sonicated for 30 minutes in a water bath prior to each use.

5.3 Media

For the cultivation of the bacteria, three distinct growth media were used. For antibiotic susceptibility testing for the given strain, Mueller-Hinton (MH) agar is recommended.[50] This was therefore used for colony forming units (CFU) measurements (for more information on these, see section 6.2), where a semi-solid medium was needed. For bioreactor experiments (see section 6.4), which called for a liquid medium, Mueller-Hinton (MH) broth was used. For dilution and plating cells a 0.9 % saline solution was mixed. This ensures an isotonic environment for the cells and imposes no osmotic pressure on the cells. The recipes for preparing growth media are given below.

5.3.1 Mueller-Hinton Broth

Mueller-Hinton broth includes beef extract and a Casein hydrolysate as a source of nutrients for bacteria and starch as an absorbant of toxic metabolites. The broth was prepared as per the instructions given by the manufacturer. 21 grams of the MH broth mixture were added to 1 l of distilled water (other volumes with the same ratio were used as well) and dissolved completely. The mixture was then autoclaved at 121 °C for 15 minutes. After cooling, the broth was stored in the refrigerator and brought to room temperature before use.

5.3.2 Mueller-Hinton Agar

Mueller-Hinton agar has a composition similar to that of MH broth with the addition of agar - the solidifying agent. The agar was, again, prepared per the manufacturer's instructions. 38 grams of the MH agar mixture were added to 1 l of distilled water (other volumes with the same ratio were used as well) and dissolved completely. The mixture was then autoclaved at 121 °C for 15 minutes. After cooling slightly, the agar was poured onto sterile Petri dishes and left to solidify. The dishes were then stored in the refrigerator and sterilized with UV light for 40 minutes before use.[52]

5.3.3 Saline

For the 0.9 % saline mixture, 4.5 g of sodium chloride (NaCl) were completely dissolved in 500 ml of distilled water. This mixture was then autoclaved at 121 °C for 15 minutes. After cooling, it was stored at room temperature until use.

Chapter 6

Methods

Numerous methods were used for the completion of this thesis. The methodology is divided into three main parts - preliminary experiments, which were aimed at gaining a deeper understanding of the parameters of the experiment, re-exposure experiments, which outline the experiment itself, and statistical methods used to process the measured data. All data and statistical analyses were done using MATLAB software version R2021b Update 1.[53]

6.1 Dilution Series

As dilution series were often utilized in this thesis, this section will provide a short explanation of how these dilution series were done. The two dilution series carried out in this thesis were two-fold dilution series and ten-fold dilution series. While a ten-fold dilution series is more useful for a broader idea of the issue at hand - for example finding the magnitude of a concentration of cells in a cell culture - a two-fold dilution series is better when the magnitude is roughly known and we need a more precise number - for example when finding the minimum inhibitory concentration for an antimicrobial. An example of such a dilution series on agar plates can be seen in Figure 6.1.

1. Eppendorf tubes were prepared in an amount corresponding to the number of dilution steps to be carried out. Eppendorf tubes were first filled with the diluting agent. For a two-fold dilution, half of the final volume was pipetted into each eppendorf tube, for a ten-fold dilution, 90 % of the final volume was pipetted into each eppendorf tube.

2. The diluted substance was then added to the first eppendorf tube. The amount varies, again, based on the dilution series. For a two-fold dilution series, half the desired volume was pipetted, for a ten-fold dilution series, 10 % of the final volume was pipetted.

3. The solution was mixed well either by vortexing or pipetting.

4. A part of the solution was removed from the tube and added into the following one for further dilution (again, 10 % of the volume was removed for a ten-fold dilution, 50 % for a two-fold dilution).

5. Steps 3 and 4 were repeated until we obtain the desired number of dilution steps. This will give us a series where each sample has half the concentration of the previous one (for a two-fold dilution series) or a tenth of the concentration of the previous member (for a ten-fold dilution series, here we get a difference in magnitude between the members).

6.2 CFU measurements

Another common method used in many experiments was the measurement of colony forming unit (CFU) concentration. An experimental procedure and example of data analysis is given in this section.

Experimental Procedure

1. Samples taken at t_0 and t_{24} were diluted using a ten-fold dilution series. Initial cultures were diluted up to 10^{-4}, while final cultures were typically diluted to 10^{-9} for final OD higher than 0.6 and to 10^{-4} for cultures with a lower OD.
2. 500 μl of each of the final three dilutions were pipetted onto fresh MH agar in duplicate (for a total of two plates of 500 μl for each dilution) and spread using a cell spreader.
3. The plates were left in the flow-box to air-dry and then placed in an incubator at 37 °C overnight.
4. After incubation, images were acquired and colonies counted using the SphereFlash automatic colony counter. The settings and sample results can be seen in the section below.
5. One t_{24} plate from each culture was stored in the fridge for further use.

Data Analysis

Below an example is given of the data obtained from CFU measurements and how it's processed. In Figure 6.1, a dilution series of reference cells after 24 hours of incubation can be seen. The dilution steps used were -7, -8, and -9, respectively. Images were obtained using an automatic colony counter. The big red circle on the plates denotes the area used to count colonies. The entire area of the plate wasn't used, as the rim and text would interfere with a clear reading. The blue circle then denotes the rim of the plate. This was used to compute a more accurate volume from which the computed colonies originate. For example: if 500 μl of cells are plated, but only 85 % of the area was counted, the volume in which the given number of colonies was found must be adjusted to get an accurate concentration. Detected colonies (based on the difference of color from background) are circled in red. Colonies evaluated as valid (based on size and other parameters) are marked with red crosses.

The results given by the SphereFlash Colony Counter software and used in this thesis are given in the table below. From the dilution factor, which can be read in the

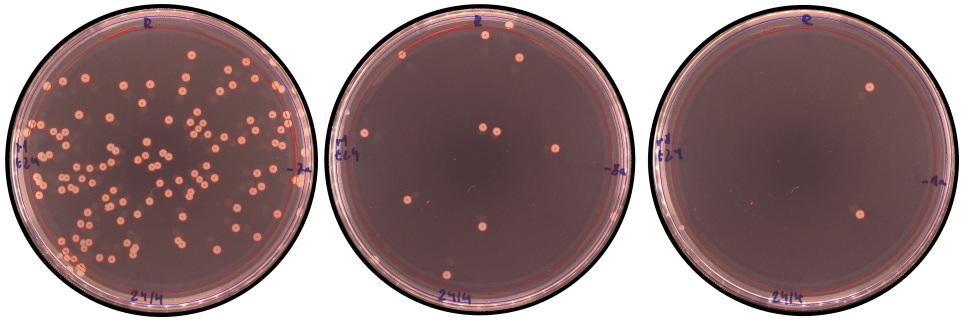

Figure 6.1: An example of images of a CFU dilution series obtained from the SphereFlash automatic colony counter.

Plate ID	Counted Colonies	Counted Volume	Inoculated Volume [ml]	Conc. [CFU/ml]
1e+07 R t24a	110	0.84	0.5	$2.6*10^9$
1e+08 R t24a	10	0.84	0.5	$2.4*10^9$
1e+09 R t24a	2	0.84	0.5	$4.7*10^9$

Table 6.1: An example of results given by the automatic colony counter and CFU concentrations computed from it.

plate ID, counted colonies, counted volume, and inoculated volume, the concentration of colony forming units was calculated using the following equation:

$$colony\_concentration = dilution\_factor \cdot \frac{counted\_colonies}{counted\_volume \cdot inoculated\_volume} \tag{6.1}$$

As can be seen from both Figure 6.1 and the Table 6.1 of counted colonies, there is a difference in the order of magnitude between the consecutive dilution steps. While the final concentrations vary slightly, the important difference is in the magnitude.

6.3 Preliminary Experiments

The diploma thesis was preceded by a semestral project, during which I spent a semester acquainting myself with laboratory work and the used method. In this preliminary project, a ZnO nanoparticle concentration of 10 μg/ml was used. Over seven re-exposure experiments no significant difference was observed. This was the main basis for the remeasuring of the minimum inhibitory concentration (MIC) of the available nanoparticles. In addition, the illumination of bioreactor tubes proved problematic, as no transparent lids are available from the manufacturer and the positioning of the light source in a perpendicular orientation proved difficult to stabilise as well. This led to the assembly of our own transparent caps as well as the design of a new bioreactor cap capable of directing the light source at the sample. Additionally, more measurements were done in order to understand the processes underway. An overview of these methods is given below.

6.3.1 3D-printed Caps

For a simpler and more consistent setup of illuminated samples, I decided to design custom caps using Tinkercad software and 3D print them. Figure 6.2 shows a cross-sectional image of the model. Figure 6.3 then shows the 3D-printe caps in use, placed on top of the bioreactors with a fibre optic cable connected to the light source. The cap was designed to sit on the bioreactors as the original cap with a 4 cm addition with a hole to lead the optic cable. The cap was designed as to have a 1 cm gap between the end of the optic cable and the cap of the falcon tube in the bioreactor.

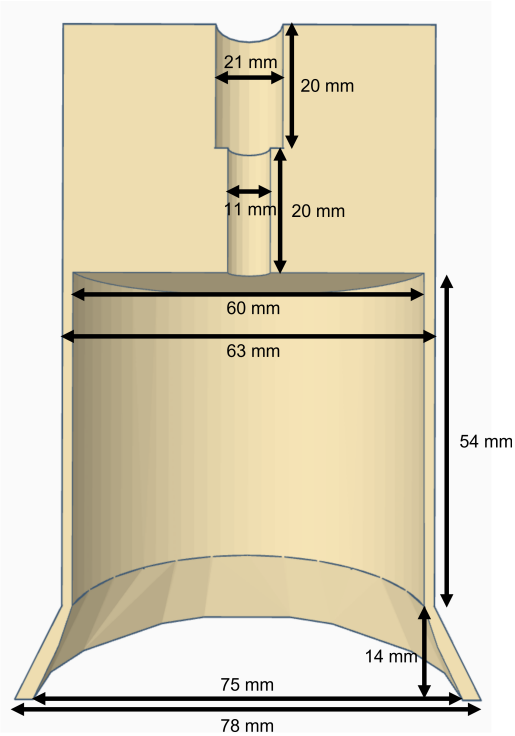

Figure 6.2: Cross section of the cap model used for illuminated samples.

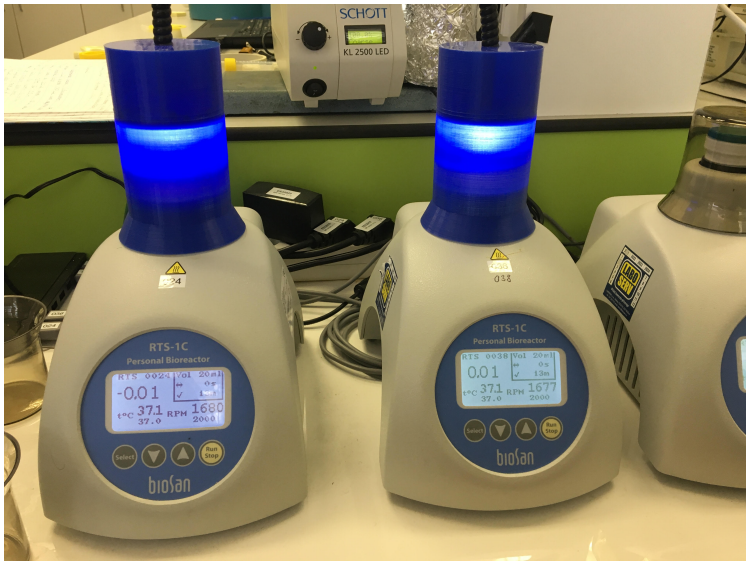

Figure 6.3: Image of the 3D-printed caps in use.

6.3.2 Bioreactor Testing

Prior to use, the bioreactors were tested for their accuracy, stability of OD measurements under illumination, with different solution volumes, and at different concentrations. The differences between the four bioreactors. Different measurements were done on all bioreactors with new and old falcon tubes, with two different concentrations of nanoparticles (50 and 200 μg/ml), with and without 100 % intensity illumination (with a 200 μg/ml concentration of nanoparticles), and with two different volumes (10 ml and 20 ml) of cells with a McFarland's density of 1.

6.3.3 Investigating the Effects of Light on *E. coli*

Although it has been shown that visible light has no profound effect on the growth of *E. coli* cells, a simple experiment was done to test this under our laboratory conditions. To find if there is any underlying effect of our intensity of light on bacteria, an experiment was done in bioreactors under 100 % intensity of illumination. The procedure is outlined below.

Experimental Procedure

1. From a stock agar plate of *E. coli* bacteria, colonies were removed using a sterile loop and resuspended in MH broth to a final McFarland density of 1.

2. This culture was then diluted using a three-step ten-fold dilution series into two falcon tubes for a final volume of 2x20 ml.

3. 100 μl of the bacterial culture was removed from each falcon tube for initial (time = 0 hours, t_0) CFU measurements.

4. The falcon tubes were placed in bioreactors and then cultivated at 37 °C and 2000 rpm with a change in spin direction every second. OD was measured every 15 minutes at 850 nm. Temperature was monitored periodically as well. The time of cultivation was 18 hours.

5. 100 μl of each culture was removed from each falcon tube for final (time = 24 hours, t_{24}) CFU measurements.

Data Analysis

The data was analyzed as outlined in Section 6.2. As there were only two samples, a Mann-Whitney U test was used. This is further explained in Section 6.5. The growth curve was blank-corrected to the initial optical density value of each sample and plotted over time.

6.3.4 Minimum Inhibitory Concentration Measurements

The minimum inhibitory concentration (MIC) of ZnO nanoparticles was conducted as outlined in chapter 4.3 using the broth microdilution method. A detailed approach is described below. For a schematic representation of the experiment setup, see Figure 6.4

Experimental Procedure

1. From a stock agar plate of *E. coli* bacteria, colonies were removed using a sterile loop and resuspended in MH broth to a final McFarland density of 1.

2. Using a four-step ten-fold dilution, the bacterial culture was diluted to a volume of 900 μl at the 10^{-3} step and 1 ml at the 10^{-4} step.

3. From a stock solution of ZnO nanoparticles (see above), a six-step, two-fold dilution series from 1024 to 32 μg/ml was made.

4. 100 μl of 10^{-3} cells were pipetted to the first three columns of a 96-well plate, while 10^{-4} cells were pipetted into the following three columns. The final row was left with no cells.

5. 100 μl of the zinc oxide dilution series from the highest concentration to the lowest were added to the plate by rows, leaving the final two rows with no zinc. This led to another two-fold dilution (of the each of the zinc solution dilution steps in the cell culture).

6. 200 μl of HPLC grade water were added to each of the six columns in the final row and 100 μl of water was added to the cells in the next-to-last row.

7. The plate was then taped over and incubated overnight at 37 °C.

8. After incubation, the plate was moved to a microplate reader, where absorbance was measured at 600 nm and 850 nm. A digital image was also procured.

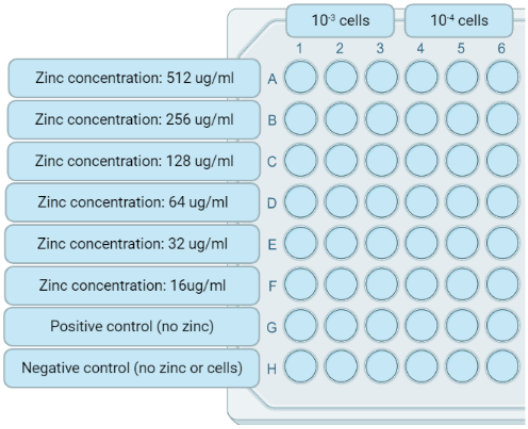

Figure 6.4: A schematic of the MIC experiment setup. This image was created using BioRender.com.

After the MIC was determined, three concentrations (200 μg/ml, 100 μg/ml, and 50 μg/ml were tested on bacterial cultures with illumination (100 % intensity) against a reference sample with no zinc and no illumination.

1. In four glass vials, colonies from a fresh agar plate containing *E. coli* cells were re-suspended in MH broth to a McFarland density of 1.

2. These cultures were then diluted using a three-step ten-fold dilution series into falcon tubes for a final volume of 18 ml.

3. To three of the cultures, the ZnO solution was added to a final concentration of 200 μg/ml, 100 μg/ml, and 50 μg/ml and final volume of 20 ml. To the final culture, 2 ml of HPLC grade water were added.

4. 1 ml of the bacterial culture was removed from each falcon tube for initial (time = 0 hours, t_0) CFU measurements.

5. The falcon tubes were placed in bioreactors and the samples containing zinc were illuminated.

6. The cells were then cultivated at 37 °C and 2000 rpm with a change in spin direction every second. OD was measured every 15 minutes at 850 nm. Temperature was monitored periodically as well. The time of cultivation was 25 hours.

7. 1 ml of each culture was removed from each falcon tube for final (time = 24 hours, t_{24}) CFU measurements.

Data Analysis

Results of the 96-well plate were analyzed using the naked eye according to the procedure outlined by the EUCAST reading guide for broth microdilution.[48] These results were then confirmed by analyzing the OD measurements of each

samples. A simple mean value on optical densities was taken and plotted against zinc concentration. The growth curves from bioreactor measurements were blank-corrected against the initial OD value of each sample and plotted over time.

6.3.5 Measuring H_2O_2 Concentrations

To find out the concentration of H_2O_2 produced from our chosen concentration of ZnO NPs, the reaction of hydrogen peroxide with titanium(IV) oxysulfate was exploited. The reaction of the colorless hydrogen peroxide with the colorless titanium oxysulfate lead to the formation of a yellow-colored peroxotitanium complex. This complex may then be detected using UV-Vis spectroscopy with a peak in absorbance at approximately 409 nm.[54] The approach used in this thesis may be seen below.

Experimental Procedure

1. From a stock solution of 2 mg/ml ZnO NPs, a three-step two-fold dilution series was done into falcon tubes to final volumes of each dilution step equal to 10 ml. The nanoparticles were diluted into HPLC grade water.
2. The solution was incubated overnight in bioreactors at 37 °C, with an illumination intensity of 100 %, rotated at 2000 rpm with a change in revolution direction every second and measurements taken every 15 minutes.
3. After 20 hours of incubation, 3 replicates (1 ml each) were removed into sterile Eppendorf tubes and centrifuged at 15,000 rpm for 30 minutes in order to remove the nanoparticles from the suspension.
4. During centrifugation, a dilution series of hydrogen peroxide was prepared as a reference. 1 ml of 30 % stock solution of H_2O_2 was added to 99 ml HPLC grade water to obtain a 1000 μM solution. In order to generate a standard curve, a six-step two-fold dilution series was done to obtain dilutions ranging from 1000 μM to 16.6 μM.
5. Each zinc and hydrogen peroxide solution was mixed in a 9:1 ratio with a 27 - 31 % titanium oxysulfate solution (9 parts of zinc or hydrogen peroxide, 1 part titanium oxysulfate).
6. 250 μl of each mixture were added to the microwell plate - hydrogen peroxide specimens in duplicate, nanoparticle specimens in triplicate. Additionally, HPLC grade water was added to two wells to complete the calibration curve. A triplicate of 250 μl of the centrifuged ZnO samples was also measured as a null sample.

Data Analysis

A calibration curve was first assembled using the measured hydrogen peroxide samples. The absorption spectra of the samples were blank corrected to the reference containing HPLC grade water and titanium oxysulfate. Values at 409 nm were then plotted onto a curve and a linear function was fitted onto these points to get a calibration curve. To find the concentration of H_2O_2 in the ZnO NP samples, the

supernantants from the zinc solutions containing titanium oxysulfate were blank-corrected to the water sample containing titanium oxysulfate. Values at 409 nm were then found and compared to the calibration curve calculated from the reference samples of known H_2O_2 concentrations.

6.3.6 ZnO NP Absorbance Measurement

To estimate the bandgap of our ZnO NPs, the absorbance profile was measured at different concentrations by UV-visible spectroscopy. The following procedure outlines how this was done.

Experimental Procedure

1. From a sonicated 1 mg/ml stock solution of ZnO NPs, 1,500 μl were removed into a sterile Eppendorf tube.

2. A three-step two-fold dilution series was made to obtain 500 μl of 1000 μg/ml, 500 μg/ml, 250 μg/ml, and 125 μg/ml. The original stock solution was then diluted ten-fold. This dilution underwent two more two-fold dilution steps, This led to three more concentrations - 100 μg/ml, 50 μg/ml, and 25 μg/ml. 400 μl of each solution were then pipetted in a descending concentration into one column of a 96-well UV-transparent plate (one concentration was put into each row). The final row was filled with HPLC grade water.

3. The plate was placed in a microplate reader. There it was shaken for 10 seconds. The absorbance of each well was then measured at wavelengths from 200 to 900 nm with a 2 nm step.

Data Analysis

The results were represented as a Tauc curve, where photon energy was plotted against the optical absorption strength. This was computed according to the following equation:

$$y = (\alpha \cdot h \cdot \nu)^2 \tag{6.2}$$

where α is equal to half the absorbance of the material at a given wavelength, h is Planck's constant and ν is the frequency of the photon at a given wavelength. The main absorption region of the curve was then fit with a linear function. The point of intersection between the x axis and the linear function is the value of the bandgap for the given material.[55]

6.4 Re-exposure Experiments

For the re-exposure experiment, cell growth was monitored using two methods - optical density measurements using bioreactors to observe the dynamics of cell growth and CFU measurements to ascertain the initial and final concentration of colony forming units (viable cells capable of forming colonies on agar). Initial concentrations

are important to measure, as the difference in initial culture may lead to a differences in the growth curves, e.g. lag phase lengths.

6.4.1 Week 1

Experimental Procedure

1. Bacterial stock was removed from the freezer and allowed to thaw at room temperature.
2. An eight-step ten-fold dilution series of bacteria into 0.9 % NaCl was done, 500 μl of the final three dilutions were plated of MH agar plates, which were incubated overnight at 37 °C.
3. One colony was then removed using a sterile loop and added to 100 ml of MH broth and cultivated overnight at 37 °C in an orbital shaker at 150 rpm.
4. From this culture, a sample was diluted into fresh MH broth to a final McFarland density of 1. This culture was subsequently diluted using a three-step ten-fold dilution to a final volume of 72 ml. This was then equally divided into 4 sterile falcon tubes (with 18 ml in each tube).
5. 2 ml of the stock solution of ZnO NPs were added to two of the falcon tubes to obtain a final zinc concentration of 100 μg/ml. 2 ml of sterile HPLC grade water were added to the remaining two tubes.
6. 1 ml of the bacterial culture was removed from each falcon tube for initial (t_0) CFU measurements.
7. The tubes were placed into the bioreactors with one zinc sample and one reference sample put under illumination (using the light set at 100 % intensity). This led to four distinct samples - a reference with no added zinc and without illumination, a culture with zinc but no illumination, a culture with illumination but no zinc, and a final culture, which was both illuminated and contained zinc.
8. The cells were then cultivated at 37 °C and 2000 rpm with a change in spin direction every second. OD was measured every 15 minutes at 850 nm. Temperature was monitored periodically as well. The time of cultivation varied from 20 to 24 hours.
9. 1 ml of each culture was removed from each falcon tube for final (t_{24}) CFU measurements.

Data Analysis

Data from the optical density measurements were blank-corrected to the initial optical density value for each sample. The data were filtered using a mean average filter with a window width of 5 samples and lengths of lag phases were then detected by thresholding at OD of 0.1.

6.4.2 Subsequent Weeks

For subsequent weeks cells used for the experiment were no longer taken from bacterial stock, but rather from t_{24} agar plates. A detailed approach can be seen below. Data analysis was done identically to week 1.

Experimental Procedure

1. Plates containing t_{24} colonies were removed from the fridge.
2. Colonies were resuspended into 4.5 ml of fresh MH broth to a McFarland density of 1. Each culture was diluted and worked with separately.
3. Each of the four cultures was diluted using a three-step ten-fold dilution into a final volume of 18 ml of MH broth in falcon tubes.
4. 2 ml of the stock solution of ZnO NPs were added to the falcon tubes containing cells previously exposed to zinc. 2 ml of HPLC grade water were added to the remaining two tubes.
5. Thereafter, the procedure followed as in Week 1 from step 6.

6.5 Statistical Analysis

Three main statistical tests were used in this thesis. As there were only a couple measurements and the data did not have a normal distribution, non-parametric tests were used. For the comparison of preliminary illumination testing, a Wilcoxon Rank-Sum test was used, as there were only two groups for comparison. For the t_0 CFU results, the Kruskal-Wallis test was used to determine, if a significantly different concentration arose withing the initial cell samples as these could have affected the length of the lag phase. For the comparison of t_{24} CFU results, a non-parametric version of a two-factor ANOVA, called the Scheirer-Ray-Hare test was used. This statistical method uses two factors which divide results into groups (in this case, the factors are light and zinc) and tests three main hypotheses - whether either factor has an effect on the final variable, or the interaction of the two factors has an effect on the final variable. Hypotheses for all tests are given below. All tests were performed using a 0.05 level of significance (α).

- Wilcoxon Rank-Sum Test
  - H_0: The mean ranks for both groups are the same.
  - H_A: The mean ranks of the two groups are significantly different from each other.
- Kruskal-Wallis Test
  - H_0: The mean ranks for all groups are the same.
  - H_A: The mean rank of at least one group is significantly different from the others.

- Scheirer-Ray-Hare Test
  - H_{0a}: The mean ranks for all light groups are the same.
  - H_{Aa}: The mean rank of at least one light group is significantly different from the others.
  - H_{0b}: The mean ranks for all zinc groups are the same.
  - H_{Ab}: The mean rank of at least one zinc group is significantly different from the others.
  - H_{0c}: There is no interaction between light and zinc.
  - H_{Ac}: There is interaction between light and zinc.

Part III

Result and Discussion

Chapter 7

Results

In this chapter, the results of the experiment will be given. A similar structure to the Materials and Methods chapter will be kept for simplicity.

7.1 Preliminary Experiments

7.1.1 Bioreactor Testing

The following experiments attempted to check the performance of the bioreactors prior to their use in the re-exposure experiments. The optical density values of different liquid types measured using the bioreactors can be seen in Tables 7.1 and 7.2. The manufacturer states the accuracy of the bioreactor as +0.1 absorbance units. In table 7.1, we can see, that there are no differences between bioreactors for samples of low optical densities and all values are within the stated accuracy. There are also no significant differences between new and used tubes, or illuminated and un-illuminated samples. However, at higher optical densities, there were significant differences between individual bioreactors. This was considered when interpreting the data from later experiments. Table 7.2 shows a difference when measuring different volumes of the same concentration of cells. This issue was easily avoided in the subsequent re-exposure experiments by keeping a stable volume over all the experiments.

Solutions:	10 ml dH_2O		50 μg/ml ZnO NPs	200 μg/ml ZnO NPs	
Bioreactor	new tube	used tube	un-illuminated	un-illuminated	illuminated
RTS024	0.09	0.07	0.02	2.18	2.19
RTS038	0.08	0.08	0.07	2.34	2.33
RTS044	0.10	0.09	0.09	2.38	2.45
RTS054	0.09	0.09	0.07	2.54	2.54

Table 7.1: Results from bioreactor calibration.

Solution:	MF1 *E. coli* suspension	
Bioreactor	10 ml	20 ml
RTS024	0.23	0.11
RTS038	0.21	0.16
RTS044	0.24	0.18
RTS054	0.24	0.18

Table 7.2: Results from bioreactor calibration.

7.1.2 Effects of Light on *E. coli*

In order to determine the effects of the intensity of light on *E. coli*, initial (t_0) CFU concentrations were measured, as well as final (t_{24}) CFU concentrations. Optical density measurements were taken during the cells' growth cycle. Boxplots showing CFU results can be seen in Figures 7.1 and 7.3 and CFU concentrations were compared using a Wilcoxon Rank Sum test. In Figure 7.2, growth curves can be seen for *E. coli* grown in the dark and illuminated with 100 % light intensity. Tables showing results from the automatic colony counter from this and all following experiments can be viewed in Appendix C.

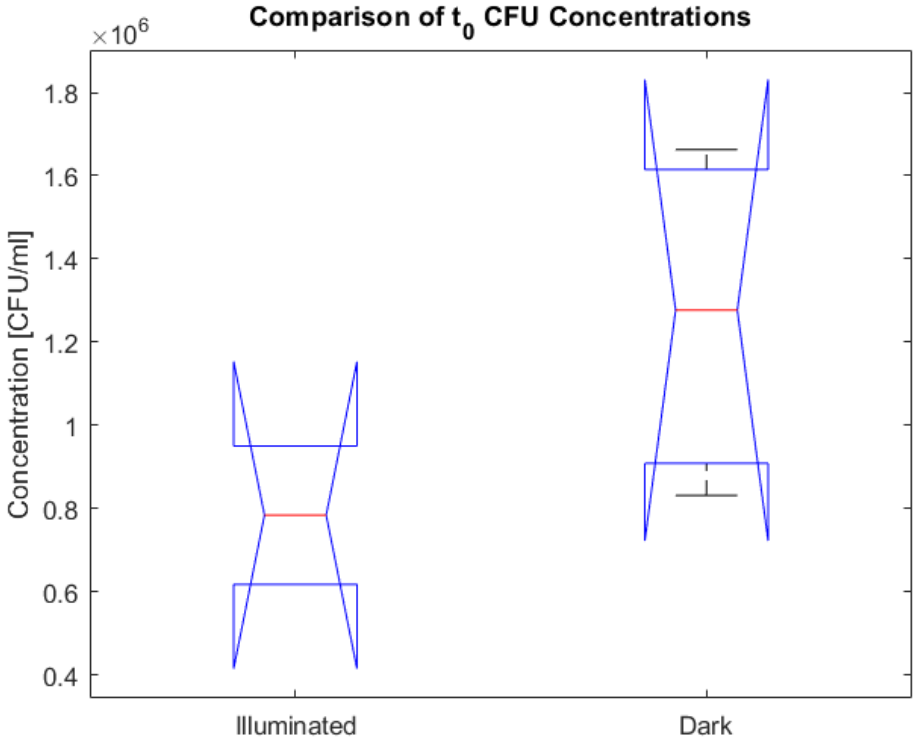

Figure 7.1: Boxplot showing the initial CFU concentration measurements from cells that will be exposed to light during growth (illuminated) and cells grown without illumination (dark).

For the initial CFU values, the Wilcoxon Rank Sum test indicated no statistically

significant difference between the illuminated sample and the reference at a 5 % significance level (W = 4, p = .27). This can also be seen in the boxplots, which show only a slight difference in the group means. What is more, both groups have a cell concentration in an order of 10^{+6}, they do not differ in an order of magnitude. We can therefore assess the growth curves assuming that both samples have similar initial conditions.

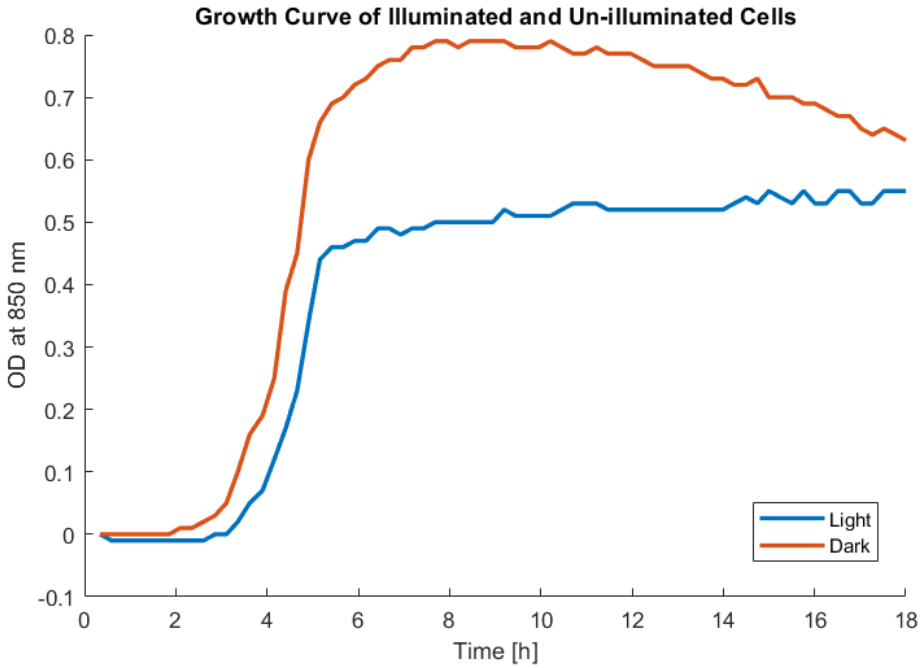

Figure 7.2: Growth curves of *E. coli* cells grown under illumination (light) and cells grown without illumination (dark).

From the growth curves, we can see a slight difference in the final optical density values (dark = 0.5, light = 0.6). Also, there is only a minimal difference between the lengths of the lag phases and from the bioreactor calibration experiments, we have seen a decreasing accuracy of optical density measurements at higher optical densities (Table 7.1). Cells without illumination had a more pronounced logarithmic growth phase compared to cells with illumination, however, the final optical density values were within the manufacturers stated accuracy of +0.1. Therefore, the main difference will be shown by endpoint CFU measurements, which could give us a better idea of the effects illumination has on cell viability.

For the endpoint CFU measurements, the Wilcoxon Rank Sum test indicated no statistically significant difference between the illuminated sample and the reference at a 5 % significance level (W = 4, p = .67). This can, again, be seen in the boxplot as well (Figure 7.3). From the results of this experiment, we can deduce there is no underlying effect of our illumination conditions on bacteria cell viability. Therefore, illumination is not a factor we need to consider as a confounding variable when assessing data in the experiment itself.

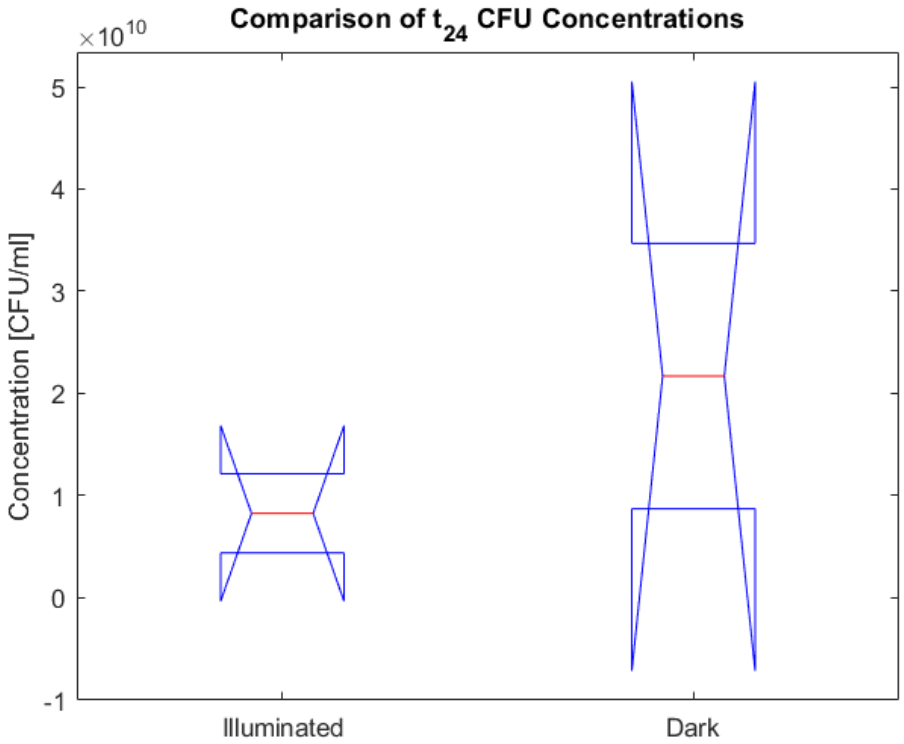

Figure 7.3: Boxplot showing the endpoint CFU concentration measurements from cells that were exposed to light during growth (illuminated) and cells grown without illumination (dark).

7.1.3 Minimum Inhibitory Concentration (MIC)

Micro-well Experiment

For the MIC experiment, wells from a 96-well plate with different concentrations of ZnO NPs were inspected and the presence or absence of bacterial growth was determined visually.

In Figure 7.4, the image of the plate can be seen along with the setup and colonies at the base of the wells reduced in size with an increasing concentration of ZnO NPs. The last distinct cell colony can be seen in wells with a 128 μg/ml concentration of ZnO. Therefore, the MIC for ZnO nanoparticles was found to be somewhere between 128 and 256 μg/ml (Figure 7.4 (b) - rows B and C). Due to its distinctly different color to that of bacterial growth, the spot observed in wells from row A was evaluated to be nanoparticle deposition at high concentrations ($>$ 256 μg/ml). Both the positive control in row G, where there were only cells without ZnO and the negative control in well H, which contained only water, showed no errors in the protocol. As all six replicates showed that bacterial growth was inhibited at the same concentration of ZnO NPs, we can say that the MIC of 128-256 μg/ml is reproducible and accept the results to be accurate. In Figure 7.5, the optical density of the wells was measured after incubation and revealed an inverse dependency with the concentration of ZnO

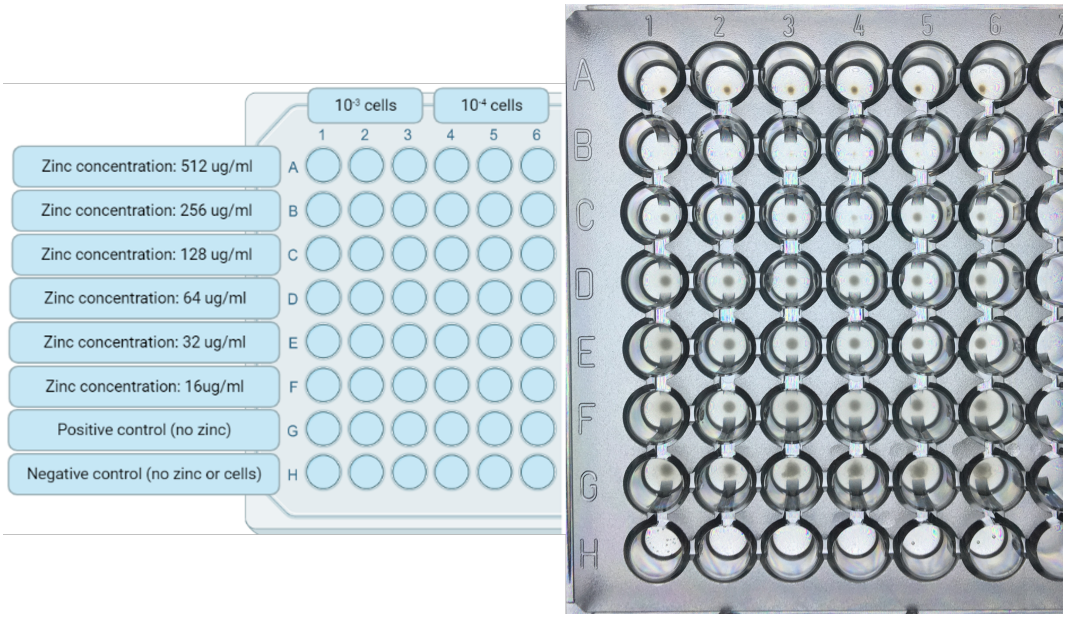

Figure 7.4: A - schematic of the MIC micro-well plate setup (created using BioRender.com). B- a digital image of the MIC micro-well plate after growth

nanoparticles can be seen. The data points denote the mean value of optical density of the six replicates. Error-bars showing standard deviation are also included.

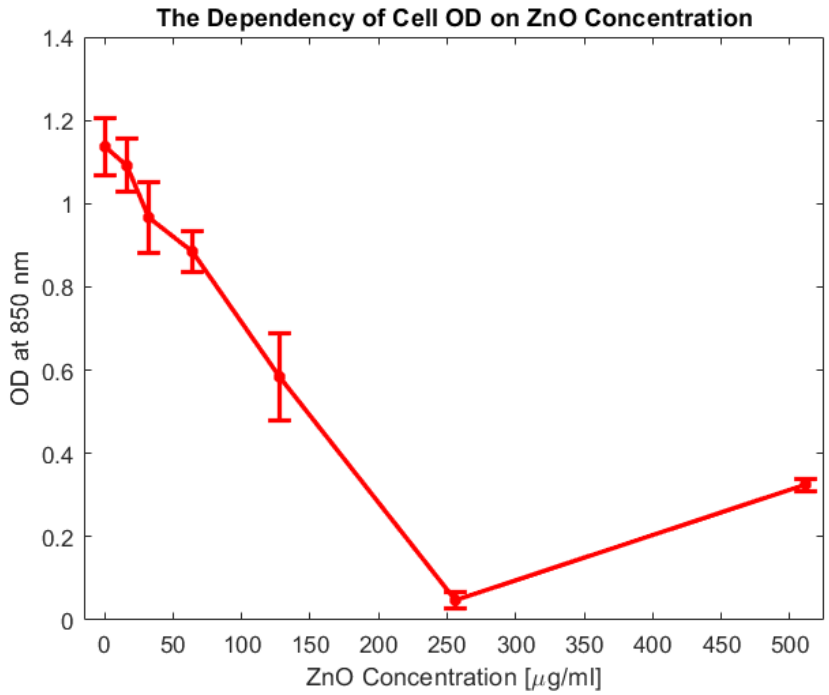

Figure 7.5: Results of mean 96-well plate MIC measurements and error bars, which denote standard deviation of the mean (n=6).

The optical density of the wells decreased with the increasing concentration of ZnO NPs. This corroborates the results as assessed with the naked eye from the 96-well plate. The only increase was seen at the highest concentration, thought to be due to a deposition of ZnO NPs on the base of the well.

Bioreactor Experiment

Based on the results of the previous MIC experiment, three concentrations of ZnO (200 μg/ml, 100 μg/ml, and 50 μg/ml) were chosen for a further exploration of their antibacterial properties using bioreactors without illumination. The results of this experiment can be seen in Figure 7.6.

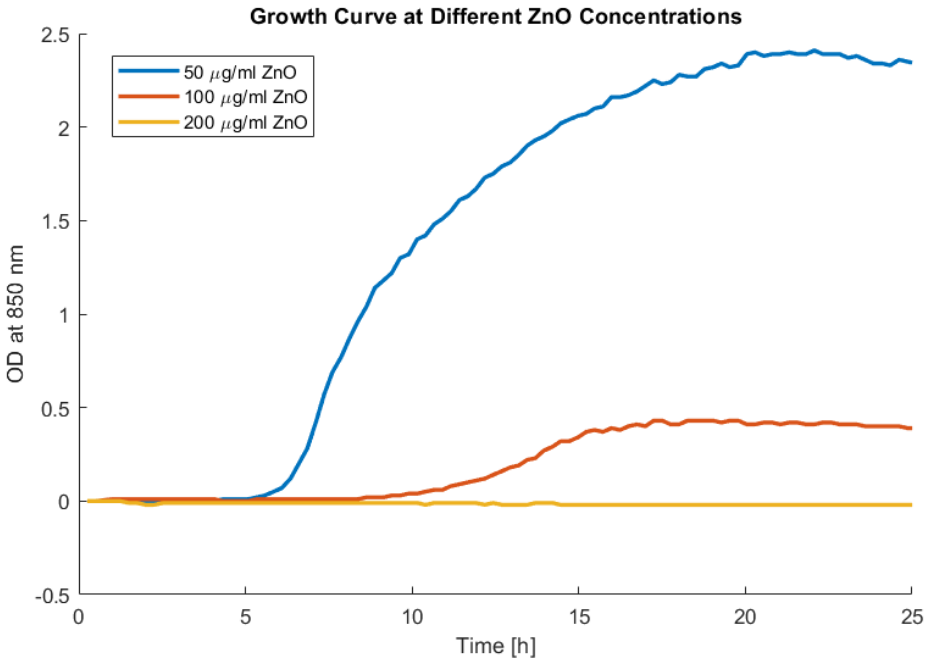

Figure 7.6: Optical density measurements of bacteria exposed to three different ZnO concentrations.

We can see that with a 50 μg/ml concentration of ZnO NPs, cells grow to an optical density greater than 2 and a lag phase of around 5 hours. This corresponds to reference values and we can therefore deduce, that this concentration has very little effect on our cells. On the other hand, a 200 μg/ml concentration of ZnO NPs leads to no growth at all. This showed, that 200 μg/ml is above the minimum inhibitory concentration and prevents growth of bacteria present in the solution. 100 μg/ml of ZnO nanoparticles led to some cell growth, though the final OD was significantly lower than that of the 50 μg/ml sample and the lag phase was also longer. A 100 μg/ml concentration seems to stress the cells (reduce their growth and lengthen their lag phase), while not killing them (some growth is still present). Therefore, this concentration of nanoparticles was chosen for the final re-exposure experiments.

7.1.4 Measuring H_2O_2 Concentrations from Illuminated ZnO NPs

Since ZnO is known to be photosensitive, I attempted to measure hydrogen peroxide that could be formed due to the illumination of deionized water containing ZnO NPs. Figure 7.7 the blank-corrected absorbance spectra of the reaction product, perititanic acid, for a range of hydrogen peroxide concentrations. A calibration curve of the maximum absorbance value as a function of hydrogen peroxide concentration was then created which can be seen in Figure 7.8.

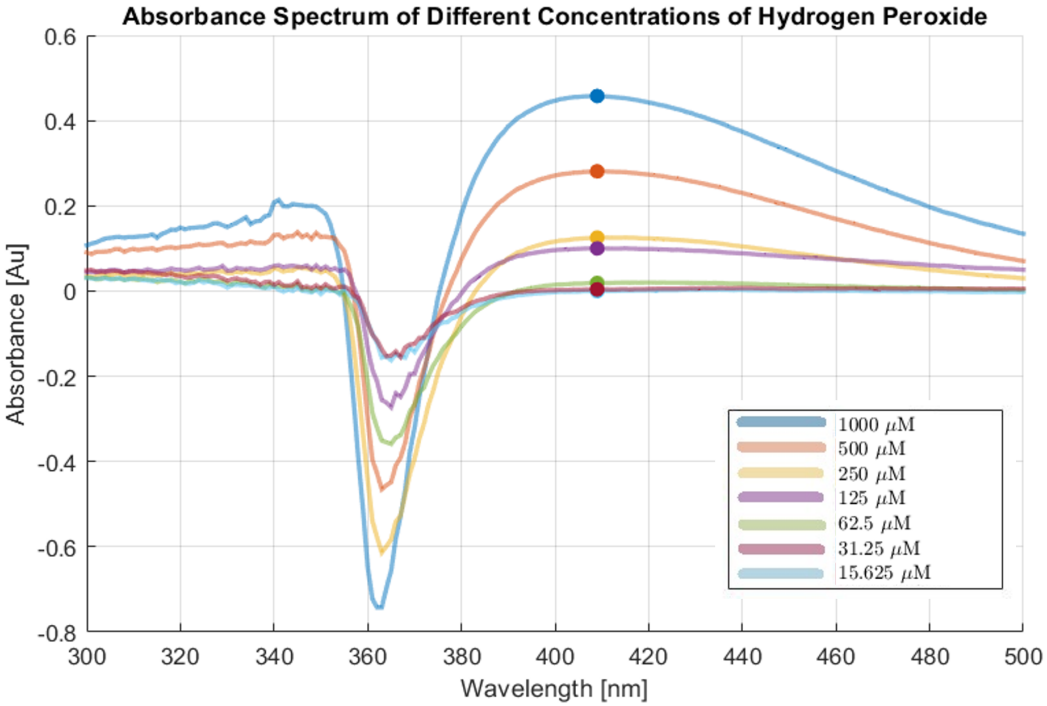

Figure 7.7: Absorbance spectra of perititanic acid for different H_2O_2 concentrations. Dots denote the absorbance maxima at 409 nm. In the image below, these absorbance values were plotted against the concentration of hydrogen peroxide in the sample for a calibration curve.

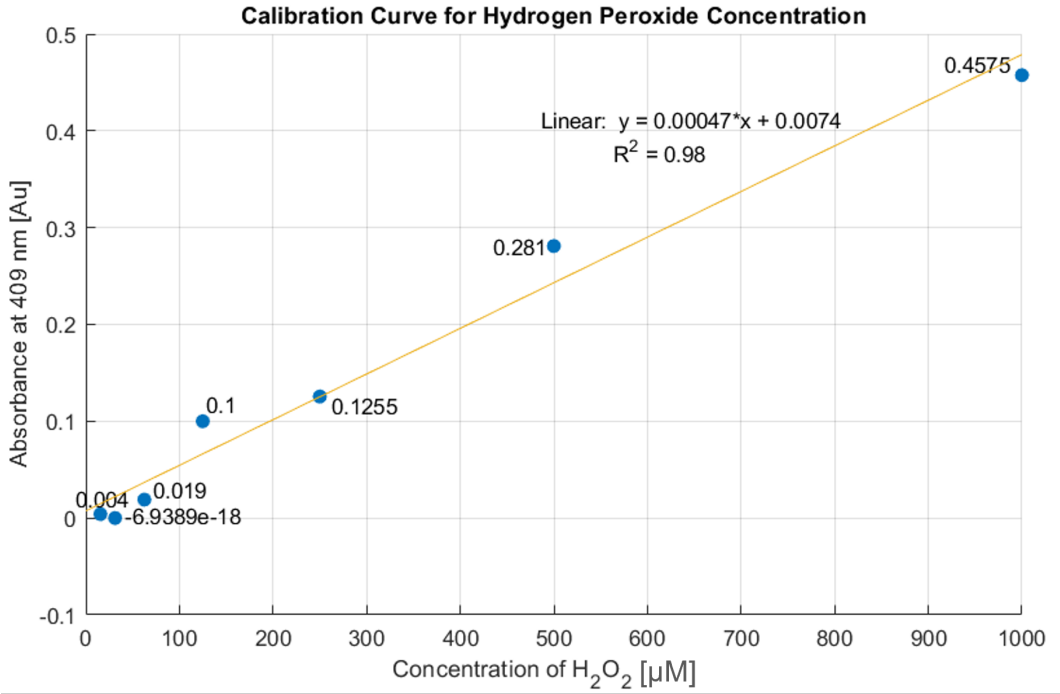

Figure 7.8: A calibration curve for hydrogen peroxide concentration detection using titanium oxysulfate. The blue points show the absorbance maxima for different concentrations of hydrogen peroxide, while the yellow line shows their linear dependency.

From the calibration curve (Figure 7.7), we can see that the dependency of absorbance at 409 nm is linear to the concentration of hydrogen peroxide in the sample. The equation of the linear dependency can be seen in the graph above along with its R^2 value ($R^2 = 0.98$), which shows a good linear relationship between the two variables. From the graphs, we can see that the limit of detection is around 16 μM of hydrogen peroxide.

For actual samples of illuminated, the spectra were blank-corrected and the value at 409 nm was read. The results can be seen in Table 7.3. For all the samples, however, the measurements were negative or close to zero. It is unlikely, therefore, that I would be able to detect hydrogen peroxide levels in the samples. This does not mean, that hydrogen peroxide or other reactive oxygen species are not being produced, but more sensitive tests would be needed to detect them.

ZnO concentration [μg/ml]	**Absorbance at 409 nm**
0	0.0500
250	-0.0050
500	0.0007
1000	-0.0098

Table 7.3: Blank-corrected absorbance values from the supernatant illuminated ZnO samples at 409 nm.

7.1.5 ZnO NP Absorbance Measurement

In order to confirm ZnO NPs can absorb visible light from the illumination source used, I first measured their UV-Vis absorbance spectra, which can be seen in Figure 7.9. In Figure 7.10, we can then see the emission spectrum of our laboratory light source. From these two images, we can see that although the light source does not emit photons of an energy where the absorbance of ZnO nanoparticles is at its maximum, there is some overlap between the spectra, especially between 400 and 450 nm. The light source could, therefore, be useful in investigating acrshortROS formation by ZnO NPs illumination with a non-bactericidal light source. More efficient ROS production could be gained by using light emitting photons in the UV spectrum, however, the light in itself would then have bactericidal effects, which could mask the effects of the nanoparticels themselves.

Absorbance of the 250 μg/ml sample was then chosen a plotted as a Tauc curve along with a linear function fit to the linear portion of the curve (Figure 7.11). From the function, the energy gap of our ZnO nanoparticles can be determined from this function as the x-axis intercept - in this case, it is 3.11 eV. This value is slightly lower than the ones found in literature (3.28 eV[39]), however, the used nanoparticles contain 6 % of an aluminium dopant, which could change the gap energy. In addition, the Tauc curve has a heavy Urbach tail (the slope of the curve at lower energies is very gradual), which could affect the results.

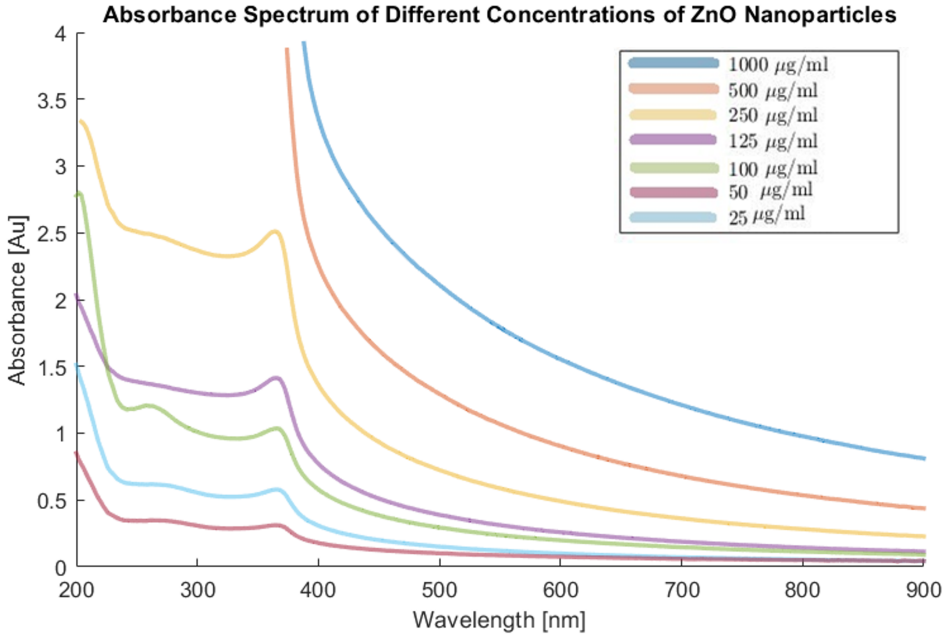

Figure 7.9: Absorbance spectra of different concentrations of ZnO NPs.

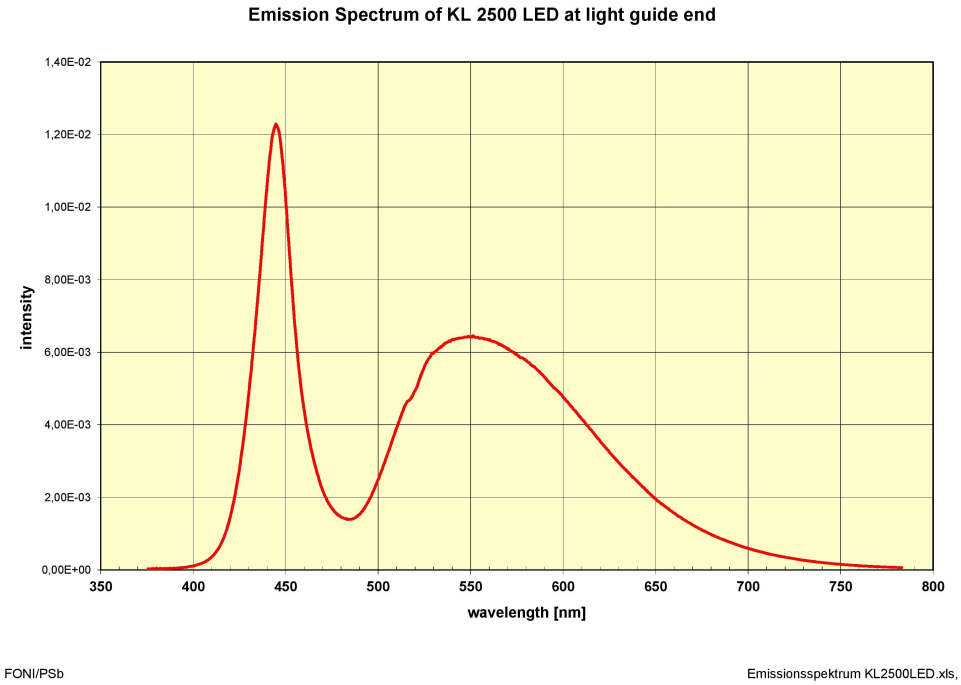

Figure 7.10: Emission spectrum of the Schott KL 2500 LED light source.[56]

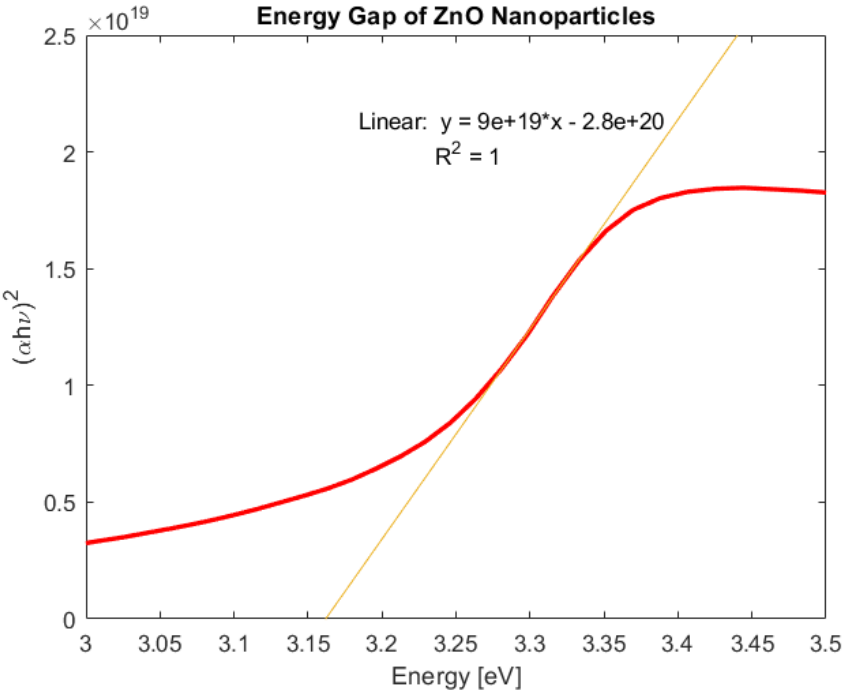

Figure 7.11: Tauc curve of 250 μg/ml ZnO nanoparticles with a fitted linear function.

7.2 Re-exposure Experiments

These experiments combined the results from the preliminary experiments and re-exposed bacteria to non-lethal concentrations of ZnO to try and detect evidence of resistance development towards ZnO exposure. Two separate re-exposure experiments (Experiment 1 and Experiment 2) were carried out, each with three re-exposure steps. The results from each experiment are further divided into re-exposures for clarity (i.e. re-exposure 1, 2, and 3). Each re-exposure section includes boxplots of initial (t_0) and endpoint (t_{24}) cell concentrations (these are shown with the y axis logarithmically scaled as we are looking for differences in an order of magnitude), a growth curve showing the change in optical density over time, and statistical analyses of these measurements. For results obtained from the automatic colony counter, please refer to tables in Appendix C. At the end of the section a graph of the progression of lag phases can be seen, as well as a graph of maximum growth rates. I will end this section with a discussion concerning the results of the experiment as a whole.

7.2.1 Experiment 1

Re-exposure 1

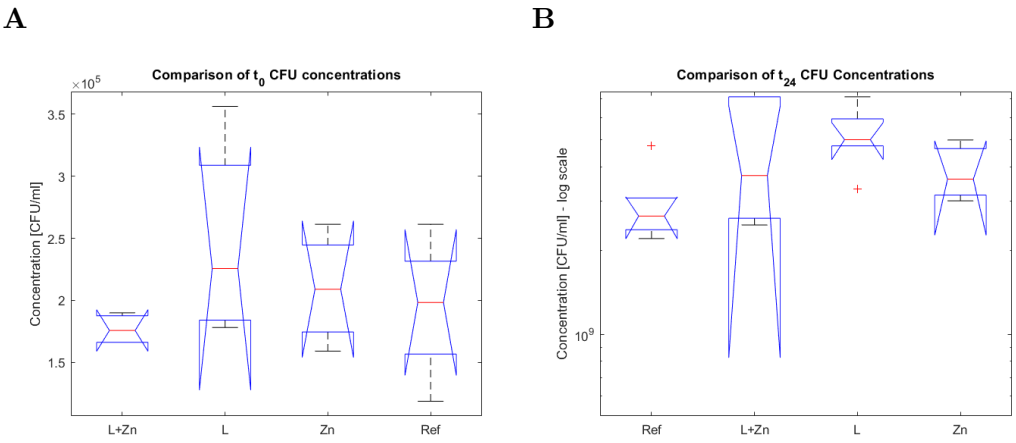

Figure 7.12: Experiment 1, re-exposure 1 CFU results. A - boxplot of initial CFU concentrations; B - boxplot of endpoint CFU concentrations. Ref - un-illuminated reference sample with no ZnO NPs, L - illuminated reference sample with no ZnO NPs, Zn - un-illuminated sample containing ZnO NPs, L+Zn - illuminated sample containing ZnO NPs.

From the boxplots, we can see that though there is a significant difference in the distribution of the groups, however, they can all be found in the same order of magnitude. This is corroborated by statistical tests. The Kruskal-Wallis test preformed on t_0 concentrations yielded the following results: $H(3) = 2.88$, $p = .41$. At a 5 % significance level we cannot, therefore, reject the null hypothesis, in other words, there is no statistically significant difference in the mean ranks of the groups. The results of the Scheirer–Ray–Hare (SRH) test are summarized in Table

7.4. From the p-values, we cannot reject the null hypothesis for the effects of light and the interaction of light and ZnO at a 5 % significance level. There seems to be a significant effect of light on the concentration of cells at t_{24} ($H(1) = 4$, $p = .045$), we can therefore reject the null hypothesis regarding the effects of light on the final cell concentration. However, the p-value is quite close to 0.05 and, more importantly, from the box plot we can see that the magnitude for the concentration over all groups is the same. The difference is statistically significant, but not significant enough to be of great interest for this experiment. The statistically significant result was most likely caused by the different distributions as well as different numbers of samples for each group.

Factor	SS	DF	H	p-value
Light	153.1	1	4.00	0.045
ZnO	1.4	1	0.037	0.847
Light x ZnO	118.0	1	3.08	0.079
Residuals	493.1	17		

Table 7.4: Results of the Scheirer-Ray-Hare test for t_{24} CFU concentrations in experiment 1, re-exposure 1. SS - sum of squares, DF - degrees of freedom

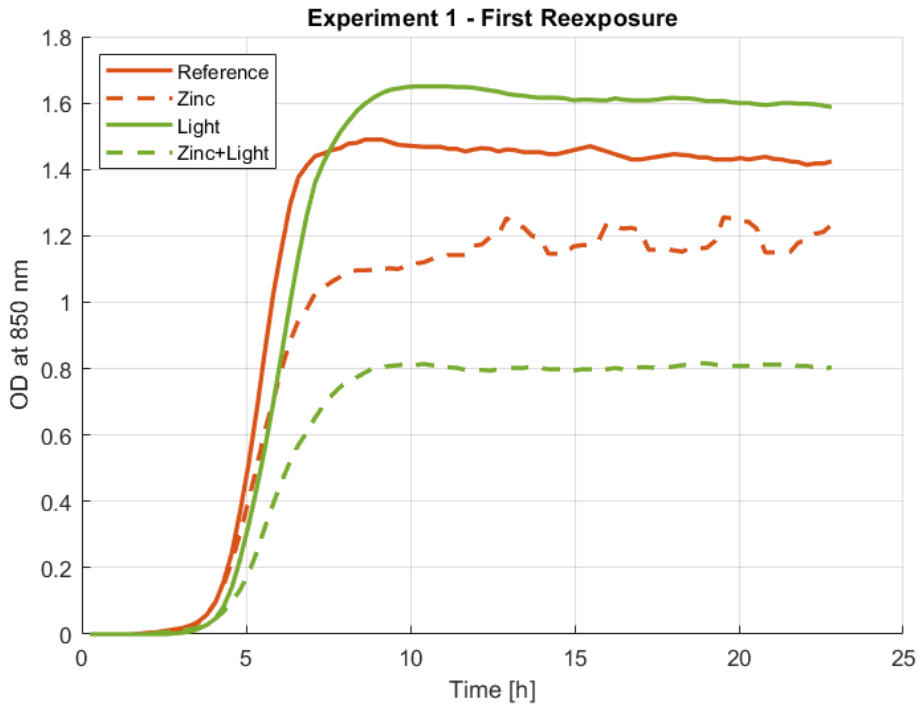

Figure 7.13: Growth curve for experiment 1, re-exposure 1 results. Red curves denote samples grown in the dark, while green curves show illuminated samples. Dashed lines then signify samples containing ZnO, while full lines show reference samples without ZnO.

From Figure 7.15, we can see, that the optical density of the samples containing

ZnO are lower than those of their respective references. However, the bioreactors have been shown to have less accuracy at higher optical densities (Table 7.1). In addition, this result is not corroborated by CFU measurements. This fact, however, raises an interesting question about the cause of this difference (which in one case is almost 100 %). One possible explanation for the observed difference in optical density is a difference in cell size or shape. In the future, variation in cell size and shape in response to illumination and/or ZnO could be further investigated using atomic force microscopy or scanning electron microscopy.

Re-exposure 2

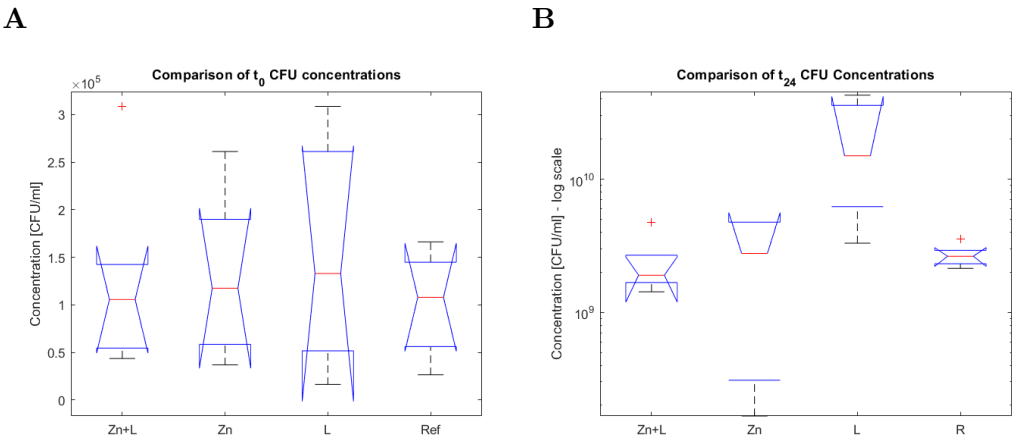

Figure 7.14: Experiment 1, re-exposure 2 CFU results. A - boxplot of initial CFU concentrations; B - boxplot of endpoint CFU concentrations. Ref - un-illuminated reference sample with no ZnO NPs, L - illuminated reference sample with no ZnO NPs, Zn - un-illuminated sample containing ZnO NPs, Zn+L - illuminated sample containing ZnO NPs.

In both cases for the second re-exposure experiments, both the boxplots and statistical tests show us no significant difference, which is corroborated by statistical tests. The Kruskal-Wallis test preformed on t_0 concentrations yielded the following results: $H(3) = 0.4$, $p = .94$. At a 5 % significance level we cannot, therefore, reject the null hypothesis, in other words, there is no statistically significant difference in the mean ranks of the groups. The results of the Scheirer–Ray–Hare (SRH) test are summarized in Table 7.5. For all factors, the p value is greater than 0.05. We cannot, therefore, reject any of the null hypotheses, in other words, no statistically significant difference was found between the samples when taking into account either of the factors (light and ZnO) or their interaction.

As in the previous re-exposure, we can see lower optical densities in samples containing ZnO, which is not corroborated by the CFU measurements. Furthermore, the growth curve of the light reference has an atypical shape. This has been seen in a number of experiments, but has no effect on CFU measurements, colony shapes or sizes. One possible cause might be air leaking into the cap of the falcon tube, which may introduce oxygen to the dividing cells. A slightly longer lag phase in the ZnO + light sample was also observed, however, the difference was only slight.

Factor	SS	DF	H	p-value
Light	6.99	1	0.22	0.638
ZnO	98.75	1	3.13	0.077
Light x ZnO	86.70	1	2.75	0.097
Residuals	379.10	15		

Table 7.5: Results of the Scheirer-Ray-Hare test for t_{24} CFU concentrations in experiment 1, re-exposure 2. SS - sum of squares, DF - degrees of freedom

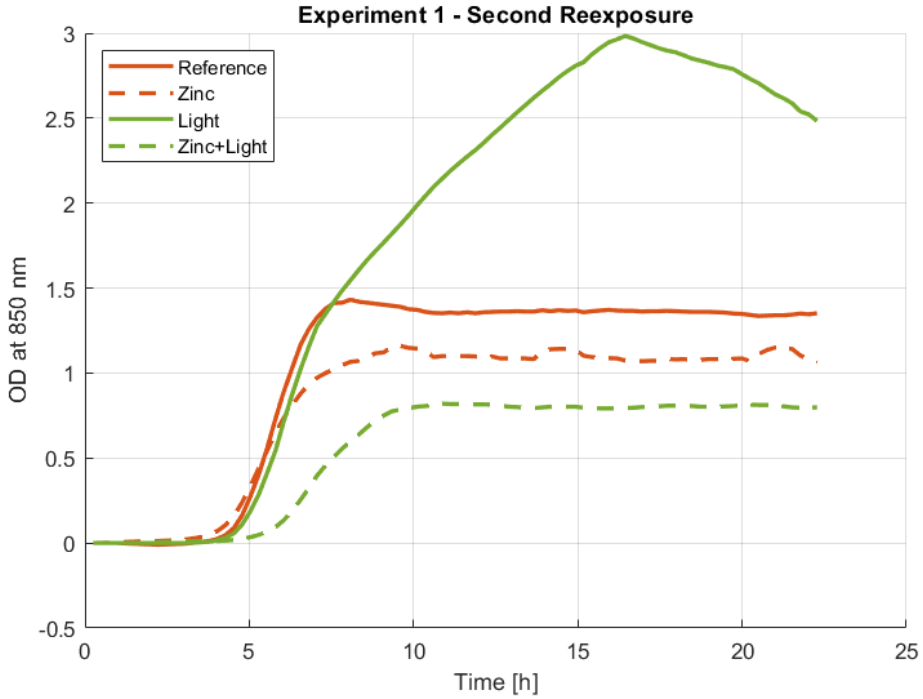

Figure 7.15: Growth curve for experiment 1, re-exposure 2 results. Red curves denote samples grown in the dark, while green curves show illuminated samples. Dashed lines then signify samples containing ZnO, while full lines show reference samples.

Re-exposure 3 - First Repetition

From the boxplots, we can see a difference in the t_0 concentrations of cells. This is confirmed by the results of the Kruskal-Wallis test: $H(3) = 15.01$, $p = .003$. At a 5 % significance level we can reject the null hypothesis, in other words, there is a statistically significant difference in the mean ranks of the groups. However, as we have seen previously, all cell concentrations are in the same order of magnitude (i,e, 10^6 CFU/ml), therefore this difference is not significant to the experiment. The boxplot for t_{24}, however, give an interesting result. As we can see, the concentration of bacterial cells exposed to ZnO is much lower than that of the other samples (by about 5 orders of magnitude). This is confirmed by the results of the Scheirer–Ray–Hare (SRH) test (Table 7.6). The p-values for light as a factor and for the interaction of light and ZnO is greater than 0.05 (0.92 and 0.27, respectively). However, the

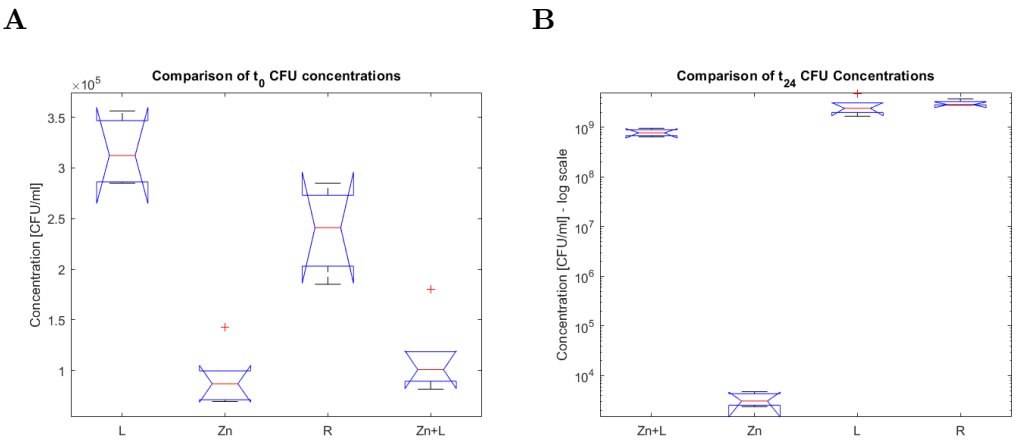

Figure 7.16: Experiment 1, re-exposure 3, first repetition CFU results. A - boxplot of initial CFU concentrations; B - boxplot of endpoint CFU concentrations. R - un-illuminated reference sample with no ZnO NPs, L - illuminated reference sample with no ZnO NPs, Zn - un-illuminated sample containing ZnO NPs, L+Zn - illuminated sample containing ZnO NPs.

effect of ZnO as a factor has a p-value smaller than 0.001. This shows a statistically significant difference between the ZnO samples.

Factor	SS	DF	H	p-value
Light	0.2	1	0.0095	0.922
ZnO	296.8	1	11.652	< 0.001
Light x ZnO	31.2	1	1.224	0.269
Residuals	78.6	13		

Table 7.6: Results of the Scheirer-Ray-Hare test for t_{24} CFU concentrations in experiment 1, re-exposure 3, first repetition. SS - sum of squares, DF - degrees of freedom

Similar results can also be seen from the growth curve, where there is no growth in the optical density of the sample including ZnO. We can also see a prolonged lag phase of the illuminated ZnO sample, which indicates that the cells are stressed. Unfortunately, t_{24} plates of the ZnO sample showed *Staphylococcus aureus* contamination. While the colonies of this bacteria are easily distinguished from that of *E. coli* as they are smaller, white in color and have sharp edges, the decrease in *E. coli* concentration may be caused by competition with these cells for nutrients in the growth medium. The measurement was, therefore, repeated.

Re-exposure 3 - Second Repetition

Figure 7.18 ahows the t_0 boxplot and we can again, see that the main difference between the groups prior to incubation is their distribution. They are all, however in the same order of magnitude (10^4 CFU/ml). The Kruskal-Wallis test also shows no significant difference ($H(3) = 4.17$, $p = .24$). At a 5 % significance level we cannot, therefore, reject the null hypothesis. Unfortunately, t_{24} dilution series for

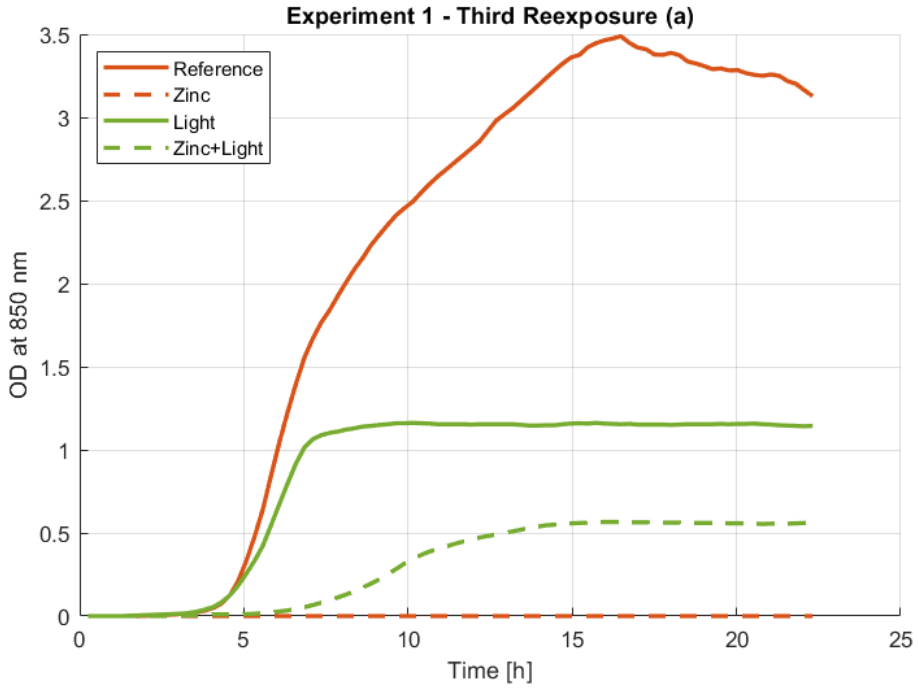

Figure 7.17: Growth curve for experiment 1, re-exposure 3, repetition 1 results. Red curves denote samples grown in the dark, while green curves show illuminated samples. Dashed lines then signify samples containing ZnO, while full lines show reference samples.

both samples including ZnO contained too many cells to be counted. A subsequent measurement was impossible due to overnight growth in the refrigerator. In addition, the growth curve (Figure 7.19 - reference) had a notable lag phase. The experiment was, therefore, repeated again.

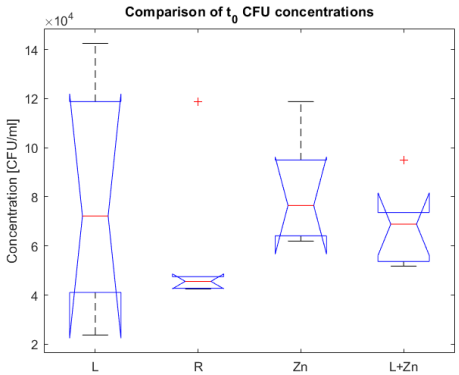

Figure 7.18: Experiment 1, re-exposure 3, repetition 2 CFU results. Boxplot of initial CFU concentrations. R - un-illuminated reference sample with no ZnO NPs, L - illuminated reference sample with no ZnO NPs, Zn - un-illuminated sample containing ZnO NPs, L+Zn - illuminated sample containing ZnO NPs.

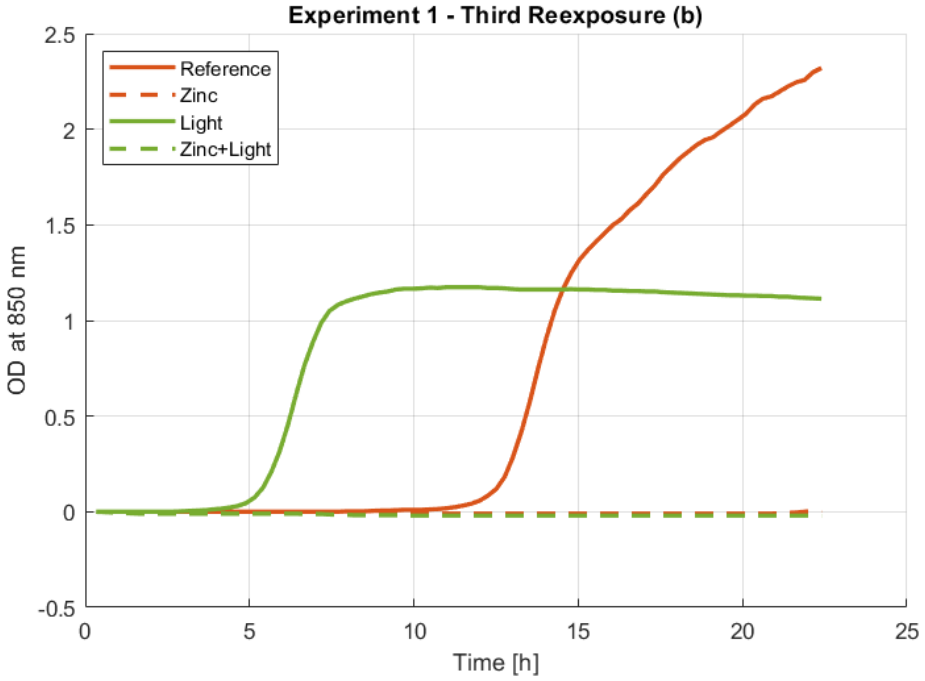

Figure 7.19: Growth curve for experiment 1, re-exposure 3, repetition 2 results. Red curves denote samples grown in the dark, while green curves show illuminated samples. Dashed lines then signify samples containing ZnO, while full lines show reference samples.

Re-exposure 3 - Third Repetition

A **B**

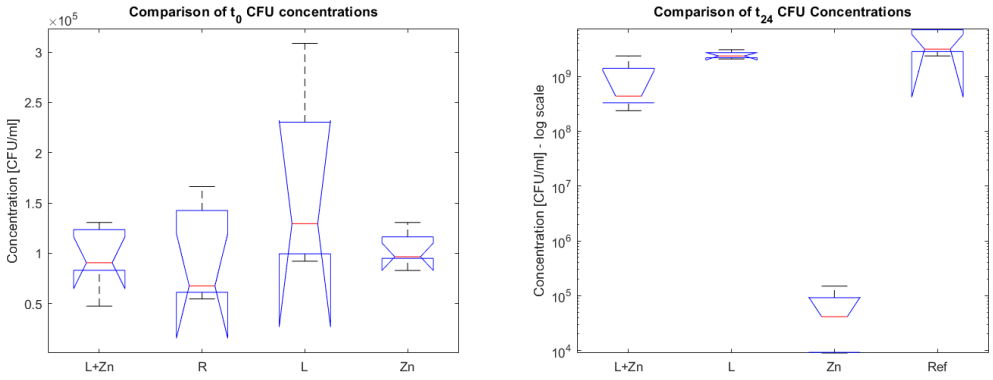

Figure 7.20: Experiment 1, re-exposure 3, repetition 3 CFU results. A - boxplot of initial CFU concentrations; B - boxplot of endpoint CFU concentrations. Ref - un-illuminated reference sample with no ZnO NPs, L - illuminated reference sample with no ZnO NPs, Zn - un-illuminated sample containing ZnO NPs, L+Zn - illuminated sample containing ZnO NPs.

From the t_0 boxplot, we can see no significant difference in the groups. This can

be seen in the result of the Kruskal-Wallis test (H(3) = 3.44, p = .33). At a 5 % significance level we cannot, therefore, reject the null hypothesis, in other words, there is no statistically significant difference in the mean ranks of the groups. The results of the Scheirer–Ray–Hare (SRH) test are summarized in Table 7.7. Even from the boxplot, however, we can see a significant difference of the sample including ZnO from the other groups by 4 to 5 orders of magnitude. This result is similar to that seen in the first repetition of this re-exposure step. However, no contamination was seen in the sample this time.

Factor	SS	DF	H	p-value
Light	0.26	1	0.0069	0.934
ZnO	513.4	1	13.378	< 0.001
Light x ZnO	137.6	1	3.59	0.058
Residuals	113.4	17		

Table 7.7: Results of the Scheirer-Ray-Hare test for t_{24} CFU concentrations in experiment 1, re-exposure 3, repetition 3. SS - sum of squares, DF - degrees of freedom

From the Schierer-Ray-Hare test, we can see that the factor of light as well as the interaction of light and ZnO have no statistically significant effect on cell concentration (p-values are .93 and .06, respectively). However, The effects of ZnO on cell concentration are pronounced (H(1) = 13.4, p < .001). We can, therefore, reject the null hypothesis that there is no difference among the groups when taking into account light as the factor.

Similar results can also be seen in the growth curve in Figure 7.21, where no growth can be seen in the ZnO sample.The illuminated ZnO sample also showed a prolonged lag phase, though no significant differences were seen in the final CFU concentrations.

As these three re-exposure steps yielded results, that showed 3 successive exposures to 100 μg/ml ZnO NPs inhibited growth, the entire experiment was repeated using fresh cells and ZnO NPs.

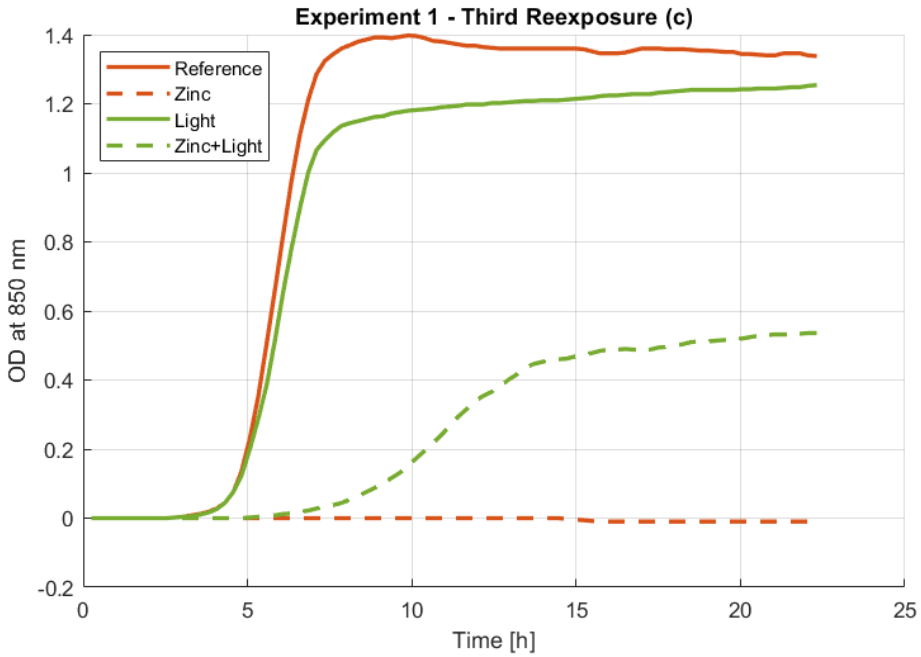

Figure 7.21: Growth curve for experiment 1, re-exposure 3, repetition 3 results. Red curves denote samples grown in the dark, while green curves show illuminated samples. Dashed lines then signify samples containing ZnO, while full lines show reference samples.

7.2.2 Experiment 2

Re-exposure 1

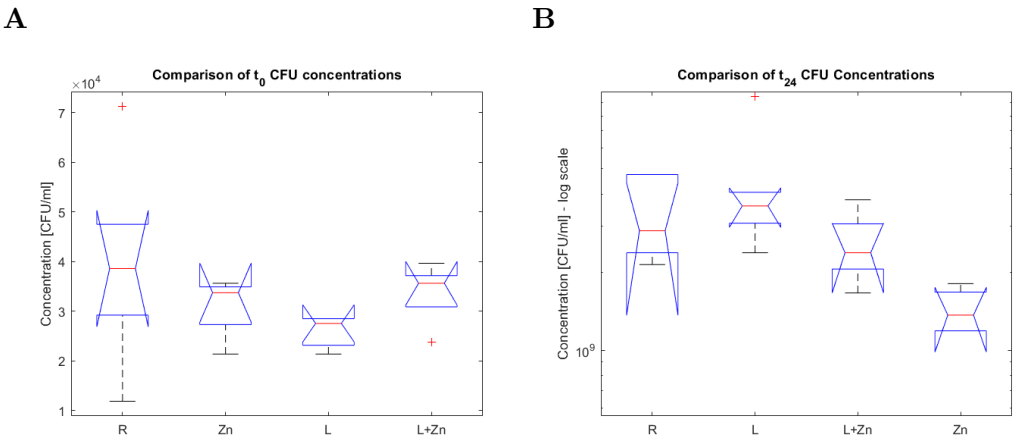

Figure 7.22: Experiment 2, re-exposure 1 CFU results. A - boxplot of initial CFU concentrations; B - boxplot of endpoint CFU concentrations. Ref - un-illuminated reference sample with no ZnO NPs, L - illuminated reference sample with no ZnO NPs, Zn - un-illuminated sample containing ZnO NPs, L+Zn - illuminated sample containing ZnO NPs..

From both the t_0 and t_{24} boxplot (Figure 7.22, we can see no significant difference in the groups. This can be seen in the result of the Kruskal-Wallis test ($H(3) = 5.44$, $p = .14$). At a 5 % significance level we cannot reject the null hypothesis, in other words, there is no statistically significant difference in the mean ranks of the groups. The results of the Scheirer–Ray–Hare (SRH) test are summarized in Table 7.8. This result is similar to some we have already seen. No statistically significant differences in concentrations were found when light was considered the factor or for the interaction of light and illumination (p-values were .12 and .37, respectively). However, a statistically significant effect of ZnO was found ($H(1) = 8.17$, $p = .004$). From the boxplot and cell concentrations, however, we can see that the difference is not in an order of magnitude and, therefore, not significant in terms of the experiment.

Factor	SS	DF	H	p-value
Light	94.1	1	2.45	0.117
ZnO	313.5	1	8.17	0.004
Light x ZnO	30.4	1	0.79	0.373
Residuals	346.7	17		

Table 7.8: Results of the Scheirer-Ray-Hare test for t_{24} CFU concentrations in experiment 1, re-exposure 3, repetition 3. SS - sum of squares, DF - degrees of freedom

From Figure 7.23, an effect of ZnO on cells is definitely noticeable. Both ZnO samples have longer lag phases, which is more pronounced in the illuminated ZnO

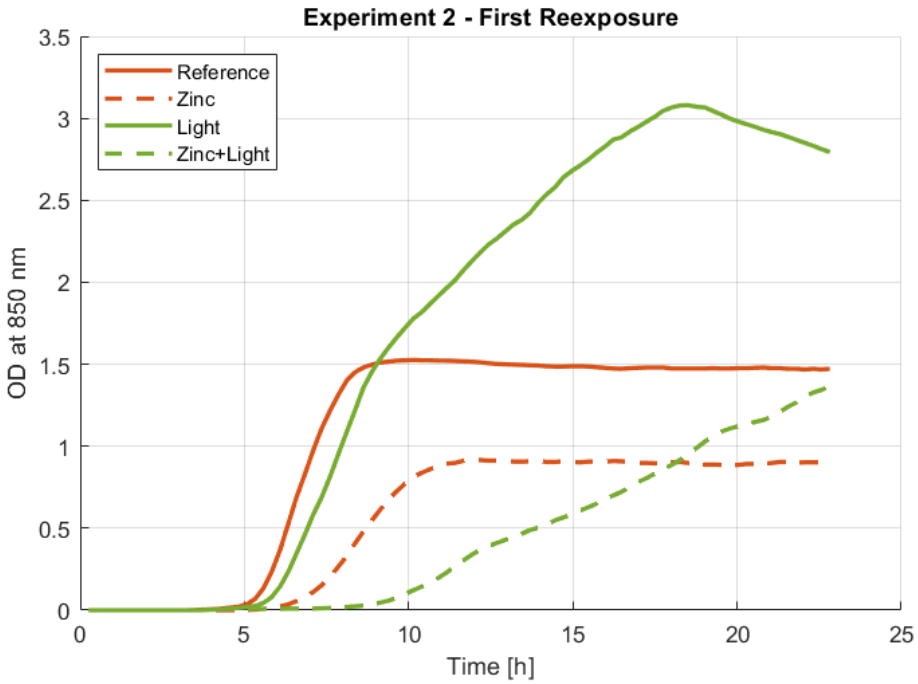

Figure 7.23: Growth curve for experiment 2, re-exposure 1 results. Red curves denote samples grown in the dark, while green curves show illuminated samples. Dashed lines then signify samples containing ZnO, while full lines show reference samples.

sample. The growth curve shape of the illuminated ZnO sample is not typical, but follows a similar trend to the reference sample and other samples I have shown in this thesis. It is again most likely caused by an insufficient isolation of the falcon tube and air infiltration.

Re-exposure 2

From both the t_0 and t_{24} boxplot (Figure 7.24, we can see no significant differences in the group values (none differ in magnitude). However, there is a visible difference in the distributions. This translates into the result of the statistical analysis. The Kruskal-Wallis test shows a significant difference between the t_0 CFU concentrations ($H(3) = 10.16$, $p = .017$). At a 5 % significance level we can reject the null hypothesis, in other words, there is a statistically significant difference in the mean ranks of the groups. As has been mentioned before, however, as long as the concentrations don't vary in an order of magnitude, it is not a significant enough difference. The results of the Scheirer–Ray–Hare (SRH) test are summarized in Table 7.9. This result also reflects the difference in sample distribution. Altough no statistically significant differences in concentrations were found when ZnO was considered the factor or for the interaction of light and illumination (p-values were .40 and .25, respectively). However, a statistically significant effect of light was found ($H(1) = 4.5$, $p = .034$). Similarly to the results of the Kruskal-Wallis test above, these results are, however, not prominent enough to be a significant result for this experiment.

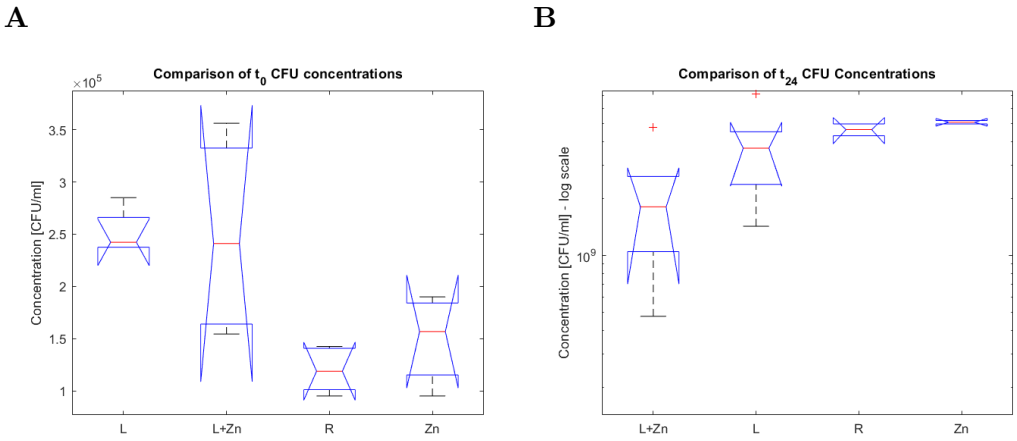

Figure 7.24: Experiment 2, re-exposure 2 CFU results. A - boxplot of initial CFU concentrations; B - boxplot of endpoint CFU concentrations. Ref - un-illuminated reference sample with no ZnO NPs, L - illuminated reference sample with no ZnO NPs, Zn - un-illuminated sample containing ZnO NPs, L+Zn - illuminated sample containing ZnO NPs.

Factor	SS	DF	H	p-value
Light	89.97	1	4.5	0.034
ZnO	14.01	1	0.7	0.402
Light x ZnO	26.93	1	1.3	0.245
Residuals	151.28	11		

Table 7.9: Results of the Scheirer-Ray-Hare test for t_{24} CFU concentrations in experiment 1, re-exposure 3, repetition 3. SS - sum of squares, DF - degrees of freedom

From Figure 7.25, the most prominent difference from the first re-exposure step is the long lag phase of the illuminated light sample. Otherwise, the growth curves are similar to previous experiments.

Re-exposure 3

From figure 7.26 A, we can see no significant difference in the groups. This is confirmed by the result of the Kruskal-Wallis test ($H(3) = 5.63$, $p = .13$). At a 5 % significance level we cannot reject the null hypothesis, in other words, there is no statistically significant difference in the mean ranks of the groups. In contrast, from Figure 7.26 B, we can see a difference in an order of magnitude of the illuminated ZnO sample from the others. This observation is supported by the results of the Scheirer–Ray–Hare (SRH) test summarized in Table 7.10. No statistically significant differences in concentrations were found when the interaction of light and illumination was considered the factor (p-value .656). However, a statistically significant effect of both ZnO ($H(1) = 6.78$, $p = .009$) and light ($H(1) = 6.32$, $p = .012$) was found. These two factors have an effect on the concentration of colony forming units in the experiment.

This result can be seen in the growth curves of the cells in Figure 7.27 as well. No

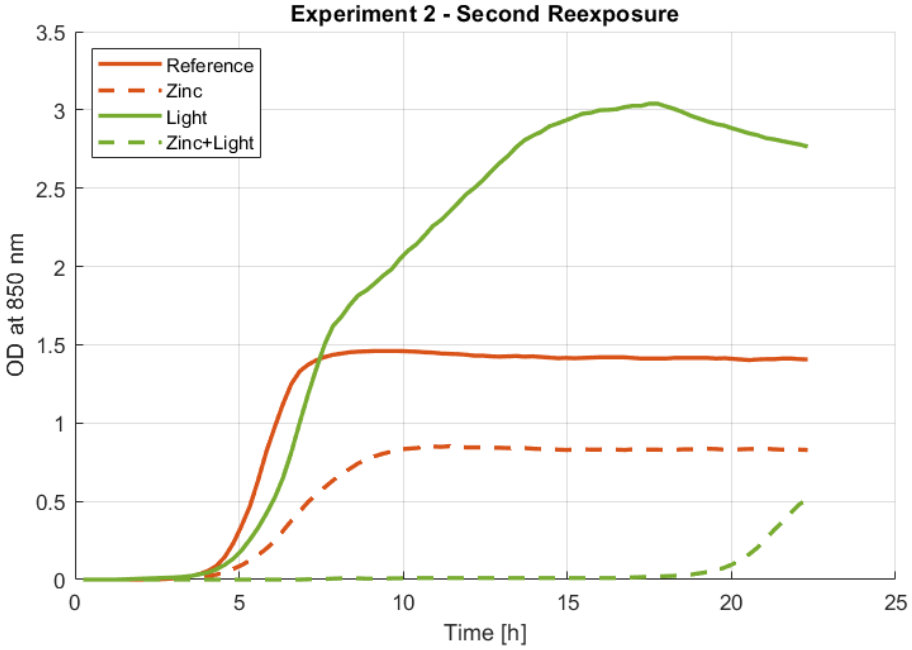

Figure 7.25: Growth curve for experiment 2, re-exposure 2 results. Red curves denote samples grown in the dark, while green curves show illuminated samples. Dashed lines then signify samples containing ZnO, while full lines show reference samples.

A **B**

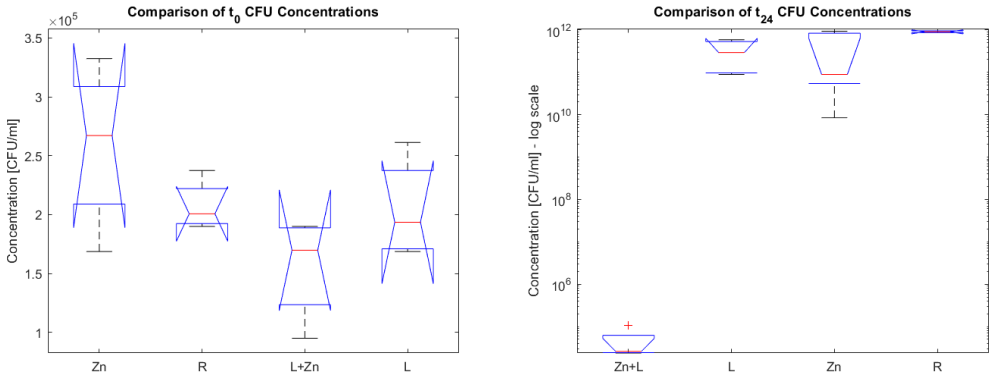

Figure 7.26: Experiment 2, re-exposure 3 CFU results. A - boxplot of initial CFU concentrations; B - boxplot of endpoint CFU concentrations. Ref - un-illuminated reference sample with no ZnO NPs, L - illuminated reference sample with no ZnO NPs, Zn - un-illuminated sample containing ZnO NPs, L+Zn - illuminated sample containing ZnO NPs.

growth was detected in the illuminated ZnO sample and the lag phase of the ZnO sample without illumination is prolonged. Both references look standard, therefore the results can be accepted as credible.

Factor	SS	DF	H	p-value
Light	143.0	1	6.32	0.012
ZnO	153.5	1	6.78	0.009
Light x ZnO	4.5	1	0.199	0.656
Residuals	79.8875	12		

Table 7.10: Results of the Scheirer-Ray-Hare test for t_{24} CFU concentrations in experiment 2, re-exposure 3. SS - sum of squares, DF - degrees of freedom

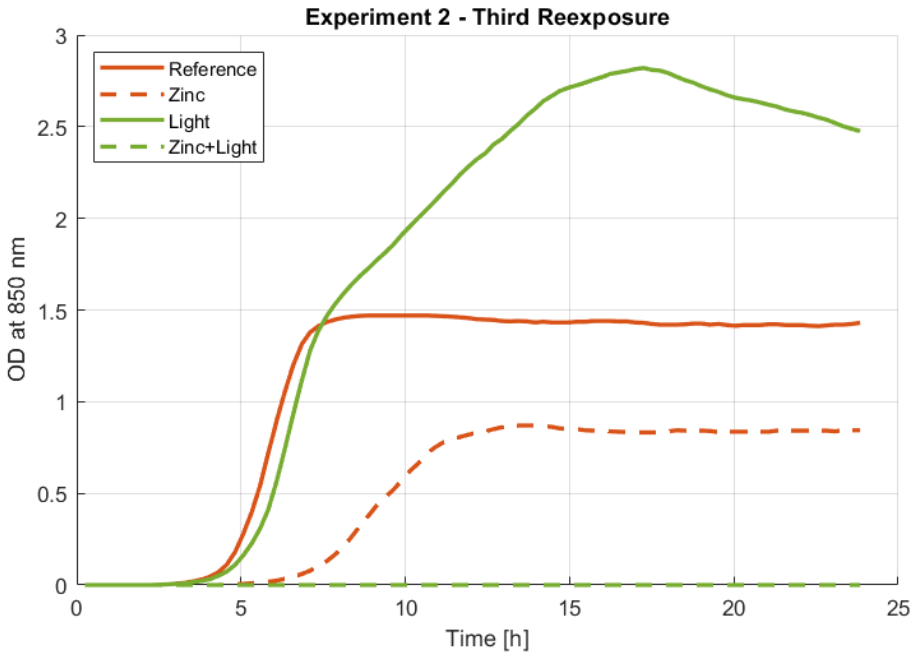

Figure 7.27: Growth curve for experiment 2, re-exposure 3 results. Red curves denote samples grown in the dark, while green curves show illuminated samples. Dashed lines then signify samples containing ZnO, while full lines show reference samples.

7.2.3 Summary of Results

In both experiments, a significant decline in cell concentration was observed by the third re-exposure in a sample containing ZnO. In the first experiment, the sample in question was the un-illuminated ZnO sample. This result was corroborated by the results of the Sheirer-Ray-Hare test. In the second experiment, the sample in question was the illuminated ZnO sample. The Scheirer-Ray-Hare test showed a significant effect of ZnO, but also an effect of illumination (however not of their interaction). This leads me to the conclusion that the presence ZnO oxide nanoparticles is the most important factor in determining the concentration of cells. The illumination source used in these experiments appeared to have no significant effect overall.

Lag Phase Lengths

In addition to the CFU measurements, I investigated the changes in lengths of lag phases of the samples over the course of the re-exposure experiments. The results can be seen in Figure 7.28 for the first experiment and Figure 7.29 for the second experiment. While the lag phases for the references are stable, the length of lag phases of ZnO samples increased gradually (with the exception of the un-illuminated ZnO sample during experiment 2). For future experiments, I would be interested to see, whether the ZnO samples which continued to grow in the third re-exposure would gradually stop growing as well. As mentioned previously, resistance towards silver nanoparticles was observed after 208 generations,[27] which would add up to a much greater number of re-exposures than tested here. A larger number of re-exposure steps may also generate different results.

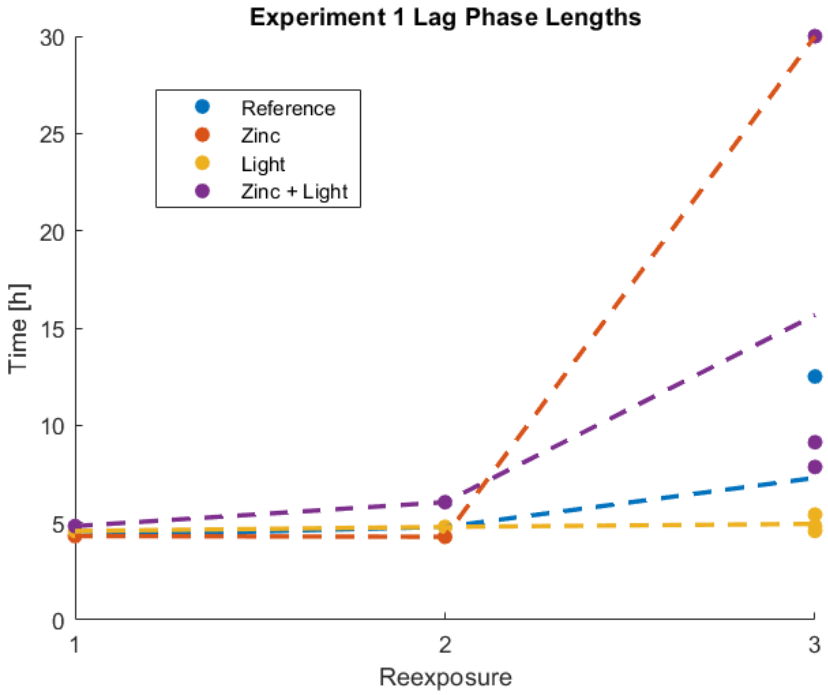

Figure 7.28: Lag phases for individual samples over the course of re-exposure experiment 1. For the final re-exposure experiment, the values from the three repetitions were averaged for the final result. Results at 30 hours denote samples, in which no growth was detected.

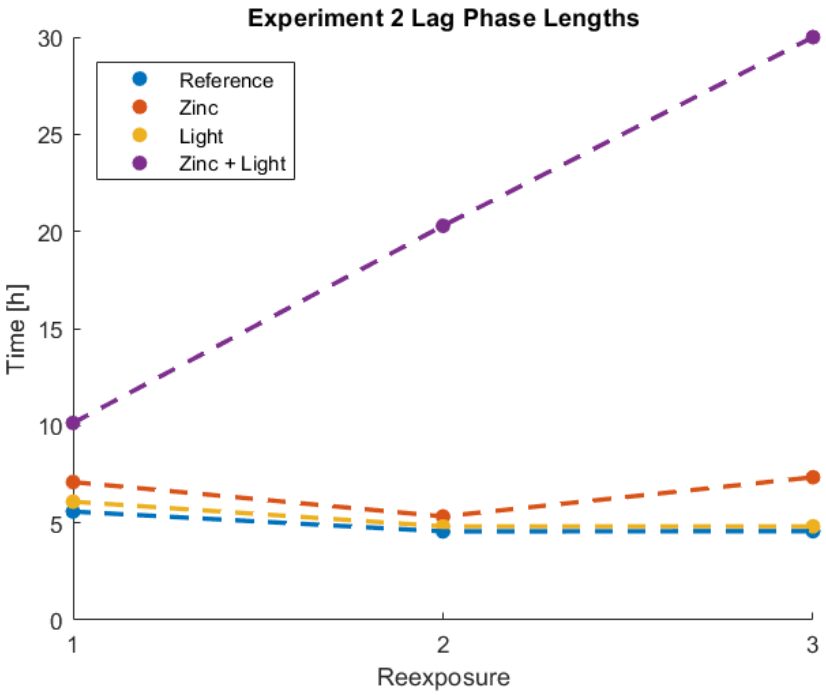

Figure 7.29: Lag phases for individual samples over the course of re-exposure experiment 2. Results at 30 hours denote samples, in which no growth was detected.

Maximum Growth Rates

Another investigated parameter for the experiments was the maximum growth rate of samples. The results of these measurements can be seen in Figure 7.30 for experiment 1 and 7.31 for experiment 2. In the graphs, two important trends can be seen. Firstly, the maximum growth rates of ZnO samples are always significantly lower than those of reference samples. Secondly, the growth rates of samples decline as their final optical densities and CFU concentrations decline. This second point is unsurprising, but supports the already stated conclusions.

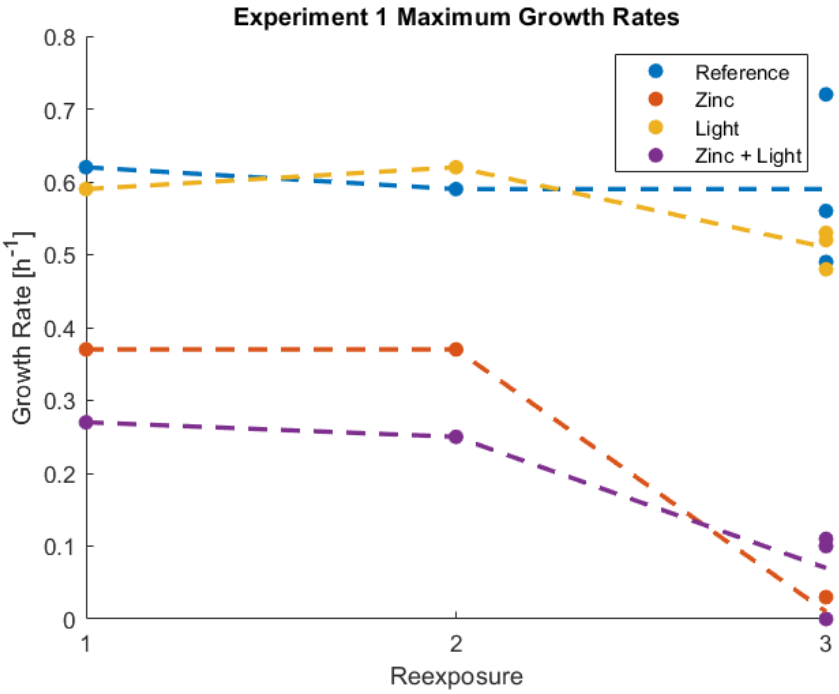

Figure 7.30: Maximum growth rates for individual samples over the course of re-exposure experiment 1. For the final re-exposure step, the values from the three repetitions were averaged for the final result.

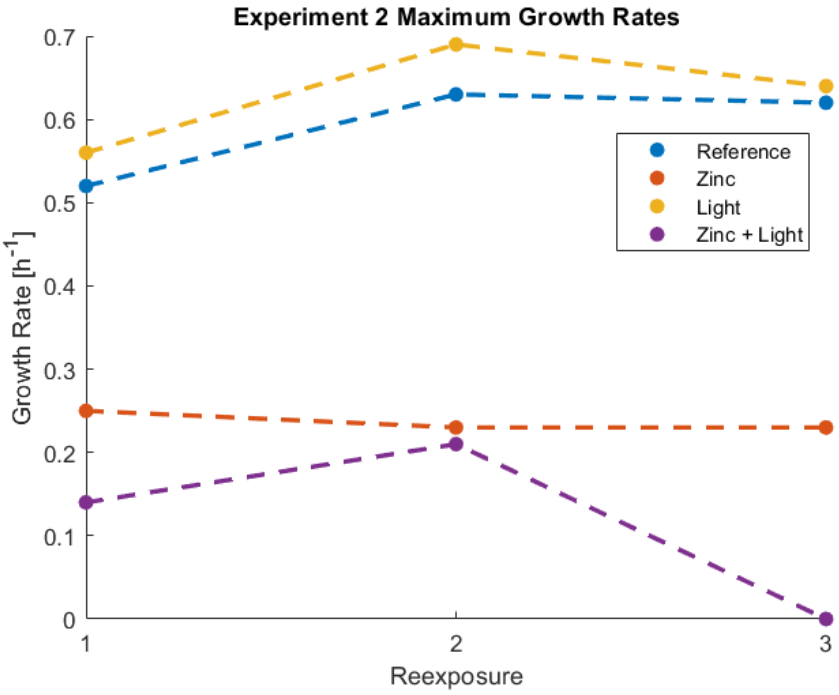

Figure 7.31: Maximum growth rates for individual samples over the course of re-exposure experiment 2.

Colonies at t_{24}

An additional finding concerns colony size and shape in response to ZnO exposure. Although this parameter was not thoroughly studied, an anomaly in the third re-exposures appeared in both experiments. A clear difference in colonies was observed in samples which displayed minimum growth (un-illuminated ZnO samples in experiment 1 and illuminated ZnO samples in experiment 2). While colonies in other experiments did not differ significantly in size or shape (sometimes fuzzier or smoother colonies appeared), the t_{24} samples with minimum growth contained both significantly different sized of colonies as well as colony shapes. These differences can be seen in Figure 7.32. While sub-figures A and B show typical colonies of t_{24} cultures, sub-figures C and D show t_{24} cultures for the third re-exposure experiment samples, which showed no growth (for experiment 1 and experiment 2, respectively). In future experiments, it may be beneficial to examine colony morphologies and shapes, as well as the shapes of the cells themselves (this may explain the comparable CFU concentrations with differing optical densities as well).

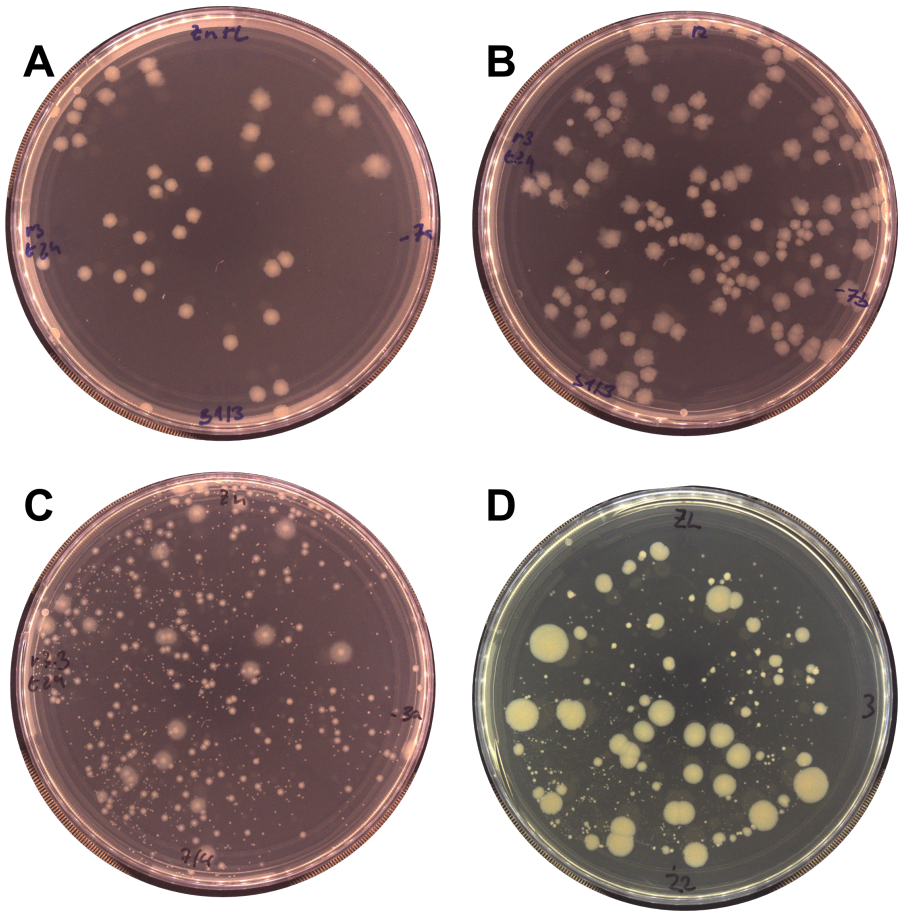

Figure 7.32: Images of t_{24} colonies. A and B show typical t_{24} colonies, while C shows t_{24} colonies of the un-illuminated ZnO sample in experiment 1, re-exposure 3, repetition 3, and D shows t_{24} colonies of the illuminated ZnO sample in experiment 2, re-exposure 3.

The MIC of the same ZnO NPs used in this study and against the same bacterial strain was previously reported to be much lower (16 μg/ml).[45] The standard protocol was originally developed for antimicrobial substances uniformly dispersed in solution and did not agglomerate, unlike nanoparticles. 50 nm ZnO particle agglomeration behavior in different liquid types recently showed cluster formation, ranging in size from hundreds of nanometers to micron-sized (the equivalent of *E. coli* cell size).[57] Such variation in particle cluster size may account for the difference in MIC, especially considering the reported influence nanoparticle size has on the antibacterial effect of ZnO. A greater understanding of ZnO NP aggregation in polar (i.e. water-based) liquids through a combination of physico-chemical experimental investigation aligned with atomic scale simulations is needed if the potential of ZnO for antibacterial applications is to be fully exploited in this "post-antibiotic" era.

Chapter 8

Conclusion

In this thesis, I investigated the effects of the long-term exposure of *Escherichia coli* cells to sub-lethal concentrations of commercial zinc oxide nanoparticles. Prior to the exposure of cells to the nanoparticles, preliminary experiments were carried out in order to determine a suitable concentration of zinc oxide nanoparticles and to uncover any underlying factors, which could affect the measurement. Subsequently, two experiments were carried out, each spanning three re-exposure experiments. Three main features were examined - the colony forming unit concentration in the cell suspension after exposure to nanoparticles, the length of the lag phase in bacterial growth curves, and the maximum growth rate of cell cultures.

From the results, a long-term effect was observed in all investigated features in cell cultures grown in a 100 μg/ml zinc oxide nanoparticle suspension. For each experiment, one sample containing zinc oxide was more noticeably affected, although both differed from their respective references. After three re-exposure steps, the final colony forming unit concentration of one of the zinc oxide samples dropped 4 - 5 orders of magnitude as opposed to the references. Statistical tests uncovered a significant effect of zinc oxide as well as an effect of light in the second experiment. However, no effect was found for the interaction of these two factors. The lag phases grew gradually in the samples containing zinc oxide. All samples containing zinc oxide had noticeably lower growth rates as opposed to the reference samples and the growth rate decreased for the zinc oxide samples with diminished growth. A surprising result was also found in the colony forming unit measurements, where the final plates containing cells exposed to zinc oxide with no growth contained abnormal shapes and sizes of colonies.

For future experiments, I would carry out more re-exposure experiments to ascertain, whether a similar effect would be observed in the second zinc oxide sample as well. Imaging of cells from the re-exposure experiments would also be beneficial, as it could show changes caused by zinc oxide as well as explain the differences in optical density values, which did not translate to CFU concentrations. A more sensitive method of hydrogen peroxide detection could also help to better map the processes in the bioreactors. Other light sources could be tested as well, as our light source didn't seem to have much effect on the cells exposed to zinc oxide.

Bibliography

[1] Y. Li, P. Leung, L. Yao, Q. Song, and E. Newton, "Antimicrobial effect of surgical masks coated with nanoparticles," *Journal of Hospital Infection*, vol. 62, pp. 58–63, jan 2006.

[2] B. Alberts, A. Johnson, P. Walter, J. Lewis, and M. Raff, *Molecular Biology of the Cell*. Norton Company, Dec. 2014.

[3] Wikipedia contributors, "Bacterial cellular morphologies — Wikipedia, the free encyclopedia," 2021. [Online; accessed 14-May-2022].

[4] M. T. Cabeen and C. Jacobs-Wagner, "Bacterial cell shape," *Nature Reviews Microbiology*, vol. 3, pp. 601–610, jul 2005.

[5] S. MRJ and K. KS, *Medical Microbiology (4th edition)*. Gavelston (TX): University of Texas Medical Branch at Gavelston, 1996.

[6] Z. Gitai, "The new bacterial cell biology: Moving parts and subcellular architecture," *Cell*, vol. 120, pp. 577–586, mar 2005.

[7] K. H. Nealson *Origins of Life and Evolution of the Biosphere*, vol. 29, no. 1, pp. 73–93, 1999.

[8] L. Wang, D. Fan, W. Chen, and E. M. Terentjev, "Bacterial growth, detachment and cell size control on polyethylene terephthalate surfaces," *Scientific Reports*, vol. 5, oct 2015.

[9] S. L. Percival and D. W. Williams, *Microbiology of Waterborne Diseases: Microbiological Aspects and Risks*. ACADEMIC PR INC, Dec. 2013.

[10] R. J. Fair and Y. Tor, "Antibiotics and bacterial resistance in the 21st century," *Perspectives in Medicinal Chemistry*, vol. 6, p. PMC.S14459, jan 2014.

[11] M. K. Taj, Z. Samreen, J. X. Ling, I. Taj, T. M. Hassani, and W. Yunlin, "*Escherichia coli* as a model organism," *International Journal of Engineering Research and Science Technology*, vol. 3, May 2014.

[12] Z. D. Blount, "The natural history of model organisms: The unexhausted potential of *E. coli*," *eLife*, vol. 4, p. e05826, mar 2015.

[13] H. Hasman, M. A. Schembri, and P. Klemm, "Antigen 43 and type 1 fimbriae determine colony morphology of iescherichia coli/i k-12," *Journal of Bacteriology*, vol. 182, pp. 1089–1095, feb 2000.

[14] M. I. Hutchings, A. W. Truman, and B. Wilkinson, "Antibiotics: past, present and future," *Current Opinion in Microbiology*, vol. 51, pp. 72–80, oct 2019.

[15] E. Leung, D. E. Weil, M. Raviglione, and H. Nakatani, "The WHO policy package to combat antimicrobial resistance," *Bulletin of the World Health Organization*, vol. 89, pp. 390–392, may 2011.

[16] I. Roca, M. Akova, F. Baquero, J. Carlet, M. Cavaleri, S. Coenen, J. Cohen, D. Findlay, I. Gyssens, O. Heure, G. Kahlmeter, H. Kruse, R. Laxminarayan, E. Liébana, L. López-Cerero, A. MacGowan, M. Martins, J. Rodríguez-Baño, J.-M. Rolain, C. Segovia, B. Sigauque, E. Tacconelli, E. Wellington, and J. Vila, "The global threat of antimicrobial resistance: science for intervention," *New Microbes and New Infections*, vol. 6, pp. 22–29, jul 2015.

[17] S. Reardon, "WHO warns against 'post-antibiotic' era," *Nature*, apr 2014.

[18] A. H. A. M. van Hoek, D. Mevius, B. Guerra, P. Mullany, A. P. Roberts, and H. J. M. Aarts, "Acquired antibiotic resistance genes: An overview," *Frontiers in Microbiology*, vol. 2, 2011.

[19] M. A. Kohanski, D. J. Dwyer, and J. J. Collins, "How antibiotics kill bacteria: from targets to networks," *Nature Reviews Microbiology*, vol. 8, pp. 423–435, may 2010.

[20] P. Singh, A. Garg, S. Pandit, V. Mokkapati, and I. Mijakovic, "Antimicrobial effects of biogenic nanoparticles," *Nanomaterials*, vol. 8, p. 1009, dec 2018.

[21] K. M. Jørgensen, T. Wassermann, P. Ø. Jensen, W. Hengzuang, S. Molin, N. Høiby, and O. Ciofu, "Sublethal ciprofloxacin treatment leads to rapid development of high-level ciprofloxacin resistance during long-term experimental evolution of pseudomonas aeruginosa," *Antimicrobial Agents and Chemotherapy*, vol. 57, pp. 4215–4221, sep 2013.

[22] A. L. Walter, D. Yang, Z. Zeng, D. Bayrock, P. E. Urriola, and G. C. Shurson, "Assessment of antibiotic resistance from long-term bacterial exposure to antibiotics commonly used in fuel ethanol production," *World Journal of Microbiology and Biotechnology*, vol. 35, apr 2019.

[23] A. J. McBain, "Selection for high-level resistance by chronic triclosan exposure is not universal," *Journal of Antimicrobial Chemotherapy*, vol. 53, pp. 772–777, mar 2004.

[24] S. Naahidi, M. Jafari, F. Edalat, K. Raymond, A. Khademhosseini, and P. Chen, "Biocompatibility of engineered nanoparticles for drug delivery," *Journal of Controlled Release*, vol. 166, pp. 182–194, mar 2013.

[25] R. Dobrucka, J. Dlugaszewska, and M. Kaczmarek, "Cytotoxic and antimicrobial effects of biosynthesized ZnO nanoparticles using of chelidonium majus extract," *Biomedical Microdevices*, vol. 20, nov 2017.

[26] J. S. Kim, E. Kuk, K. N. Yu, J.-H. Kim, S. J. Park, H. J. Lee, S. H. Kim, Y. K. Park, Y. H. Park, C.-Y. Hwang, Y.-K. Kim, Y.-S. Lee, D. H. Jeong, and M.-H. Cho, "Antimicrobial effects of silver nanoparticles," *Nanomedicine: Nanotechnology, Biology and Medicine*, vol. 3, pp. 95–101, mar 2007.

[27] A. Panáček, L. Kvítek, M. Smékalová, R. Večeřová, M. Kolář, M. Röderová, F. Dyčka, M. Šebela, R. Prucek, O. Tomanec, and R. Zbořil, "Bacterial resistance to silver nanoparticles and how to overcome it," *Nature Nanotechnology*, vol. 13, pp. 65–71, dec 2017.

[28] C. Angelé-Martínez, K. V. T. Nguyen, F. S. Ameer, J. N. Anker, and J. L. Brumaghim, "Reactive oxygen species generation by copper(II) oxide nanoparticles determined by DNA damage assays and EPR spectroscopy," *Nanotoxicology*, vol. 11, pp. 278–288, feb 2017.

[29] A. I. El-Batal, G. S. El-Sayyad, A. El-Ghamery, and M. Gobara, "Response surface methodology optimization of melanin production by streptomyces cyaneus and synthesis of copper oxide nanoparticles using gamma radiation," *Journal of Cluster Science*, vol. 28, pp. 1083–1112, oct 2016.

[30] H. A. Foster, I. B. Ditta, S. Varghese, and A. Steele, "Photocatalytic disinfection using titanium dioxide: spectrum and mechanism of antimicrobial activity," *Applied Microbiology and Biotechnology*, vol. 90, pp. 1847–1868, apr 2011.

[31] K. S. Siddiqi and A. Husen, "Green synthesis, characterization and uses of palladium/platinum nanoparticles," *Nanoscale Research Letters*, vol. 11, nov 2016.

[32] B. L. da Silva, M. P. Abuçafy, E. B. Manaia, J. A. O. Junior, B. G. Chiari-Andréo, R. C. R. Pietro, and L. A. Chiavacci, "Relationship between structure and antimicrobial activity of zinc oxide nanoparticles: An overview," *International Journal of Nanomedicine*, vol. Volume 14, pp. 9395–9410, dec 2019.

[33] J. Jiang, J. Pi, and J. Cai, "The advancing of zinc oxide nanoparticles for biomedical applications," *Bioinorganic Chemistry and Applications*, vol. 2018, pp. 1–18, jul 2018.

[34] P. S. Bedi and A. Kaur, "An overview on uses of zinc oxide nanoparticles," *World Journal of Pharmacy and Pharmaceutical Sciences*, vol. 4, no. 12, p. 1177–1196, 2015.

[35] D. Sharma, J. Rajput, B. Kaith, M. Kaur, and S. Sharma, "Synthesis of ZnO nanoparticles and study of their antibacterial and antifungal properties," *Thin Solid Films*, vol. 519, pp. 1224–1229, nov 2010.

[36] A. Sirelkhatim, S. Mahmud, A. Seeni, N. H. M. Kaus, L. C. Ann, S. K. M. Bakhori, H. Hasan, and D. Mohamad, "Review on zinc oxide nanoparticles: Antibacterial activity and toxicity mechanism," *Nano-Micro Letters*, vol. 7, pp. 219–242, apr 2015.

[37] J. T. Hancock, R. Desikan, and S. Neill, "Role of reactive oxygen species in cell signalling pathways," *Biochemical Society Transactions*, vol. 29, pp. 345–349, may 2001.

[38] R. M. Day and Y. J. Suzuki, "Cell proliferation, reactive oxygen and cellular glutathione.," *Dose-response : a publication of International Hormesis Society*, vol. 3, pp. 425–442, May 2006.

[39] R. Kumar, A. Umar, G. Kumar, and H. S. Nalwa, "Antimicrobial properties of ZnO nanomaterials: A review," *Ceramics International*, vol. 43, pp. 3940–3961, apr 2017.

[40] K. Feris, C. Otto, J. Tinker, D. Wingett, A. Punnoose, A. Thurber, M. Kongara, M. Sabetian, B. Quinn, C. Hanna, and D. Pink, "Electrostatic interactions affect nanoparticle-mediated toxicity to gram-negative bacterium *Pseudomonas aeruginosa* PAO1," *Langmuir*, vol. 26, pp. 4429–4436, dec 2009.

[41] G. Porcheron, A. Garénaux, J. Proulx, M. Sabri, and C. M. Dozois, "Iron, copper, zinc, and manganese transport and regulation in pathogenic enterobacteria: correlations between strains, site of infection and the relative importance of the different metal transport systems for virulence," *Frontiers in Cellular and Infection Microbiology*, vol. 3, 2013.

[42] O. R. Vasile, I. Serdaru, E. Andronescu, R. Truşcă, V. A. Surdu, O. Oprea, A. Ilie, and B. Ş. Vasile, "Influence of the size and the morphology of ZnO nanoparticles on cell viability," *Comptes Rendus Chimie*, vol. 18, pp. 1335–1343, dec 2015.

[43] C. O. Dimkpa, J. E. McLean, D. W. Britt, and A. J. Anderson, "Antifungal activity of ZnO nanoparticles and their interactive effect with a biocontrol bacterium on growth antagonism of the plant pathogen fusarium graminearum," *BioMetals*, vol. 26, pp. 913–924, aug 2013.

[44] C. P. Adams, K. A. Walker, S. O. Obare, and K. M. Docherty, "Size-dependent antimicrobial effects of novel palladium nanoparticles," *PLoS ONE*, vol. 9, p. e85981, jan 2014.

[45] D. Rutherford, J. Jíra, K. Kolářová, I. Matolínová, J. Mičová, Z. Remeš, and B. Rezek, "Growth inhibition of gram-positive and gram-negative bacteria by zinc oxide hedgehog particles," *International Journal of Nanomedicine*, vol. Volume 16, pp. 3541–3554, may 2021.

[46] A. Ali, A.-R. Phull, and M. Zia, "Elemental zinc to zinc nanoparticles: is ZnO NPs crucial for life? synthesis, toxicological, and environmental concerns," *Nanotechnology Reviews*, vol. 7, pp. 413–441, sep 2018.

[47] V. V. Shinde, D. S. Dalavi, S. S. Mali, C. K. Hong, J. H. Kim, and P. S. Patil, "Surfactant free microwave assisted synthesis of ZnO microspheres: Study of their antibacterial activity," *Applied Surface Science*, vol. 307, pp. 495–502, jul 2014.

[48] "The european committee on antimicrobial susceptibility testing. *EUCAST reading guide for broth microdilution, version 4.0*," Jan. 2022.

[49] "The european committee on antimicrobial susceptibility testing. *Antimicrobial susceptibility testing, EUCAST disk diffusion method version 10.0*," Jan. 2022.

[50] L. C. Reimer, J. S. Carbasse, J. Koblitz, C. Ebeling, A. Podstawka, and J. Overmann, "Bacidive/i in 2022: the knowledge base for standardized bacterial and archaeal data," *Nucleic Acids Research*, vol. 50, pp. D741–D746, oct 2021.

[51] "Einstufung von prokaryonten (bacteria und archaea) in risikogruppen," *Technische Regeln für Biologische Arbeitsstoffe*, vol. TRBA 466, Dec. 2020.

[52] "Product data sheet: Mueller-hinton agar."

[53] MATLAB, *9.11.0.1809720 (R2021b Update 1)*. Natick, Massachusetts: The MathWorks Inc., 2021.

[54] T. D. . N. E. M. . C. D. V. . F. Reniers, "Hydrogen peroxide generated by an atmospheric he-o_2-h_2o flowing postdischarge: production mechanisms and absolute quantification," *22nd International Symposium on Plasma Chemistry*, 2015.

[55] J. B. Coulter and D. P. Birnie, "Assessing tauc plot slope quantification: ZnO thin films as a model system," *physica status solidi (b)*, vol. 255, p. 1700393, sep 2017.

[56] Schott, "Kl fiber optic light sources."

[57] D. Rutherford, J. Jíra, K. Kolářová, I. Matolínová, Z. Remeš, J. Kuliček, D. Padmanaban, P. Maguire, D. Mariotti, and B. Rezek, "Plasma-synthesised zinc oxide nanoparticle behavior in liquids," in *NANOCON 2021 Conference Proeedings*, TANGER Ltd., 2021.

Appendices

Appendix A

Laboratory Equipment and Scientific Instruments

- KL 2500 LED light ..... Schott
- ABT 320-4M analytical balance ..... Kern
- Sonorex digitec DT 31 ultrasonic bath ..... Bandelin
- 2840 ELV-D vertical autoclave ..... Schoeller Tuttnauer
- RTS-1C personal bioreactors ..... Biosan
- ZX3 Advanced vortex mixer ..... Velp Scientifica
- MPW-150R centrifuge ..... MPW Medical Instruments
- DEN-1B McFarland Densitometer ..... Biosan
- EPOCH2 Gen5 microplate reader ..... BioTek
- SphereFlash automatic colony counter ..... iUL

Appendix B

Materials

- Zinc oxide nanopowder, <50 nm particle size (BET), /97 % ..... Sigma
- HPLC grade water ..... ROTH
- Titanium(IV) oxysulfate in sulfuric acid (27 - 31 %) ..... Sigma
- Mueller-Hinton Broth ..... Oxoid
- Mueller-Hinton Agar ..... Roth
- Sodium chloride (NaCl) ..... Penta
- *E. coli* (Migula 1895) ..... Czech Collection of Microorganisms

Appendix C

CFU Measurements

Plate Id	Method	Counted Colonies	Counted Volume	Volume	Input Values	Concentration	Comments
1e+05 Ec_Illuminated_a	Fuzzy	4	0.842094719	0.5	26 ;85.0 ;0.8	950011.8948	
1e+04 Ec_Illuminated_b	Fuzzy	26	0.842094719	0.5	26 ;85.0 ;0.8	617507.7316	
1e+05 Ec_Dark_a	Fuzzy	7	0.842094719	0.5	26 ;85.0 ;0.8	1662520.816	
1e+05 Ec_Dark_b	Fuzzy	7	0.842094719	1	26 ;85.0 ;0.8	831260.408	
1e+04 Ec_Dark_c	Fuzzy	66	0.842094719	0.5	26 ;85.0 ;0.8	3135039.253	
1e+04 Ec_Dark_d	Fuzzy	83	0.842094719	1	26 ;85.0 ;0.8	985637.3409	

Table C.1: Preliminary light experiment automatic colony counter t_0 CFU results. Plate Id gives the dilution factor and illumination conditions. The "Method" column gives the method of colony detection used by the colony counter software. Counted Volume gives the percentage of inoculated volume included in cell detection. Volume gives the volume of plated cells in ml. Input Values gives 3 figures - the threshold to the background, the diameter of the computed part of the Petri dish and the minimal colony diameter in mm.

Plate Id	Method	Counted Colonies	Counted Volume	Volume	Input Values	Concentration	Comments
1e+08 Ec_Illuminated t24a	Fuzzy	51	0.842094719	0.5	25 ;85.0 ;0.35	12112651659	
1e+07 Ec_Illuminated t24b	Fuzzy	184	0.842094719	0.5	25 ;85.0 ;0.35	4370054716	
1e+06 Ec_Illuminated t24c	Fuzzy	852	0.842094719	0.5	25 ;85.0 ;0.35	2023525336	
1e+08 Ec_Dark t24a	Fuzzy	146	0.842094719	0.5	25 ;85.0 ;0.35	34675434161	
1e+07 Ec_Dark t24b	Fuzzy	366	0.842094719	0.5	25 ;85.0 ;0.3	8692608838	
1e+06 Ec_Dark t24c	Fuzzy	610	0.842094719	0.5	25 ;85.0 ;0.3	1448768140	

Table C.2: Preliminary light experiment automatic colony counter t_{24} CFU results. Plate Id gives the dilution factor and illumination conditions. The "Method" column gives the method of colony detection used by the colony counter software. Counted Volume gives the percentage of inoculated volume included in cell detection. Volume gives the volume of plated cells in ml. Input Values gives 3 figures - the threshold to the background, the diameter of the computed part of the Petri dish and the minimal colony diameter in mm.

Plate Id	Method	Counted Colonies	Counted Volume	Volume	Input Values	Concentration	Comments
1e+02 Ra	Fuzzy	372	0.842024744	0.5	25 ;85.0 ;1.8	88358.44857	
1e+02 Rb	Fuzzy	303	0.842024744	0.5	25 ;85.0 ;1.8	71969.3815	
1e+03 Ra	Fuzzy	132	0.842024744	0.5	25 ;85.0 ;1.8	313529.9788	
1e+03 Rb	Fuzzy	119	0.842024744	0.5	25 ;85.0 ;1.8	282652.0263	
1e+04 Ra	Fuzzy	31	0.842024744	0.5	25 ;85.0 ;1.8	736320.4048	
1e+04 Rb	Fuzzy	33	0.842024744	0.5	25 ;85.0 ;1.8	783824.947	
1e+02 Zn50a	Fuzzy	373	0.842024744	0.5	25 ;85.0 ;1.8	88595.97128	
1e+02 Zn50b	Fuzzy	432	0.842024744	0.5	25 ;85.0 ;1.8	102609.8112	
1e+03 Zn50a	Fuzzy	154	0.842024744	0.5	25 ;85.0 ;1.8	365784.9753	
1e+03 Zn50b	Fuzzy	141	0.842024744	0.5	25 ;85.0 ;1.8	334907.0228	
1e+04 Zn50a	Fuzzy	37	0.842024744	0.5	25 ;85.0 ;1.8	878834.0315	
1e+04 Zn50b	Fuzzy	35	0.842024744	0.5	25 ;85.0 ;1.8	831329.4893	
1e+02 Zn100a	Sharp	423	0.842024744	0.5	25 ;85.0 ;0.3	100472.1068	
1e+02 Zn100b	Fuzzy	281	0.842094719	0.5	30 ;85.0 ;1.8	66738.33561	
1e+03 Zn100a	Fuzzy	117	0.842094719	0.5	30 ;85.0 ;1.8	277878.4792	
1e+03 Zn100b	Fuzzy	118	0.842094719	0.5	30 ;85.0 ;1.8	280253.509	
1e+04 Zn100a	Fuzzy	26	0.842094719	0.5	30 ;85.0 ;1.8	617507.7316	
1e+04 Zn100b	Fuzzy	28	0.842094719	0.5	30 ;85.0 ;1.8	665008.3264	
1e+02 Zn200a	Fuzzy	278	0.842094719	0.5	15 ;85.0 ;0.8	66025.82669	
1e+02 Zn200b	Fuzzy	280	0.842094719	0.5	15 ;85.0 ;0.8	66500.83264	
1e+03 Zn200a	Fuzzy	81	0.842094719	0.5	15 ;85.0 ;0.8	192377.4087	
1e+03 Zn200b	Fuzzy	79	0.842094719	0.5	15 ;85.0 ;0.8	187627.3492	
1e+04 Zn200a	Fuzzy	13	0.842094719	0.5	15 ;85.0 ;0.8	308753.8658	
1e+04 Zn200b	Fuzzy	27	0.842094719	0.5	15 ;85.0 ;0.8	641258.029	

Table C.3: Preliminary MIC bioreactor experiment automatic colony counter t_0 CFU results. Plate Id gives the dilution factor and ZnO concentration (R denotes no ZnO present). The "Method" column gives the method of colony detection used by the colony counter software. Counted Volume gives the percentage of inoculated volume included in cell detection. Volume gives the volume of plated cells in ml. Input Values gives 3 figures - the threshold to the background, the diameter of the computed part of the Petri dish and the minimal colony diameter in mm.

Plate Id	Method	Counted Colonies	Counted Volume	Volume	Input Values	Concentration	Comments
1e+02 Zn200b	Fuzzy	3	0.848781645	0.5	25 ;89.0 ;1.8	706.8955877	
1e+02 Zn200a	Fuzzy	10	0.848781645	0.5	25 ;89.0 ;1.8	2356.318626	
1e+03 Zn200a	Fuzzy	1	0.848781645	0.5	25 ;89.0 ;1.8	2356.318626	
1e+03 Zn200b	Fuzzy	2	0.848781645	0.5	25 ;89.0 ;1.8	4712.637251	
1e+04 Zn200a	Fuzzy	0	0.848781645	0.5	25 ;89.0 ;1.8	0	
1e+04 Zn200b	Fuzzy	0	0.848781645	0.5	25 ;89.0 ;1.8	0	
1e+04 Zn100b	Fuzzy	126	0.848781645	0.5	25 ;89.0 ;1.8	2968961.468	
1e+04 Zn100a	Fuzzy	173	0.848781645	0.5	25 ;89.0 ;1.8	4076431.223	
1e+05 Zn100b	Fuzzy	258	0.848781645	0.5	25 ;89.0 ;1.8	60793020.54	
1e+05 Zn100b	Fuzzy	273	0.848781645	0.5	25 ;89.0 ;1.8	64327498.48	
1e+06 Zn100b	Fuzzy	140	0.848781645	0.5	25 ;89.0 ;1.8	329884607.6	
1e+06 Zn100a	Fuzzy	126	0.848781645	0.5	25 ;89.0 ;1.8	296896146.8	
1e+06 Zn50a	Fuzzy	608	0.848781645	0.5	25 ;89.0 ;1.3	1432641724	
1e+06 Zn50b	Fuzzy	470	0.848781645	0.5	25 ;89.0 ;1.3	1107469754	
1e+07 Zn50a	Fuzzy	224	0.848781645	0.5	25 ;89.0 ;1.3	5278153722	
1e+07 Zn50b	Fuzzy	199	0.848781645	0.5	25 ;89.0 ;1.3	4689074065	
1e+08 Zn50a	Fuzzy	21	0.848781645	0.5	25 ;89.0 ;1.3	4948269114	
1e+08 Zn50b	Fuzzy	39	0.848781645	0.5	25 ;89.0 ;1.3	9189642640	
1e+07 Rb	Fuzzy	39	0.848781645	0.5	25 ;89.0 ;1.3	918964264	
1e+06 Ra	Fuzzy	185	0.848781645	0.5	25 ;89.0 ;1.3	435918945.8	
1e+06 Rb	Fuzzy	255	0.848781645	0.5	25 ;89.0 ;1.3	600861249.6	
1e+07 Ra	Fuzzy	37	0.848781645	0.5	25 ;89.0 ;1.3	871837891.5	
1e+08 Ra	Fuzzy	4	0.848781645	0.5	25 ;89.0 ;1.8	942527450.3	
1e+08 Rb	Fuzzy	1	0.848781645	0.5	25 ;89.0 ;1.8	235631862.6	

Table C.4: Preliminary MIC bioreactor experiment automatic colony counter t_{24} CFU results. Plate Id gives the dilution factor and ZnO concentration (R denotes no ZnO present). The "Method" column gives the method of colony detection used by the colony counter software. Counted Volume gives the percentage of inoculated volume included in cell detection. Volume gives the volume of plated cells in ml. Input Values gives 3 figures - the threshold to the background, the diameter of the computed part of the Petri dish and the minimal colony diameter in mm.

Plate Id	Method	Counted Colonies	Counted Volume	Volume	Input Values	Concentration	Comments
1e+02 L+Zn t0a	Fuzzy	590	0.842024744	0.5	25 ;85.0 ;0.8	140138.3995	
1e+02 L+Zn t0b	Fuzzy	581	0.842024744	0.5	25 ;85.0 ;0.8	138000.6951	
1e+03 L+Zn t0a	Fuzzy	80	0.842024744	0.5	25 ;85.0 ;0.8	190018.1689	
1e+03 L+Zn t0b	Fuzzy	78	0.842024744	0.5	25 ;85.0 ;0.8	185267.7147	
1e+04 L+Zn t0a	Fuzzy	7	0.842024744	0.5	25 ;85.0 ;0.8	166265.8978	
1e+04 L+Zn t0b	Fuzzy	7	0.842024744	0.5	25 ;85.0 ;0.8	166265.8978	
1e+02 L t0a	Fuzzy	612	0.842024744	0.5	25 ;85.0 ;0.8	145363.8992	
1e+02 L t0b	Fuzzy	582	0.842024744	0.5	25 ;85.0 ;0.8	138238.2179	
1e+03 L t0a	Fuzzy	75	0.842024744	0.5	25 ;85.0 ;0.8	178142.0333	
1e+03 L t0b	Fuzzy	80	0.842024744	0.5	25 ;85.0 ;0.8	190018.1689	
1e+04 L t0a	Fuzzy	11	0.842024744	0.5	25 ;85.0 ;0.8	261274.9822	
1e+04 L t0b	Fuzzy	15	0.842024744	0.5	25 ;85.0 ;0.8	356284.0666	
1e+02 Zn t0a	Fuzzy	688	0.842024744	0.5	25 ;85.0 ;0.8	163415.6252	
1e+02 Zn t0b	Fuzzy	586	0.842024744	0.5	25 ;85.0 ;0.8	139188.3087	
1e+03 Zn t0a	Fuzzy	96	0.842024744	0.5	25 ;85.0 ;0.8	228021.8026	
1e+03 Zn t0b	Fuzzy	67	0.842024744	0.5	25 ;85.0 ;0.8	159140.2164	
1e+04 Zn t0a	Fuzzy	8	0.842024744	0.5	25 ;85.0 ;0.8	190018.1689	
1e+04 Zn t0b	Fuzzy	11	0.842024744	0.5	25 ;85.0 ;0.8	261274.9822	
1e+02 Ref t0a	Fuzzy	567	0.842024744	0.5	25 ;85.0 ;0.8	134675.3772	
1e+02 Ref t0b	Fuzzy	693	0.842024744	0.5	25 ;85.0 ;0.8	164603.2388	
1e+03 Ref t0a	Fuzzy	85	0.842024744	0.5	25 ;85.0 ;0.8	201894.3044	
1e+03 Ref t0b	Fuzzy	82	0.842024744	0.5	25 ;85.0 ;0.8	194768.6231	
1e+04 Ref t0a	Fuzzy	11	0.842024744	0.5	25 ;85.0 ;0.8	261274.9822	
1e+04 Ref t0b	Fuzzy	5	0.842024744	0.5	25 ;85.0 ;0.8	118761.3555	

Table C.5: Experiment 1, re-exposure 1 automatic colony counter results for initial CFU concentration and the computed concentration. Plate Id gives the dilution factor, measured group and other cell specifications. The "Method" column gives the method of colony detection used by the colony counter software. Counted Volume gives the percentage of inoculated volume included in cell detection. Volume gives the volume of plated cells in ml. Input Values gives 3 figures - the threshold to the background, the diameter of the computed part of the Petri dish and the minimal colony diameter in mm.

Plate Id	Method	Counted Colonies	Counted Volume	Volume	Input Values	Concentration	Comments
1e+09 Ref t24b	Fuzzy	1	0.842126966	0.5	25 ;85.0 ;1.3	2374938793	
1e+09 Ref t24a	Fuzzy	2	0.842126966	0.5	25 ;85.0 ;1.3	4749877586	
1e+08 Ref t24b	Fuzzy	11	0.842126966	0.5	25 ;85.0 ;1.3	2612432672	
1e+08 Ref t24a	Fuzzy	13	0.842126966	0.5	25 ;85.0 ;1.3	3087420431	
1e+07 Ref t24a	Fuzzy	114	0.842126966	0.5	25 ;85.0 ;0.8	2707430224	
1e+07 Ref t24b	Fuzzy	93	0.842126966	0.5	25 ;85.0 ;0.8	2208693077	
1e+09 L+Zn t24b	Fuzzy	3	0.842126966	0.5	25 ;85.0 ;0.8	7124816378	
1e+09 L+Zn t24a	Fuzzy	3	0.842126966	0.5	25 ;85.0 ;0.8	7124816378	
1e+08 L+Zn t24b	Fuzzy	11	0.842126966	0.5	25 ;85.0 ;0.8	2612432672	
1e+08 L+Zn t24a	Fuzzy	20	0.842126966	0.5	25 ;85.0 ;0.8	4749877586	
1e+07 L+Zn t24b	Fuzzy	113	0.842126966	0.5	25 ;85.0 ;0.8	2683680836	
1e+07 L+Zn t24a	Fuzzy	104	0.842126966	0.5	25 ;85.0 ;0.8	2469936344	
1e+09 L t24b	Fuzzy	3	0.842126966	0.5	25 ;85.0 ;0.8	7124816378	
1e+09 L t24a	Fuzzy	2	0.842126966	0.5	25 ;85.0 ;0.8	4749877586	
1e+08 L t24b	Fuzzy	25	0.842126966	0.5	25 ;85.0 ;0.3	5937346982	
1e+08 L t24a	Fuzzy	21	0.842126966	0.5	25 ;85.0 ;0.3	4987371465	
1e+07 L t24b	Fuzzy	211	0.842126966	0.5	25 ;85.0 ;0.3	5011120853	
1e+07 L t24b	Fuzzy	140	0.842126966	0.5	25 ;85.0 ;0.3	3324914310	
1e+08 Zn t24b	Fuzzy	21	0.842126966	0.5	25 ;85.0 ;0.3	4987371465	
1e+07 Zn t24b	Fuzzy	152	0.842126966	0.5	25 ;85.0 ;0.3	3609906965	
1e+07 Zn t24a	Fuzzy	127	0.842126966	0.5	25 ;85.0 ;0.3	3016172267	

Table C.6: Experiment 1, re-exposure 1 automatic colony counter results for endpoint CFU concentration and the computed concentration. Plate Id gives the dilution factor, measured group and other cell specifications. The "Method" column gives the method of colony detection used by the colony counter software. Counted Volume gives the percentage of inoculated volume included in cell detection. Volume gives the volume of plated cells in ml. Input Values gives 3 figures - the threshold to the background, the diameter of the computed part of the Petri dish and the minimal colony diameter in mm.

Plate Id	Method	Counted Colonies	Counted Volume	Volume	Input Values	Concentration	Comments
1e+02 Zn+L t0a	Fuzzy	230	0.842126966	0.5	30 ;85.0 ;2.3	54623.59223	
1e+02 Zn+L t0b	Fuzzy	184	0.842126966	0.5	30 ;85.0 ;2.3	43698.87379	
1e+03 Zn+L t0a	Fuzzy	49	0.842126966	0.5	30 ;85.0 ;2.3	116372.0008	
1e+03 Zn+L t0b	Fuzzy	40	0.842126966	0.5	30 ;85.0 ;2.3	94997.55171	
1e+04 Zn+L t0a	Fuzzy	6	0.842126966	0.5	30 ;85.0 ;2.3	142496.3276	
1e+04 Zn+L t0b	Fuzzy	13	0.842126966	0.5	30 ;85.0 ;2.3	308742.0431	
1e+02 Zn t0a	Fuzzy	247	0.842126966	0.5	30 ;85.0 ;2.3	58660.98818	
1e+02 Zn t0b	Fuzzy	156	0.842126966	0.5	30 ;85.0 ;2.3	37049.04517	
1e+03 Zn t0a	Fuzzy	55	0.842126966	0.5	30 ;85.0 ;2.3	130621.6336	
1e+03 Zn t0b	Fuzzy	44	0.842126966	0.5	30 ;85.0 ;2.3	104497.3069	
1e+04 Zn t0a	Fuzzy	11	0.842126966	0.5	30 ;85.0 ;2.3	261243.2672	
1e+04 Zn t0b	Fuzzy	8	0.842126966	0.5	25 ;85.0 ;2.3	189995.1034	
1e+02 L t0a	Fuzzy	69	0.842126966	0.5	25 ;85.0 ;2.3	16387.07767	
1e+02 L t0b	Fuzzy	218	0.842126966	0.5	25 ;85.0 ;2.3	51773.66568	
1e+03 L t0a	Fuzzy	50	0.842126966	0.5	25 ;85.0 ;2.3	118746.9396	
1e+03 L t0b	Fuzzy	62	0.842126966	0.5	25 ;85.0 ;2.3	147246.2052	
1e+04 L t0a	Fuzzy	11	0.842126966	0.5	25 ;85.0 ;2.3	261243.2672	
1e+04 L t0b	Fuzzy	13	0.842126966	0.5	25 ;85.0 ;2.3	308742.0431	
1e+02 Ref t0a	Fuzzy	112	0.842126966	0.5	25 ;85.0 ;2.3	26599.31448	
1e+02 Ref t0b	Fuzzy	237	0.842126966	0.5	25 ;85.0 ;2.3	56286.04939	
1e+03 Ref t0a	Fuzzy	61	0.842126966	0.5	25 ;85.0 ;2.3	144871.2664	
1e+03 Ref t0b	Fuzzy	51	0.842126966	0.5	25 ;85.0 ;2.3	121121.8784	
1e+04 Ref t0a	Fuzzy	7	0.842126966	0.5	25 ;85.0 ;2.3	166245.7155	
1e+04 Ref t0b	Fuzzy	4	0.842126966	0.5	25 ;85.0 ;1.3	94997.55171	

Table C.7: Experiment 1, re-exposure 2 automatic colony counter results for initial CFU concentration and the computed concentration. Plate Id gives the dilution factor, measured group and other cell specifications. The "Method" column gives the method of colony detection used by the colony counter software. Counted Volume gives the percentage of inoculated volume included in cell detection. Volume gives the volume of plated cells in ml. Input Values gives 3 figures - the threshold to the background, the diameter of the computed part of the Petri dish and the minimal colony diameter in mm.

Plate Id	Method	Counted Colonies	Counted Volume	Volume	Input Values	Concentration	Comments
1e+09 Zn+L t24b	Fuzzy	0	0.842126966	0.5	25 ;85.0 ;1.0	0	
1e+09 Zn+L t24a	Fuzzy	2	0.842126966	0.5	25 ;85.0 ;1.0	4749877586	
1e+08 Zn+L t24b	Fuzzy	6	0.842126966	0.5	25 ;85.0 ;1.0	1424963276	
1e+08 Zn+L t24a	Fuzzy	8	0.842126966	0.5	25 ;85.0 ;1.0	1899951034	
1e+07 Zn+L t24b	Fuzzy	84	0.842126966	0.5	25 ;85.0 ;1.0	1994948586	
1e+07 Zn+L t24a	Fuzzy	74	0.842126966	0.5	25 ;85.0 ;1.0	1757454707	
1e+09 Zn t24b	Fuzzy	2	0.842126966	0.5	25 ;85.0 ;1.0	4749877586	
1e+09 Zn t24a	Fuzzy	2	0.842126966	0.5	25 ;85.0 ;1.0	4749877586	
1e+07 Zn t24b	Fuzzy	13	0.842126966	0.5	25 ;85.0 ;1.0	308742043.1	
1e+07 Zn t24a	Fuzzy	7	0.842126966	0.5	25 ;85.0 ;1.0	166245715.5	
1e+07 Zn t24b	Fuzzy	135	0.842126966	0.5	25 ;85.0 ;1.0	3206167370	
1e+07 Zn t24a	Fuzzy	98	0.842126966	0.5	25 ;85.0 ;1.0	2327440017	
1e+09 L t24b	Fuzzy	687	0.842126966	0.5	25 ;85.0 ;1.0	1.63E+12	
1e+09 L t24a	Fuzzy	621	0.842126966	0.5	25 ;85.0 ;1.0	1.47E+12	
1e+08 L t24b	Fuzzy	691	0.842126966	0.5	25 ;85.0 ;1.0	1.64E+11	
1e+08 L t24a	Fuzzy	904	0.842126966	0.5	25 ;85.0 ;1.0	2.15E+11	
1e+07 L t24b	Fuzzy	500	0.842126966	0.5	25 ;85.0 ;1.0	11874693964	
1e+09 L t24	Fuzzy	18	0.842126966	0.5	26 ;85.0 ;1.0	42748898270	A
1e+08 L t24	Fuzzy	63	0.842126966	0.5	27 ;85.0 ;1.0	14962114395	A
1e+07 L t24	Fuzzy	139	0.842126966	0.5	28 ;85.0 ;1.0	3301164922	A
1e+07 L t24a	Fuzzy	683	0.842126966	0.5	25 ;85.0 ;1.0	16220831955	
1e+09 R t24b	Fuzzy	0	0.842126966	0.5	25 ;85.0 ;1.0	0	
1e+09 R t24a	Fuzzy	1	0.842126966	0.5	25 ;85.0 ;1.0	2374938793	
1e+08 R t24b	Fuzzy	15	0.842126966	0.5	25 ;85.0 ;1.0	3562408189	
1e+08 R t24a	Fuzzy	9	0.842126966	0.5	25 ;85.0 ;1.0	2137444914	
1e+07 R t24b	Fuzzy	114	0.842126966	0.5	25 ;85.0 ;1.0	2707430224	
1e+07 R t24a	Fuzzy	111	0.842126966	0.5	25 ;85.0 ;1.0	2636182060	

Table C.8: Experiment 1, re-exposure 2, automatic colony counter results for endpoint CFU concentration and the computed concentration. Plate Id gives the dilution factor, measured group and other cell specifications. The "Method" column gives the method of colony detection used by the colony counter software. Counted Volume gives the percentage of inoculated volume included in cell detection. Volume gives the volume of plated cells in ml. Input Values gives 3 figures - the threshold to the background, the diameter of the computed part of the Petri dish and the minimal colony diameter in mm. In the comments section, samples with the letter A were remeasured 24 hours after incubation.

Plate Id	Method	Counted Colonies	Counted Volume	Volume	Input Values	Concentration	Comments
1e+02 L t0b	Fuzzy	653	0.842126966	0.5	25 ;85.0 ;1.3	155083.5032	
1e+02 L t0a	Fuzzy	663	0.842126966	0.5	25 ;85.0 ;1.3	157458.442	
1e+03 L t0b	Fuzzy	121	0.842126966	0.5	25 ;85.0 ;1.3	287367.5939	
1e+03 L t0a	Fuzzy	142	0.842126966	0.5	25 ;85.0 ;1.3	337241.3086	
1e+04 L t0b	Fuzzy	12	0.842126966	0.5	25 ;85.0 ;1.3	284992.6551	
1e+04 L t0a	Fuzzy	15	0.842126966	0.5	25 ;85.0 ;1.3	356240.8189	
1e+02 Zn t0b	Fuzzy	313	0.842126966	0.5	25 ;85.0 ;1.3	74335.58421	
1e+02 Zn t0a	Fuzzy	293	0.842126966	0.5	25 ;85.0 ;1.3	69585.70663	
1e+03 Zn t0b	Fuzzy	42	0.842126966	0.5	25 ;85.0 ;1.3	99747.4293	
1e+03 Zn t0a	Fuzzy	42	0.842126966	0.5	25 ;85.0 ;1.3	99747.4293	
1e+04 Zn t0b	Fuzzy	6	0.842126966	0.5	25 ;85.0 ;1.3	142496.3276	
1e+04 Zn t0a	Fuzzy	3	0.842126966	0.5	25 ;85.0 ;1.3	71248.16378	
1e+02 R t0b	Fuzzy	483	0.842126966	0.5	25 ;85.0 ;1.3	114709.5437	
1e+02 R t0a	Fuzzy	534	0.842126966	0.5	25 ;85.0 ;1.3	126821.7315	
1e+03 R t0a	Fuzzy	93	0.842126966	0.5	25 ;85.0 ;1.3	220869.3077	
1e+03 R t0b	Fuzzy	78	0.842126966	0.5	25 ;85.0 ;1.3	185245.2258	
1e+04 R t0a	Fuzzy	12	0.842126966	0.5	25 ;85.0 ;1.3	284992.6551	
1e+04 R t0b	Fuzzy	11	0.842126966	0.5	25 ;85.0 ;1.3	261243.2672	
1e+02 Zn+L t0b	Fuzzy	377	0.842126966	0.5	25 ;85.0 ;1.3	89535.19249	
1e+02 Zn+L t0a	Fuzzy	344	0.842126966	0.5	25 ;85.0 ;1.3	81697.89447	
1e+03 Zn+L t0b	Fuzzy	76	0.842126966	0.5	25 ;85.0 ;1.3	180495.3483	
1e+03 Zn+L t0a	Fuzzy	45	0.842126966	0.5	25 ;85.0 ;1.3	106872.2457	
1e+04 Zn+L t24b	Fuzzy	4	0.842126966	0.5	25 ;85.0 ;1.3	94997.55171	
1e+04 Zn+L t24a	Fuzzy	5	0.842126966	0.5	25 ;85.0 ;1.3	118746.9396	

Table C.9: Experiment 1, re-exposure 3, repetition 1 automatic colony counter results for initial CFU concentration and the computed concentration. Plate Id gives the dilution factor, measured group and other cell specifications. The "Method" column gives the method of colony detection used by the colony counter software. Counted Volume gives the percentage of inoculated volume included in cell detection. Volume gives the volume of plated cells in ml. Input Values gives 3 figures - the threshold to the background, the diameter of the computed part of the Petri dish and the minimal colony diameter in mm.

Plate Id	Method	Counted Colonies	Counted Volume	Volume	Input Values	Concentration	Comments
1e+09 Zn+L t24a	Fuzzy	0	0.842126966	0.5	25 ;85.0 ;2.0	0	
1e+09 Zn+L t24b	Fuzzy	0	0.842126966	0.5	25 ;85.0 ;2.0	0	
1e+08 Zn+L t24a	Fuzzy	4	0.842126966	0.5	25 ;85.0 ;2.0	949975517.1	
1e+08 Zn+L t24b	Fuzzy	3	0.842126966	0.5	25 ;85.0 ;2.0	712481637.8	
1e+07 Zn+L t24a	Fuzzy	35	0.842126966	0.5	25 ;85.0 ;2.0	831228577.5	
1e+07 Zn+L t24b	Fuzzy	27	0.842126966	0.5	25 ;85.0 ;2.0	641233474.1	
1e+04 Zn t24a	Fuzzy	0	0.842126966	0.5	25 ;85.0 ;2.0	0	
1e+04 Zn t24b	Fuzzy	0	0.842126966	0.5	25 ;85.0 ;2.0	0	
1e+03 Zn t24a	Fuzzy	0	0.842126966	0.5	25 ;85.0 ;2.0	0	
1e+03 Zn t24b	Fuzzy	1	0.842126966	0.5	25 ;85.0 ;2.0	2374.938793	
1e+02 Zn t24a	Fuzzy	20	0.842126966	0.5	25 ;85.0 ;2.0	4749.877586	
1e+02 Zn t24b	Fuzzy	13	0.842126966	0.5	25 ;85.0 ;2.0	3087.420431	
1e+09 L t24a	Fuzzy	1	0.842126966	0.5	25 ;85.0 ;1.0	2374938793	
1e+09 L t24b	Fuzzy	2	0.842126966	0.5	25 ;85.0 ;1.0	4749877586	
1e+08 L t24a	Fuzzy	13	0.842126966	0.5	25 ;85.0 ;1.0	3087420431	
1e+08 L t24b	Fuzzy	7	0.842126966	0.5	25 ;85.0 ;1.0	1662457155	
1e+07 L t24a	Fuzzy	103	0.842126966	0.5	25 ;85.0 ;1.0	2446186957	
1e+07 L t24b	Fuzzy	83	0.842126966	0.5	25 ;85.0 ;1.0	1971199198	
1e+09 R t24a	Fuzzy	0	0.842126966	0.5	25 ;85.0 ;1.0	0	
1e+09 R t24b	Fuzzy	0	0.842126966	0.5	25 ;85.0 ;1.0	0	
1e+08 R t24a	Fuzzy	12	0.842126966	0.5	25 ;85.0 ;1.0	2849926551	
1e+08 R t24b	Fuzzy	12	0.842126966	0.5	25 ;85.0 ;1.0	2849926551	
1e+07 R t24a	Fuzzy	157	0.842126966	0.5	25 ;85.0 ;1.0	3728653905	
1e+07 R t24b	Fuzzy	117	0.842126966	0.5	25 ;85.0 ;1.0	2778678388	

Table C.10: Experiment 1, re-exposure 3, repetition 1 automatic colony counter results for endpoint CFU concentration and the computed concentration. Plate Id gives the dilution factor, measured group and other cell specifications. The "Method" column gives the method of colony detection used by the colony counter software. Counted Volume gives the percentage of inoculated volume included in cell detection. Volume gives the volume of plated cells in ml. Input Values gives 3 figures - the threshold to the background, the diameter of the computed part of the Petri dish and the minimal colony diameter in mm.

Plate Id	Method	Counted Colonies	Counted Volume	Volume	Input Values	Concentration	Comments
1e+04 L t0a	Fuzzy	1	0.842126966	0.5	25 ;85.0 ;1.8	23749.38793	
1e+04 L t0b	Fuzzy	6	0.842126966	0.5	25 ;85.0 ;1.8	142496.3276	
1e+03 L t0a	Fuzzy	36	0.842126966	0.5	25 ;85.0 ;1.8	85497.79654	
1e+03 L t0b	Fuzzy	50	0.842126966	0.5	25 ;85.0 ;1.8	118746.9396	
1e+02 L t0b	Fuzzy	248	0.842126966	0.5	25 ;85.0 ;1.8	58898.48206	
1e+02 L t0b	Fuzzy	173	0.842126966	0.5	25 ;85.0 ;1.8	41086.44112	
1e+04 R t0a	Fuzzy	5	0.842126966	0.5	25 ;85.0 ;1.8	118746.9396	
1e+04 R t0b	Fuzzy	2	0.842126966	0.5	25 ;85.0 ;1.8	47498.77586	
1e+03 R t0a	Fuzzy	20	0.842126966	0.5	25 ;85.0 ;1.8	47498.77586	
1e+03 R t0b	Fuzzy	18	0.842126966	0.5	25 ;85.0 ;1.8	42748.89827	
1e+02 R t0a	Fuzzy	184	0.842126966	0.5	25 ;85.0 ;0.8	43698.87379	
1e+02 R t0b	Fuzzy	179	0.842126966	0.5	25 ;85.0 ;0.8	42511.40439	
1e+04 Zn t0a	Fuzzy	5	0.842126966	0.5	25 ;85.0 ;0.8	118746.9396	
1e+04 Zn t0b	Fuzzy	4	0.842126966	0.5	25 ;85.0 ;0.8	94997.55171	
1e+03 Zn t0a	Fuzzy	37	0.842126966	0.5	25 ;85.0 ;0.8	87872.73533	
1e+03 Zn t0b	Fuzzy	27	0.842126966	0.5	25 ;85.0 ;0.8	64123.34741	
1e+02 Zn t0a	Fuzzy	274	0.842126966	0.5	25 ;85.0 ;0.8	65073.32292	
1e+02 Zn t0b	Fuzzy	261	0.842126966	0.5	25 ;85.0 ;0.8	61985.90249	
1e+02 L+Zn t0b	Fuzzy	226	0.842126966	0.5	25 ;85.0 ;0.8	53673.61672	
1e+02 L+Zn t0a	Fuzzy	218	0.842126966	0.5	25 ;85.0 ;0.8	51773.66568	
1e+03 L+Zn t0b	Fuzzy	31	0.842126966	0.5	25 ;85.0 ;0.8	73623.10258	
1e+03 L+Zn t0a	Fuzzy	28	0.842126966	0.5	25 ;85.0 ;0.8	66498.2862	
1e+04 L+Zn t0a	Fuzzy	3	0.842126966	0.5	25 ;85.0 ;0.8	71248.16378	
1e+04 L+Zn t0b	Fuzzy	4	0.842126966	0.5	25 ;85.0 ;0.8	94997.55171	

Table C.11: Experiment 1, re-exposure 3, repetition 2 automatic colony counter results for initial CFU concentration and the computed concentration. Plate Id gives the dilution factor, measured group and other cell specifications. The "Method" column gives the method of colony detection used by the colony counter software. Counted Volume gives the percentage of inoculated volume included in cell detection. Volume gives the volume of plated cells in ml. Input Values gives 3 figures - the threshold to the background, the diameter of the computed part of the Petri dish and the minimal colony diameter in mm.

Plate Id	Method	Counted Colonies	Counted Volume	Volume	Input Values	Concentration	Comments
1e+09 L t24a	Fuzzy	1	0.842126966	0.5	25 ;85.0 ;1.3	2374938793	
1e+09 L t24b	Fuzzy	3	0.842126966	0.5	25 ;85.0 ;1.3	7124816378	
1e+08 L t24a	Fuzzy	12	0.842126966	0.5	25 ;85.0 ;0.8	2849926551	
1e+08 L t24b	Fuzzy	11	0.842126966	0.5	25 ;85.0 ;0.8	2612432672	
1e+08 L t24b	Fuzzy	18	0.842126966	0.5	25 ;85.0 ;0.3	4274889827	
1e+07 L t24a	Fuzzy	105	0.842126966	0.5	25 ;85.0 ;0.3	2493685732	
1e+07 L t24b	Fuzzy	131	0.842126966	0.5	25 ;85.0 ;0.3	3111169819	
1e+01 L+Zn t24a	Fuzzy	2567	0.842126966	0.5	25 ;85.0 ;0.3	60964.67881	
1e+01 L+Zn t24b	Fuzzy	1461	0.842126966	0.5	25 ;85.0 ;0.3	34697.85576	
1e+02 L+Zn t24a	Fuzzy	395	0.842126966	0.5	25 ;85.0 ;0.3	93810.08231	
1e+02 L+Zn t24b	Fuzzy	438	0.842126966	0.5	25 ;85.0 ;0.3	104022.3191	
1e+03 L+Zn t24a	Fuzzy	57	0.842126966	0.5	25 ;85.0 ;0.8	135371.5112	
1e+03 L+Zn t24b	Fuzzy	55	0.842126966	0.5	25 ;85.0 ;0.8	130621.6336	
1e+09 R t24a	Fuzzy	1	0.842126966	0.5	25 ;85.0 ;0.8	2374938793	
1e+09 R t24b	Fuzzy	5	0.842126966	0.5	25 ;85.0 ;0.8	11874693964	
1e+08 R t24b	Fuzzy	38	0.842126966	0.5	25 ;85.0 ;0.8	9024767413	
1e+08 R t24a	Fuzzy	23	0.842126966	0.5	25 ;85.0 ;0.8	5462359223	
1e+07 R t24b	Fuzzy	171	0.842126966	0.5	25 ;85.0 ;0.8	4061145336	
1e+07 R t24a	Fuzzy	199	0.842126966	0.5	25 ;85.0 ;0.8	4726128198	

Table C.12: Experiment 1, re-exposure 3, repetition 2 automatic colony counter results for endpoint CFU concentration and the computed concentration. Plate Id gives the dilution factor, measured group and other cell specifications. The "Method" column gives the method of colony detection used by the colony counter software. Counted Volume gives the percentage of inoculated volume included in cell detection. Volume gives the volume of plated cells in ml. Input Values gives 3 figures - the threshold to the background, the diameter of the computed part of the Petri dish and the minimal colony diameter in mm.

Plate Id	Method	Counted Colonies	Counted Volume	Volume	Input Values	Concentration	Comments
1e+04 L+Zn t0vb	Fuzzy	2	0.842126966	0.5	25 ;85.0 ;0.8	47498.77586	
1e+04 L+Zn t0a	Fuzzy	4	0.842126966	0.5	25 ;85.0 ;0.8	94997.55171	
1e+03 L+Zn t0a	Fuzzy	55	0.842126966	0.5	25 ;85.0 ;0.8	130621.6336	
1e+03 L+Zn t0b	Fuzzy	52	0.842126966	0.5	25 ;85.0 ;0.8	123496.8172	
1e+02 L+Zn t0b	Fuzzy	350	0.842126966	0.5	25 ;85.0 ;0.8	83122.85775	
1e+02 L+Zn t0a	Fuzzy	363	0.842126966	0.5	25 ;85.0 ;0.8	86210.27818	
1e+04 R t0b	Fuzzy	7	0.842126966	0.5	25 ;85.0 ;0.8	166245.7155	
1e+04 R t0a	Fuzzy	6	0.842126966	0.5	25 ;85.0 ;0.8	142496.3276	
1e+03 R t0a	Fuzzy	23	0.842126966	0.5	25 ;85.0 ;0.8	54623.59223	
1e+03 R t0b	Fuzzy	30	0.842126966	0.5	25 ;85.0 ;0.8	71248.16378	
1e+02 R t0b	Fuzzy	269	0.842126966	0.5	25 ;85.0 ;0.8	63885.85353	
1e+02 R t0a	Fuzzy	258	0.842126966	0.5	25 ;85.0 ;0.8	61273.42085	
1e+04 L t0a	Fuzzy	0	0.842126966	0.5	25 ;85.0 ;0.8	0	
1e+04 L t0b	Fuzzy	13	0.842126966	0.5	25 ;85.0 ;0.8	308742.0431	
1e+03 L t0b	Fuzzy	64	0.842126966	0.5	25 ;85.0 ;0.8	151996.0827	
1e+03 L t0a	Fuzzy	45	0.842126966	0.5	25 ;85.0 ;0.8	106872.2457	
1e+02 L t0b	Fuzzy	502	0.842126966	0.5	25 ;85.0 ;0.8	119221.9274	
1e+02 L t0a	Fuzzy	388	0.842126966	0.5	25 ;85.0 ;0.8	92147.62516	
1e+04 Zn t0a	Fuzzy	4	0.842126966	0.5	25 ;85.0 ;0.8	94997.55171	
1e+04 Zn t0b	Fuzzy	4	0.842126966	0.5	25 ;85.0 ;0.8	94997.55171	
1e+03 Zn t0b	Fuzzy	55	0.842126966	0.5	25 ;85.0 ;0.8	130621.6336	
1e+03 Zn t0a	Fuzzy	49	0.842126966	0.5	25 ;85.0 ;0.8	116372.0008	
1e+02 Zn t0a	Fuzzy	413	0.842126966	0.5	25 ;85.0 ;0.3	98084.97214	
1e+02 Zn t0b	Fuzzy	349	0.842126966	0.5	25 ;85.0 ;0.3	82885.36387	

Table C.13: Experiment 1, re-exposure 3, repetition 3 automatic colony counter results for initial CFU concentration and the computed concentration. Plate Id gives the dilution factor, measured group and other cell specifications. The "Method" column gives the method of colony detection used by the colony counter software. Counted Volume gives the percentage of inoculated volume included in cell detection. Volume gives the volume of plated cells in ml. Input Values gives 3 figures - the threshold to the background, the diameter of the computed part of the Petri dish and the minimal colony diameter in mm.

Plate Id	Method	Counted Colonies	Counted Volume	Volume	Input Values	Concentration	Comments
1e+09 L+Zn t24a	Fuzzy	1	0.842126966	0.5	25 ;85.0 ;1.5	2374938793	
1e+09 L+Zn t24b	Fuzzy	0	0.842126966	0.5	25 ;85.0 ;1.5	0	
1e+08 L+Zn t24a	Fuzzy	0	0.842126966	0.5	25 ;85.0 ;1.5	0	
1e+08 L+Zn t24b	Fuzzy	1	0.842126966	0.5	25 ;85.0 ;1.5	237493879.3	
1e+07 L+Zn t24a	Fuzzy	18	0.842126966	0.5	25 ;85.0 ;1.5	427488982.7	
1e+07 L+Zn t24b	Fuzzy	19	0.842126966	0.5	25 ;85.0 ;1.5	451238370.6	
1e+09 L t24a	Fuzzy	1	0.842126966	0.5	25 ;85.0 ;1.5	2374938793	
1e+09 L t24b	Fuzzy	0	0.842126966	0.5	25 ;85.0 ;1.5	0	
1e+08 L t24a	Fuzzy	13	0.842126966	0.5	25 ;85.0 ;1.5	3087420431	
1e+08 L t24b	Fuzzy	11	0.842126966	0.5	25 ;85.0 ;1.5	2612432672	
1e+07 L t24a	Fuzzy	88	0.842126966	0.5	25 ;85.0 ;1.5	2089946138	
1e+07 L t24b	Fuzzy	94	0.842126966	0.5	25 ;85.0 ;1.5	2232442465	
1e+03 Zn t24a	Fuzzy	31	0.842126966	0.5	25 ;85.0 ;1.5	73623.10258	
1e+03 Zn t24b	Fuzzy	63	0.842126966	0.5	25 ;85.0 ;1.5	149621.1439	
1e+02 Zn t24a	Fuzzy	39	0.842126966	0.5	25 ;85.0 ;1.0	9262.261292	
1e+02 Zn t24b	Fuzzy	387	0.842126966	0.5	25 ;85.0 ;1.0	91910.13128	
1e+01 Zn t24a	Fuzzy	403	0.842126966	0.5	25 ;85.0 ;1.0	9571.003335	
1e+01 Zn t24b	Fuzzy	379	0.842126966	0.5	25 ;85.0 ;1.0	9001.018025	
1e+09 R t24a	Fuzzy	3	0.842126966	0.5	25 ;85.0 ;1.0	7124816378	
1e+09 R t24b	Fuzzy	3	0.842126966	0.5	25 ;85.0 ;1.0	7124816378	
1e+08 R t24a	Fuzzy	10	0.842126966	0.5	25 ;85.0 ;1.0	2374938793	
1e+08 R t24b	Fuzzy	12	0.842126966	0.5	25 ;85.0 ;1.0	2849926551	
1e+07 R t24a	Fuzzy	131	0.842126966	0.5	25 ;85.0 ;1.0	3111169819	
1e+07 R t24b	Fuzzy	135	0.842126966	0.5	25 ;85.0 ;1.0	3206167370	

Table C.14: Experiment 1, re-exposure 3, repetition 3 automatic colony counter results for endpoint CFU concentration and the computed concentration. Plate Id gives the dilution factor, measured group and other cell specifications. The "Method" column gives the method of colony detection used by the colony counter software. Counted Volume gives the percentage of inoculated volume included in cell detection. Volume gives the volume of plated cells in ml. Input Values gives 3 figures - the threshold to the background, the diameter of the computed part of the Petri dish and the minimal colony diameter in mm.

Plate Id	Method	Counted Colonies	Counted Volume	Volume	Input Values	Concentration	Comments
1e+04 R t0a	Fuzzy	3	0.842126966	0.5	25 ;85.0 ;0.8	71248.16378	
1e+04 R t0b	Fuzzy	2	0.842126966	0.5	25 ;85.0 ;0.8	47498.77586	
1e+03 R t0b	Fuzzy	5	0.842126966	0.5	25 ;85.0 ;0.8	11874.69396	
1e+03 R t0a	Fuzzy	18	0.842126966	0.5	25 ;85.0 ;0.8	42748.89827	
1e+02 R t0a	Fuzzy	145	0.842126966	0.5	25 ;85.0 ;0.8	34436.6125	
1e+02 R t0b	Fuzzy	123	0.842126966	0.5	25 ;85.0 ;0.8	29211.74715	
1e+04 Zn t0a	Fuzzy	0	0.842126966	0.5	25 ;85.0 ;0.8	0	
1e+04 Zn t0b	Fuzzy	0	0.842126966	0.5	25 ;85.0 ;0.8	0	
1e+03 Zn t0a	Fuzzy	15	0.842126966	0.5	25 ;85.0 ;0.3	35624.08189	
1e+03 Zn t0b	Fuzzy	9	0.842126966	0.5	25 ;85.0 ;0.8	21374.44914	
1e+02 Zn t0a	Fuzzy	144	0.842126966	0.5	25 ;85.0 ;0.8	34199.11862	
1e+02 Zn t0b	Fuzzy	140	0.842126966	0.5	25 ;85.0 ;0.8	33249.1431	
1e+04 L t0a	Fuzzy	1	0.842126966	0.5	25 ;85.0 ;0.8	23749.38793	
1e+04 L t0b	Fuzzy	0	0.842126966	0.5	25 ;85.0 ;0.8	0	
1e+03 L t0a	Fuzzy	12	0.842126966	0.5	25 ;85.0 ;0.8	28499.26551	
1e+03 L t0b	Fuzzy	9	0.842126966	0.5	25 ;85.0 ;0.8	21374.44914	
1e+02 L t0a	Fuzzy	120	0.842126966	0.5	25 ;85.0 ;0.8	28499.26551	
1e+02 L t0b	Fuzzy	116	0.842126966	0.5	25 ;85.0 ;0.8	27549.29	
1e+04 L+Zn t0b	Fuzzy	0	0.842126966	0.5	25 ;85.0 ;0.8	0	
1e+04 L+Zn t0a	Fuzzy	1	0.842126966	0.5	25 ;85.0 ;0.8	23749.38793	
1e+03 L+Zn t0b	Fuzzy	14	0.842126966	0.5	25 ;85.0 ;0.8	33249.1431	
1e+03 L+Zn t0a	Fuzzy	15	0.842126966	0.5	25 ;85.0 ;0.3	35624.08189	
1e+02 L+Zn t0a	Fuzzy	153	0.842126966	0.5	25 ;85.0 ;0.3	36336.56353	
1e+02 L+Zn t0b	Fuzzy	167	0.842126966	0.5	25 ;85.0 ;0.3	39661.47784	

Table C.15: Experiment 2, re-exposure 1 automatic colony counter results for initial CFU concentration and the computed concentration. Plate Id gives the dilution factor, measured group and other cell specifications. The "Method" column gives the method of colony detection used by the colony counter software. Counted Volume gives the percentage of inoculated volume included in cell detection. Volume gives the volume of plated cells in ml. Input Values gives 3 figures - the threshold to the background, the diameter of the computed part of the Petri dish and the minimal colony diameter in mm.

Plate Id	Method	Counted Colonies	Counted Volume	Volume	Input Values	Concentration	Comments
1e+07 R t24b	Fuzzy	133	0.842126966	0.5	25 ;85.0 ;0.8	3158668594	
1e+07 R t24a	Fuzzy	110	0.842126966	0.5	25 ;85.0 ;0.8	2612432672	
1e+08 R t24b	Fuzzy	9	0.842126966	0.5	25 ;85.0 ;0.8	2137444914	
1e+08 R t24a	Fuzzy	10	0.842126966	0.5	25 ;85.0 ;0.8	2374938793	
1e+09 R t24b	Fuzzy	2	0.842126966	0.5	25 ;85.0 ;0.8	4749877586	
1e+09 R t24a	Fuzzy	2	0.842126966	0.5	25 ;85.0 ;0.8	4749877586	
1e+07 L t24b	Fuzzy	171	0.842126966	0.5	25 ;85.0 ;0.8	4061145336	
1e+07 L t24a	Fuzzy	153	0.842126966	0.5	25 ;85.0 ;0.8	3633656353	
1e+08 L t24b	Fuzzy	15	0.842126966	0.5	25 ;85.0 ;0.8	3562408189	
1e+08 L t24a	Fuzzy	13	0.842126966	0.5	25 ;85.0 ;0.8	3087420431	
1e+09 L t24b	Fuzzy	4	0.842126966	0.5	25 ;85.0 ;0.8	9499755171	
1e+09 L t24a	Fuzzy	1	0.842126966	0.5	25 ;85.0 ;0.8	2374938793	
1e+07 L+Zn t24b	Fuzzy	119	0.842126966	0.5	25 ;85.0 ;0.8	2826177163	
1e+07 L+Zn t24a	Fuzzy	92	0.842126966	0.5	25 ;85.0 ;0.8	2184943689	
1e+08 L+Zn t24b	Fuzzy	16	0.842126966	0.5	25 ;85.0 ;0.8	3799902068	
1e+08 L+Zn t24a	Fuzzy	7	0.842126966	0.5	25 ;85.0 ;0.8	1662457155	
1e+09 L+Zn t24b	Fuzzy	1	0.842126966	0.5	25 ;85.0 ;0.8	2374938793	
1e+09 L+Zn t24a	Fuzzy	0	0.842126966	0.5	25 ;85.0 ;0.8	0	
1e+07 Zn t24b	Fuzzy	65	0.842126966	0.5	25 ;85.0 ;0.8	1543710215	
1e+07 Zn t24a	Fuzzy	76	0.842126966	0.5	25 ;85.0 ;0.8	1804953483	
1e+08 Zn t24b	Fuzzy	5	0.842126966	0.5	25 ;85.0 ;0.8	1187469396	
1e+08 Zn t24a	Fuzzy	5	0.842126966	0.5	25 ;85.0 ;0.8	1187469396	
1e+09 Zn t24b	Fuzzy	0	0.842126966	0.5	25 ;85.0 ;0.8	0	
1e+09 Zn t24a	Fuzzy	0	0.842126966	0.5	25 ;85.0 ;0.8	0	

Table C.16: Experiment 2, re-exposure 1 automatic colony counter results for endpoint CFU concentration and the computed concentration. Plate Id gives the dilution factor, measured group and other cell specifications. The "Method" column gives the method of colony detection used by the colony counter software. Counted Volume gives the percentage of inoculated volume included in cell detection. Volume gives the volume of plated cells in ml. Input Values gives 3 figures - the threshold to the background, the diameter of the computed part of the Petri dish and the minimal colony diameter in mm.

Plate Id	Method	Counted Colonies	Counted Volume	Volume	Input Values	Concentration	Comments
1e+02 L t0b	Fuzzy	559	0.842126966	0.5	25 ;85.0 ;0.8	132759.0785	
1e+02 L t0a	Fuzzy	607	0.842126966	0.5	25 ;85.0 ;0.8	144158.7847	
1e+03 L t0b	Fuzzy	104	0.842126966	0.5	25 ;85.0 ;0.8	246993.6344	
1e+03 L t0a	Fuzzy	100	0.842126966	0.5	25 ;85.0 ;0.8	237493.8793	
1e+04 L t0b	Fuzzy	10	0.842126966	0.5	25 ;85.0 ;0.8	237493.8793	
1e+04 L t0a	Fuzzy	12	0.842126966	0.5	25 ;85.0 ;0.8	284992.6551	
1e+02 L+Zn t0b	Fuzzy	659	0.842126966	0.5	25 ;85.0 ;0.8	156508.4664	
1e+02 L+Zn t0a	Fuzzy	468	0.842126966	0.5	25 ;85.0 ;0.8	111147.1355	
1e+03 L+Zn t0b	Fuzzy	65	0.842126966	0.5	25 ;85.0 ;0.8	154371.0215	
1e+03 L+Zn t0a	Fuzzy	73	0.842126966	0.5	25 ;85.0 ;0.8	173370.5319	
1e+04 L+Zn t0b	Fuzzy	13	0.842126966	0.5	25 ;85.0 ;0.8	308742.0431	
1e+04 L+Zn t0a	Fuzzy	15	0.842126966	0.5	25 ;85.0 ;0.8	356240.8189	
1e+04 R t0a	Fuzzy	4	0.842126966	0.5	25 ;85.0 ;0.8	94997.55171	
1e+04 R t0b	Fuzzy	5	0.842126966	0.5	25 ;85.0 ;0.8	118746.9396	
1e+03 R t0a	Fuzzy	59	0.842126966	0.5	25 ;85.0 ;0.8	140121.3888	
1e+03 R t0b	Fuzzy	60	0.842126966	0.5	25 ;85.0 ;0.8	142496.3276	
1e+02 R t0a	Fuzzy	497	0.842126966	0.5	25 ;85.0 ;0.8	118034.458	
1e+02 R t0b	Fuzzy	434	0.842126966	0.5	25 ;85.0 ;0.8	103072.3436	
1e+04 Zn t0a	Fuzzy	4	0.842126966	0.5	25 ;85.0 ;0.8	94997.55171	
1e+04 Zn t0b	Fuzzy	8	0.842126966	0.5	25 ;85.0 ;0.8	189995.1034	
1e+03 Zn t0a	Fuzzy	57	0.842126966	0.5	25 ;85.0 ;0.3	135371.5112	
1e+03 Zn t0b	Fuzzy	75	0.842126966	0.5	25 ;85.0 ;0.3	178120.4095	
1e+02 Zn t0a	Fuzzy	468	0.842126966	0.5	25 ;85.0 ;0.3	111147.1355	
1e+02 Zn t0b	Fuzzy	557	0.842126966	0.5	25 ;85.0 ;0.3	132284.0908	

Table C.17: Experiment 2, re-exposure 2 automatic colony counter results for initial CFU concentration and the computed concentration. Plate Id gives the dilution factor, measured group and other cell specifications. The "Method" column gives the method of colony detection used by the colony counter software. Counted Volume gives the percentage of inoculated volume included in cell detection. Volume gives the volume of plated cells in ml. Input Values gives 3 figures - the threshold to the background, the diameter of the computed part of the Petri dish and the minimal colony diameter in mm.

Plate Id	Method	Counted Colonies	Counted Volume	Volume	Input Values	Concentration	Comments
1e+09 L+Zn t24a	Fuzzy	0	0.842126966	0.5	25 ;85.0 ;1.3	0	
1e+09 L+Zn t24b	Fuzzy	2	0.842126966	0.5	25 ;85.0 ;1.3	4749877586	
1e+08 L+Zn t24a	Fuzzy	2	0.842126966	0.5	25 ;85.0 ;1.3	474987758.6	
1e+08 L+Zn t24b	Fuzzy	8	0.842126966	0.5	25 ;85.0 ;1.3	1899951034	
1e+07 L+Zn t24a	Fuzzy	52	0.842126966	0.5	25 ;85.0 ;1.3	1234968172	
1e+07 L+Zn t24b	Fuzzy	76	0.842126966	0.5	25 ;85.0 ;1.3	1804953483	
1e+07 L t24b	Fuzzy	160	0.842126966	0.5	25 ;85.0 ;1.3	3799902068	
1e+07 L t24a	Fuzzy	151	0.842126966	0.5	25 ;85.0 ;1.3	3586157577	
1e+08 L t24b	Fuzzy	6	0.842126966	0.5	25 ;85.0 ;1.3	1424963276	
1e+08 L t24a	Fuzzy	19	0.842126966	0.5	25 ;85.0 ;1.3	4512383706	
1e+09 L t24b	Fuzzy	3	0.842126966	0.5	25 ;85.0 ;1.3	7124816378	
1e+09 L t24a	Fuzzy	1	0.842126966	0.5	25 ;85.0 ;1.3	2374938793	
1e+07 R t24b	Fuzzy	209	0.842126966	0.5	25 ;85.0 ;1.3	4963622077	
1e+07 R t24a	Fuzzy	181	0.842126966	0.5	25 ;85.0 ;1.3	4298639215	
1e+07 Zn t24b	Fuzzy	218	0.842126966	0.5	25 ;85.0 ;1.3	5177366568	
1e+07 Zn t24a	Fuzzy	209	0.842126966	0.5	25 ;85.0 ;1.3	4963622077	

Table C.18: Experiment 2, re-exposure 2 automatic colony counter results for endpoint CFU concentration and the computed concentration. Plate Id gives the dilution factor, measured group and other cell specifications. The "Method" column gives the method of colony detection used by the colony counter software. Counted Volume gives the percentage of inoculated volume included in cell detection. Volume gives the volume of plated cells in ml. Input Values gives 3 figures - the threshold to the background, the diameter of the computed part of the Petri dish and the minimal colony diameter in mm.

Plate Id	Method	Counted Colonies	Counted Volume	Volume	Input Values	Concentration	Comments
1e+04 Zn t0a	Fuzzy	12	0.842126966	0.5	25 ;85.0 ;0.65	284992.6551	
1e+04 Zn t0b	Fuzzy	14	0.842126966	0.5	25 ;85.0 ;0.65	332491.431	
1e+03 Zn t0a	Fuzzy	71	0.842126966	0.5	25 ;85.0 ;0.65	168620.6543	
1e+03 Zn t0b	Fuzzy	105	0.842126966	0.5	25 ;85.0 ;0.65	249368.5732	
1e+02 Zn t0a	Fuzzy	683	0.842126966	0.5	25 ;85.0 ;0.65	162208.3195	
1e+02 Zn t0b	Fuzzy	648	0.842126966	0.5	25 ;85.0 ;0.65	153896.0338	
1e+04 R t0a	Fuzzy	10	0.842126966	0.5	25 ;85.0 ;0.65	237493.8793	
1e+04 R t0b	Fuzzy	8	0.842126966	0.5	25 ;85.0 ;0.65	189995.1034	
1e+03 R t0a	Fuzzy	82	0.842126966	0.5	25 ;85.0 ;0.65	194744.981	
1e+03 R t0b	Fuzzy	87	0.842126966	0.5	25 ;85.0 ;0.65	206619.675	
1e+02 R t0a	Fuzzy	615	0.842126966	0.5	25 ;85.0 ;0.65	146058.7358	
1e+02 R t0b	Fuzzy	690	0.842126966	0.5	25 ;85.0 ;0.65	163870.7767	
1e+04 L+Zn t0a	Fuzzy	8	0.842126966	0.5	25 ;85.0 ;0.65	189995.1034	
1e+04 L+Zn t0b	Fuzzy	4	0.842126966	0.5	25 ;85.0 ;0.65	94997.55171	
1e+03 L+Zn t0a	Fuzzy	64	0.842126966	0.5	25 ;85.0 ;0.65	151996.0827	
1e+03 L+Zn t0b	Fuzzy	79	0.842126966	0.5	25 ;85.0 ;0.65	187620.1646	
1e+02 L+Zn t0a	Fuzzy	516	0.842126966	0.5	25 ;85.0 ;0.65	122546.8417	
1e+02 L+Zn t0b	Fuzzy	596	0.842126966	0.5	25 ;85.0 ;0.65	141546.352	
1e+04 L t0a	Fuzzy	11	0.842126966	0.5	25 ;85.0 ;0.65	261243.2672	
1e+04 L t0b	Fuzzy	9	0.842126966	0.5	25 ;85.0 ;0.65	213744.4914	
1e+03 L t0a	Fuzzy	71	0.842126966	0.5	25 ;85.0 ;0.65	168620.6543	
1e+03 L t0b	Fuzzy	73	0.842126966	0.5	25 ;85.0 ;0.65	173370.5319	
1e+02 L t0a	Fuzzy	640	0.842126966	0.5	25 ;85.0 ;0.65	151996.0827	
1e+02 L t0b	Fuzzy	660	0.842126966	0.5	25 ;85.0 ;0.65	156745.9603	

Table C.19: Experiment 2, re-exposure 3 automatic colony counter results for initial CFU concentration and the computed concentration. Plate Id gives the dilution factor, measured group and other cell specifications. The "Method" column gives the method of colony detection used by the colony counter software. Counted Volume gives the percentage of inoculated volume included in cell detection. Volume gives the volume of plated cells in ml. Input Values gives 3 figures - the threshold to the background, the diameter of the computed part of the Petri dish and the minimal colony diameter in mm.

Plate Id	Method	Counted Colonies	Counted Volume	Volume	Input Values	Concentration	Comments
1e+04 Zn+L t24a	Fuzzy	0	0.842126966	0.5	25 ;85.0 ;1.5	0	
1e+04 Zn+L t24b	Fuzzy	1	0.842126966	0.5	25 ;85.0 ;1.5	23749.38793	
1e+03 Zn+L t24a	Fuzzy	45	0.842126966	0.5	25 ;85.0 ;0.5	106872.2457	
1e+03 Zn+L t24b	Fuzzy	20	0.842126966	0.5	25 ;85.0 ;0.5	47498.77586	
1e+02 Zn+L t24a	Fuzzy	109	0.842126966	0.5	25 ;85.0 ;0.5	25886.83284	
1e+02 Zn+L t24b	Fuzzy	103	0.842126966	0.5	25 ;85.0 ;0.5	24461.86957	
1e+09 L t24a	Fuzzy	203	0.842126966	0.5	25 ;85.0 ;0.3	4.82E+11	
1e+09 L t24b	Fuzzy	248	0.842126966	0.5	25 ;85.0 ;0.3	5.89E+11	
1e+08 L t24a	Fuzzy	442	0.842126966	0.5	25 ;85.0 ;0.3	1.05E+11	
1e+08 L t24b	Fuzzy	377	0.842126966	0.5	25 ;85.0 ;0.3	89535192488	
1e+07 L t24a	Fuzzy	752	0.842126966	0.5	25 ;85.0 ;0.3	17859539722	
1e+07 L t24b	Fuzzy	579	0.842126966	0.5	25 ;85.0 ;0.3	13750895610	
1e+09 Zn t24a	Fuzzy	341	0.842126966	0.5	25 ;85.0 ;0.3	8.10E+11	
1e+09 Zn t24b	Fuzzy	394	0.842126966	0.5	25 ;85.0 ;0.3	9.36E+11	
1e+08 Zn t24a	Fuzzy	295	0.842126966	0.5	25 ;85.0 ;0.3	70060694387	
1e+08 Zn t24b	Fuzzy	377	0.842126966	0.5	25 ;85.0 ;0.3	89535192488	
1e+07 Zn t24a	Fuzzy	742	0.842126966	0.5	25 ;85.0 ;0.3	17622045842	
1e+07 Zn t24b	Fuzzy	357	0.842126966	0.5	25 ;85.0 ;0.3	8478531490	
1e+09 R t24a	Fuzzy	402	0.842126966	0.5	25 ;85.0 ;0.3	9.55E+11	
1e+09 R t24b	Fuzzy	365	0.842126966	0.5	25 ;85.0 ;0.3	8.67E+11	
1e+08 R t24a	Fuzzy	758	0.842126966	0.5	25 ;85.0 ;0.3	1.80E+11	
1e+08 R t24b	Fuzzy	791	0.842126966	0.5	25 ;85.0 ;0.3	1.88E+11	
1e+07 R t24a	Fuzzy	866	0.842126966	0.5	25 ;85.0 ;0.3	20566969945	
1e+07 R t24b	Fuzzy	911	0.842126966	0.5	25 ;85.0 ;0.3	21635692402	

Table C.20: Experiment 2, re-exposure 3 automatic colony counter results for endpoint CFU concentration and the computed concentration. Plate Id gives the dilution factor, measured group and other cell specifications. The "Method" column gives the method of colony detection used by the colony counter software. Counted Volume gives the percentage of inoculated volume included in cell detection. Volume gives the volume of plated cells in ml. Input Values gives 3 figures - the threshold to the background, the diameter of the computed part of the Petri dish and the minimal colony diameter in mm.

Appendix D

Contents of Attached CD

Folder	Contents
3D_cap	3D model of the designed cap in `.stl` format
Thesis	The master's thesis in `.pdf` format